1968

Thermal residual stresses in hot-rolled steel members, December 1968

G. A. Alpsten

LEHIGH UNIVERSITY INSTITUTE OF RESEARCH

Residual Stresses in Thick Welded Plates

THERMAL RESIDUAL STRESSES IN HOT-ROLLED STEEL MEMBERS

by
Goran A. Alpsten

December, 1968

Fritz Engineering Laboratory Report No. 337.3

THERMAL RESIDUAL STRESSES IN HOT-ROLLED STEEL MEMBERS

by

Goran A. Alpsten

Fritz Engineering Laboratory
Department of Civil Engineering
Lehigh University
Bethlehem, Pennsylvania

December, 1968

Fritz Laboratory Report No. 337.3

TABLE OF CONTENTS

ABSTRACT

A method for calculating thermal residual stresses in hot-rolled steel members is presented. The method is based on a computation of the temperature and thermal stress distributions throughout the cooling process using a finite-difference method and simulating the actual conditions, including variable material coefficients.

Several computations of residual stresses in rolled plates and H-shapes were carried out using an electronic computer with the purpose of studying (1) the mechanism of formation of thermal residual stresses, (2) the possible influence of various manufacturing conditions upon residual stresses, (3) the effect of variations in material properties, and (4) the effect of shape geometry. The eventual aim of this study was to make possible predictions of thermal residual stresses in hot-rolled plates and shapes.

From the study it was found that shape geometry and cooling conditions are the principal factors which influence the formation of thermal residual stresses in hot-rolled members.

The computations were correlated with experimental measurements of the temperature distribution during cooling of H-shapes. Comparisons were made also with measured residual stress distributions. In general, the experimental results are in conformity with the predictions.

Since the results obtained theoretically have correlated well with the experimental data, the method is expected to be of practical use in the prediction of thermal residual stresses in hot-rolled plates and shapes. Also, analogous methods should be useful for the prediction of temperature-time history and residual stress resulting from other thermal manufacturing and fabrication processes, such as flame-cutting, welding, and heat-treatment.

INTRODUCTION

Purpose and Scope

Residual stresses in structural members can play an important role in buckling, fatigue, stress corrosion, and brittle fracture. Therefore, the actual magnitude and distribution of residual stresses as well as the factors which influence the formation of residual stresses in structural elements are of considerable significance.

Residual stresses result from all types of manufacturing and fabrication processes used in practice, for instance, hot-rolling, flame-cutting, and welding. Residual stresses in hot-rolled steel sections are of great importance, not only because hot-rolled H-shapes are used extensively in structural members subjected to compressive loads, but also because hot-rolled universal-mill plates can form the component plates of welded built-up shapes. Recent studies have indicated that the initial residual stresses existing in the component plates can constitute the major part of the residual stresses in welded shapes, especially in shapes built up of thick universal-mill plates.[1]

An investigation of residual stresses can be experimental or theoretical, or a combination. The actual residual stress distribution in a single specimen can be verified only by experimental measurements. However, accurate measurements of residual

stresses are very tedious and expensive and it is practically impossible to carry out measurements on more than a few specimens out of all existing types of different shapes. Moreover, the residual stress distribution may vary from specimen to specimen, implying several measurements to be made on each shape to obtain a statistically significant result.

In an experimental study, it is very difficult to separate the factor considered and thus eliminate the possible variations due to all other variables. On the other hand, for a systematic investigation of residual stresses and the variables which influence their formation, theoretical methods appear useful. It is only through theoretical studies that the mechanism for formation of residual stresses can be understood in detail.

The objective of the investigation reported in the paper was to study thermal residual stresses in hot-rolled steel plates and shapes. Such stresses are formed due to the non-uniform temperature distribution during cooling after rolling. A method was developed for theoretical prediction of these particular stresses. The method is based on a calculation of the temperature and the resulting thermal stress distribution throughout the cooling process, and simulating the actual cooling conditions, including variable material coefficients.

The topics of the study can be summarized as follows:

-- to study the mechanism for formation of thermal residual stresses in hot-rolled plates and shapes

-- to investigate the possible influence of various fabrication conditions upon residual stresses

-- to investigate the influence of variations in material properties upon residual stresses

-- to study the effect of shape geometry

-- to make possible predictions of thermal residual stresses in hot-rolled plates and shapes

-- to suggest areas for further experimental investigations.

The paper is based on a dissertation[2] to which reference may be made for detailed information throughout the paper.

Short Review of the Manufacturing Procedure

Figure 1 shows the schematic arrangement of a typical mill for the rolling of structural shapes. A similar arrangement is used for the rolling of plates. The material enters the mill in the form of a bloom of rectangular cross section. Depending upon the temperature of the entering bloom it may be necessary to reheat it in a furnace to a temperature of 2200-2400°F.

The bloom is then rolled in a number of passes in two or more rolling stands. In each pass the cross section is reduced in a certain manner until the shape has reached its final cross section in the finishing stand. Figure 2 shows the rolling in one of the last passes.

After finish-rolling, the material is conveyed to a hot saw where it is cut into lengths which can be conveniently handled. The member is then allowed to cool down to ambient temperature on a cooling bed, that is, a metal structure which permits the air to circulate around the rolled members. The detailed arrangement of the plates or shapes on the cooling bed varies with different mill practice and different shape of the material.

Residual stresses will result after the cooling because of the non-uniform temperature distribution through the cross-section during the cooling process. These residual stresses existing after cooling will be referred to as "thermal residual stresses" or "cooling residual stresses" and are the topic of the present paper.

Due to uneven cooling conditions on the cooling bed, many members are crooked after cooling. Therefore, most shapes have to be straightened in some manner. This is accomplished in a roller-straightener or a gag press.

In the roller-straightener the member is passed through a number of rolls which bend the shape in alternating directions about its weak axis. This is, at least theoretically, a continuous process, affecting the whole length of the member. However, the adjustment of the rolls in the roller-straightening machine is made manually. Therefore, the effect on residual stresses can

be expected to vary from almost no change at all to a complete modification of the stress distribution from cooling. The cooling residual stresses, however, will always form the basic residual stress pattern.

The roller-straighteners used today have a limited capacity and many shapes have to be straightened in a gag press. In the "gagging" procedure only fractions of the total length of the shape are affected, leaving parts of the length with the cooling residual stress distribution unchanged.

Finally, there is no assurance that a member is straightened at all. Practical measurements have indicated that residual stresses in delivered plates and shapes often show the basic pattern to be expected from the cooling process.

Previous Work

While the presence of residual stresses in general had been pointed out by F. Neumann and others in the middle of the nineteenth century, a study by M. Roš in 1930 appears to be the first published work dealing specifically with the residual stress distribution in a hot-rolled shape.

Roš assumed that the temperature distribution in an H-shape during cooling after rolling could be considered uniform through the entire flanges and also uniform through the web as indicated

in Fig. 3. Due to the difference in thickness between flanges and web, there would be a difference in temperature during cooling, the thinner web cooling faster. The temperature difference ΔT existing in the temperature range where the material changes from plastic to elastic behavior would cause residual stresses after cooling down to ambient temperature. The distribution of these residual stresses as determined by the assumed temperature distribution is shown in Fig. 3 and the magnitude could be computed from two simple equations, also shown in Fig. 3. Substituting some typical coefficients, Roš could obtain an estimate of the magnitude of stresses as

$$\sigma_f \approx 0.04 \text{ to } 0.06\ \Delta T \qquad \text{(ksi) in the flanges}$$

and

$$\sigma_w \approx -0.11 \text{ to } 0.12\ \Delta T \qquad \text{(ksi) in the web}$$

where ΔT is measured in °F.

The principle of thermal residual stress formation as proposed by Roš is basically the same as used in more recent investigations. However, his assumed temperature distribution was too crude to permit a quantitative or maybe even a qualitative prediction of the actual residual stress distribution. Finally, Roš concluded that the temperature differences in normal rolling practice must be negligible. This conclusion was based on some sectioning tests which showed no evidence of residual stress.

Experimental measurements for residual stress determination which have been carried out since that time have shown that the conclusion drawn by Roš on the magnitude of residual stresses in hot-rolled shapes was not true. J. Mathar reported in 1933 what appears to be the first complete measurements of residual stresses in a structural shape. Measured stresses in two wide-flange H-shapes DIP 20 (nearest equivalent 8WF40) are shown in Fig. 4 after Mathar. Figure 4a gives the variation of the residual stress at the center of the web. The stress is more or less constant in the central part of the beam length and decreases to zero at the ends. The distribution of residual stress in that cross section which showed maximum residual stress in the web was also measured and the results are given in Fig. 4b. Remarkable enough, the measured distribution was almost completely reversed when compared to the pattern predicted by Roš (Fig. 3). The flanges were subject to compressive stresses of varying magnitude, whereas the web showed high tensile stresses, near the yield stress of the material. From similar measurements carried out at that time by other investigators[5,6] it was noted that the residual stress in the web could also be compressive. An average stress in the web of approximately -10 ksi[5] was reported for the same shape as used in Mathar's investigations and -24 ksi[6] was measured in a shape DIP 42½ (nearest equivalent 16WF96).

A considerable number of measurements of residual stresses in hot-rolled shapes reported in the literature up to the present

time and a majority of them carried out at Lehigh University[7,8,9] have shown also that residual stresses in the web can be compressive as well as tensile. The distribution in the flanges appears to be less erratic, normally with compressive residual stresses at the flange tips and tensile stresses at the junction between the flange and web.

A theoretical study of residual stresses in hot-rolled plates and H-shapes was conducted by Huber[8]. However, the study for H-shapes was based on an assumed strain distribution corresponding to an assumed temperature distribution and this approach was, therefore, basically the same as that used by Roš.

METHOD FOR CALCULATION OF THERMAL RESIDUAL STRESS

The temperature during hot-rolling is normally 1700°F or more, which is sufficiently high to allow recrystallization to occur during or after rolling. This means that the material can contain no stresses immediately after rolling and, for a discussion of thermal stress, we can consider the material as being perfectly plastic.

The formation of thermal residual stresses in hot-rolled members can be studied by examining the temperature and stress history from the instant of finish-rolling up to the time when ambient temperature is reached throughout the member. The residual stresses are the final thermal stress distribution at ambient temperature.

Generally, the temperature and stress formations are mutually interrelated in a complex way. However, if the strain rate is small compared to the temperature rate it is possible to formulate equations for the temperature state, independently of the stress-strain state.

An analytical temperature-time solution is practically impossible under the conditions prevailing in the considered case with complicated boundary conditions and variable coefficients. Numerical methods based on finite-difference methods can, however, be used for the solution. The number of numerical operations

involved in such methods necessitates the use of an electronic computer. The fact that the temperature is obtained in a numerical form only is actually no restriction since the subsequent thermal stress analysis is made by numerical methods.

A computer program based on a finite-difference method was developed for the calculation of cooling residual stresses in hot-rolled H-shapes. A number of simplifications or restrictions had to be made and will be discussed in detail later in the paper.

The following variables generally affect the cooling behavior and their influence was to be studied.

1. Temperature magnitude and distribution at finish-rolling.
2. Geometry of the cross section.
3. Exterior cooling conditions; for instance, temperature of the surrounding atmosphere, circulation of air around the shape, and cooling bed arrangement.
4. Interior cooling conditions; internal temperature at arrival to the cooling bed and conditions caused by the position of shape on cooling bed and with respect to adjacent cooling shapes.
5. Thermo-physical properties: thermal conductivity, density, specific heat, latent heat involved in phase transformations, and surface coefficient of heat transfer.
6. Mechanical properties: coefficient of linear expansion and stress-strain relationship (modulus of elasticity and yield stress for elastic-perfectly-plastic material).

A similar computer program was developed for the calculation of cooling residual stresses in members of rectangular cross section, for instance, blooms, billets, and universal-mill plates.

TEMPERATURE ANALYSIS

Theory and Assumptions

The governing equations for three-dimensional heat flow in a solid body under non-stationary conditions may be written

$$\frac{\partial}{\partial x}\left(k\frac{\partial T}{\partial x}\right)+\frac{\partial}{\partial y}\left(k\frac{\partial T}{\partial y}\right)+\frac{\partial}{\partial z}\left(k\frac{\partial T}{\partial z}\right)+Q=\rho c_p\frac{\partial T}{\partial t}+\frac{E\alpha}{1-2\nu}\left(\frac{\partial \varepsilon_x}{\partial t}+\frac{\partial \varepsilon_y}{\partial t}+\frac{\partial \varepsilon_z}{\partial t}\right) \quad (1)$$

and

$$-k\frac{\partial T}{\partial n}=h\left(T-T_{atm.}\right) \quad (2)$$

where

- k = thermal conductivity
- Q = generated heat energy
- ρ = density
- c_p = specific heat
- T = temperature
- E = modulus of elasticity
- α = coefficient of linear expansion
- ν = Poisson's ratio
- ε = mechanical strain
- h = surface coefficient of heat transfer
- x, y, z = Cartesian coordinates
- t = time
- n = coordinate normal to surface

The first equation is a generalized Fourier heat-conduction equation, valid for the interior of the body, whereas the second equation forms the boundary condition and is valid at the surface

of the body. In this study, coefficients generally were assumed to be variable with temperature.

While an analytical solution of this problem is practically impossible, certain assumptions have to be made even in the case of numerical methods. The following assumptions were made in this analysis:

1. An initial temperature distribution in the rolled member as well as the temperature of the atmosphere surrounding the cooling shape are known.
2. The conditions are considered to be two-dimensional, that is, the axial heat flow in the member is neglected. (This assumption is justifiable with the exception of regions close to the ends of the member.)
3. The member and the boundary conditions are symmetrical about both axes of the cross-sectional plane.
4. The material is considered homogeneous and isotropic throughout the cross section; the material coefficients are known as functions of temperature.
5. The heat transfer conditions from the shape surface to the atmosphere are known; no external or internal heat source is acting during cooling.

Considering the assumptions which have been stated above the following simplifications of Eq. (1) can be made. For a body subjected to cooling in the atmosphere (assumption 5) with no sharp variations in the temperature-time history, the coupling effect of temperature and strain can be neglected.[10] This means that the second term of the right member of Eq. (1) is

negligible. Further, Q = 0 since there is no heat generated in the body. Finally, from assumption 2 it follows that the third derivative of the left member of Eq. (1) vanishes. Equation (1) now can be simplified to

$$\frac{\partial}{\partial x}\left(k\frac{\partial T}{\partial x}\right)+\frac{\partial}{\partial y}\left(k\frac{\partial T}{\partial y}\right)=\rho c_p\frac{\partial T}{\partial t} \qquad (3)$$

Formulation of Finite-Difference Relationships

For a finite-difference solution the cross section must be subdivided into a mesh, Fig. 5. The mesh spacing for H-shapes was made variable in order to limit the number of mesh points.(13)

The common "explicit finite-difference method" used to solve transient thermal flow problems is based on a representation of the geometrical derivatives in Eq. (3) by finite central differences and of the time derivative by a finite forward difference. This means that the unknown temperature $T_{i,j,k+1}$ can be expressed in terms of the known temperatures $T_{i,j,k}$, $T_{i-1,j,k}$, $T_{i+1,j,k}$, $T_{i,j-1,k}$, and $T_{i,j+1,k}$ at the previous time interval. See Fig. 6a. However, a numerical stability criterion is involved in this method, restricting the possible time interval to

$$\Delta t \leq \frac{1}{2\frac{k}{\rho c_p}\left(\frac{1}{\Delta x^2}+\frac{1}{\Delta y^2}\right)} \qquad (4)$$

Substituting $\frac{k}{\rho c_p} \sim 0.3$ ft^2/hr (valid for carbon steel) and $\Delta x = \Delta y \sim 0.005$ ft into Eq. (4) gives $\Delta t \lesssim 0.1$ sec. Thus for

the subdivision chosen the time interval in the calculations must be chosen to be less than 0.1 sec. This means that the complete temperature field over the whole cross section must be computed at least 600 times for each minute of the cooling period. Narrow mesh spacings will lead to very tedious computations, even when using a high speed computer.

For this reason, another method was used which is based on a principle developed by Peaceman and Rachford in 1955[11]. The principle, referred to as the implicit alternating direction (IAD) method, is illustrated schematically in Fig. 6b. One of the geometrical derivatives is always represented by a forward difference and this derivative is taken in alternating directions. It has been proven that the IAD method is stable for a rectangular integration region and an arbitrary time interval Δt.[12] Numerical studies have shown that the method is stable for arbitrary time intervals also for more complex shapes of the integration region.

The detailed derivation of the finite-difference equations for the interior and the boundary of the cross section in this application of the IAD method is given in Ref. 2.

The calculation is started at the assumed initial state of temperature. The temperature field after the first time interval

is then computed, integrating in one direction of the cross section. After the next time interval the temperature is computed in the other direction and the computation then continues following a step-by-step procedure and integrating in alternating directions.

A finite-difference equation can be formulated for each mesh point at a certain time interval. Since the number of unknown temperatures is equal to the number of mesh points, the problem can be solved provided the coefficients are known. The equations for each time interval will form a number of comparatively simple equation systems. The coefficient matrix to each equation system contains coefficients different from zero only in the diagonal and in the two adjacent disgonals. The equation systems can, therefore, be solved relatively easily.

Thermo-Physical Coefficients

The coefficients which enter Eqs. (2) and (3) are the thermal conductivity k, the density ρ, the specific heat c_p, and the surface coefficient of heat transfer h. In the preceding sections it was assumed that these coefficients were known. The means for consideration of the actual thermo-physical properties were part of the reported investigation but are discussed in detail elsewhere.[2,13] The variation of properties with temperature was included as well as the effect of phase transformations.

Figures 7 through 9 show the variation of k, c_p, and h with temperature for carbon steels. Upper and lower bounds for test data found in a literature survey[2] are indicated with dashed curves in the diagrams. Solid curves represent the relationships used in the computations. A constant value of 490 lb/ft^3 was chosen for the density. This gives a better approximation of the physical behavior than the use of the actual, variable density.[2,13]

The discontinuity in c_p at 1200-1400°F is a result of the phase transformation, austenite → ferrite + cementite. This was dealt with in a manner different from earlier studies.[2,13,14,15,16]

The surface coefficient of heat transfer includes the effect of convection, conduction and radiation. In the computations a geometrical reduction factor was applied to h to take into account the fact that the free heat transfer may be obstructed, for instance, on the inner surfaces of the flanges and on the web. This factor was computed according to Lambert's cosine law for heat radiation. A further reduction due to the external conditions during cooling can be used in the computations, when applicable.

The material coefficients which enter the computation of the temperature field at a certain instant, t_{2n+1}, (see Fig. 6b) are the average values in the time interval between the previous time, t_{2n}, and the time considered, t_{2n+1}. Since only the temperatures at t_{2n} are known at that moment, the coefficients can not be evaluated before the temperatures at t_{2n+1} are calculated.

This complication was solved with an iterative method. As a first guess the coefficients were evaluated from temperatures which were extrapolated linearly in time from the previous and the next to the previous temperatures at the considered mesh point. Approximate values for all coefficients could be obtained in this way. Using the approximate coefficients, a preliminary temperature field was calculated as described in the previous section.

With the preliminary temperature field, new improved values for the coefficients were evaluated for the average of the previous temperature and the computed preliminary temperature. Using these improved values, the temperature field was calculated again.

The iteration may be continued to give any prescribed accuracy. From numerical studies in the present application, it was found that the error after one iteration, as described above, is negligible.

Results of Temperature Computations

A flow diagram of the computer program for temperature determination is shown in Fig. 10. The computations were carried out in a computer type CDC 3600. The machine time needed for a complete computation including thermal stress calculation ranged from about 1 to 3 minutes for a cooling period of 30 to 90 minutes.

Numerical studies of a specific case (same conditions as in the computations shown in Fig. 11) indicated that while the

ordinary explicit finite-difference method would require approximately 40,000 time intervals to be computed, the prescribed accuracy could be obtained with 200 time intervals when using the IAD method. Although the number of numerical operations involved in each time interval of the IAD method is 10-20 times that of the explicit method, it may be concluded that the IAD method is far more efficient for these calculations.

The computed time-temperature curves for a European shape 'HE 200 B', approximately equivalent to the 8WF40, and using average curves for the material coefficients, are shown in Fig. 11. Three different curves are given, corresponding to three different locations in the cross section (that is, the temperature in three out of the 71 mesh points used are shown). The initial temperature was assumed to be 1830°F (1000°C), uniform through the cross section. This temperature corresponds to the average temperature in practice at, or immediately before, the finish-rolling.

In the beginning of the cooling the flange tips and the web point cool much faster than the point at the junction between flange and web. When the coolest part reaches the phase transformation temperature ($\approx$ 1340°F), the cooling curves tend to level out due to the transformation heat. After some time the transformation is finished and the cooling curves then proceed with a slope almost as if they were a continuation of the curves before

the transformation, the cooling only being delayed for a certain time. The curves continue smoothly until the temperature of the whole cross section eventually approaches the ambient temperature (assumed equal to room temperature).

In Fig. 11 it can be seen that there is a fairly large temperature gradient through the cross section. These temperature differences are the cause of residual stresses to be formed after cooling. No residual stresses would result from a temperature which is uniform or planely distributed across the section during cooling.

The temperature differences over the web and over the flange from the computation in Fig. 11 are drawn in Fig. 12. The temperature differences increase at first very rapidly, reach a maximum and then start to decrease, indicating that the material transformation has started in the coolest point. After a time the curves increase again (for the flange points a very small increase) corresponding to the situation when transformation has started in the hotter point while the transformation is finished in the other point. A new maximum is then reached, marking the situation where the transformation is finished in both points, and after that the temperature differences decrease gradually to zero as ambient temperature is reached.

Actually, the relevant parameter for the formation of residual stresses is not time but rather temperature. As will be

shown later, the critical temperature differences are those existing in the temperature region where the material changes from perfectly plastic to elastic-plastic condition (see also the discussion according to Roš). Therefore, the temperature differences as a function of the temperature is the most apt background for a discussion of residual stress formation. In Fig. 13 has been redrawn the upper diagram of Fig. 12, but with the temperature difference as a function of the temperature in the web point. This diagram indicates that the effect of the phase transformation is significant in a major portion of the cooling process.

Computations of the same kind as those illustrated in Figs. 11 through 13 were obtained for a large number of different cases. The results of these computations may be summarized briefly:

-- the effect of the assumed initial temperature distribution is negligible in the critical region (below the transformation temperature) provided the assumed temperature is chosen sufficiently high.
-- Small variations in the thermo-physical properties have only a small influence upon the computed thermal behavior.
-- Shape geometry has a significant effect upon the absolute temperature as well as the relative temperature state.
-- Cooling conditions can have a significant effect upon the absolute and relative temperature state.

Results of Temperature Measurements

Experimental investigations of the cooling behavior were carried out to study the applicability of the computations and to make possible a comparison between computed and experimental results. A number of cooling tests were made with specimens heated in a furnace to the same temperature as used in the computations (that is, the finish-rolling temperature or somewhat higher). Several thermo-couples were mounted to the central cross section of the specimens to measure the temperature in different points over the cross section. The ends of the specimen were insulated to simulate the two-dimensional cooling conditions prevailing in a long shape. After the furnace temperature was obtained uniformly through the cross section, the specimen was taken out of the furnace and allowed to cool freely in air down to ambient temperature.

The accuracy of the temperature measurement was estimated as ±10°F. The error in the relative temperature measurement was kept to within ±10°F.

Experimental cooling curves for the same shape as in the computations in Figs. 11 through 13 are shown in Fig. 14. The curves give the average temperature at symmetrically located gage points. A comparison with the computed cooling curves in Fig. 11 reveals that the general behavior of computed and experimental cooling curves is very similar.

Figure 15 gives the results from repeated cooling tests with the same specimen, now plotted in the form of temperature difference as a function of time. (The thermo-couple in the web center became loose in one of the cooling tests so only three curves are shown in the upper diagram). A comparison with the computed results (dashed lines in Fig. 15, taken from Fig. 12) for this shape and based upon average material data from the literature shows that the difference between computed and experimental results is of the same order as the variation between repeated measurements.

In two of the tests, there was an unintentional axial heat flow due to unsuitable insulation shields at the ends of the specimen; the first test was accelerated and the second test delayed due to the influence of the axial heat flow. However, the measured temperature differences were still at the same level as for the other two tests.

In Figure 16 the upper diagram from Figure 15 has been redrawn, now with temperature as a parameter. This diagram reveals the actual similarity between the different test results and the computed results. The significance of this basis for comparison will be further demonstrated in the following section.

In conclusion, it may be stated that there is a fairly good agreement between experimental results and the results computed

from average coefficient curves. Similar agreement was obtained also from repeated tests on a different shape. Therefore, it appears possible to compute the time-temperature history during cooling with a reasonable accuracy, provided the actual cooling conditions and the actual geometry are simulated in the computation.

THERMAL STRESS ANALYSIS

Theory and Assumptions

A number of methods for thermal stress analysis have been presented in the literature. Because of the complex conditions certain assumptions must be made. A summary of some previous methods used for calculation of welding residual stresses can be found in Ref. 17. As pointed out there, most previous methods consider neither plastic deformations nor the actual equilibrium conditions.

Solutions based on an analytical analysis for simple geometry and boundary conditions have been reported.[11] However, for more complex shapes and variable coefficients such solutions are presently not developed. Other investigations which included variable coefficients[17,18] were based upon a step-by-step analysis with a stepwise algebraic addition of the thermal stress existing before the time interval considered and an incremental stress formed during this time interval.

The model for the thermal stress formation as used in the present investigation is different from the methods previously mentioned. Before the method is discussed further in detail it is pertinent to summarize the assumptions made in this study.

(1) The material is elastic-perfectly-plastic at all temperatures.

(2) The mechanical material coefficients (coefficient of linear expansion, modulus of elasticity and yield stress) are known as functions of temperature.

(3) Only longitudinal stresses in the member are considered.

(4) Plane sections remain plane.

The principle for the thermal stress calculation is illustrated in Fig. 17. The two stress-strain curves shown represent the conditions in a certain mesh point (i,j) at the start of and at the end of the time interval considered. The same mesh system was used for stress analysis as was employed previously for the temperature computation. (The variable mesh spacing was chosen in such a way that all points were located in the center of the corresponding cross-sectional elements).

The formal procedure to obtain the unknown stress at a certain mesh point and after a certain time interval is simply to add the elastic strain existing prior to the time interval considered and the incremental strain (in Fig. 17 assumed to be negative) and enter the stress-strain curve for this strain as shown in Fig. 17. The incremental strain is determined from the thermal strain and compatibility and equilibrium conditions. The principle and the details of the procedure will be discussed further in the next section.

Formulation of Stress-Strain Equations

Consider a certain mesh point (i,j). The stress and strain existing at a certain time t_k are designated $\sigma_{i,j,k}$ and $\varepsilon_{i,j,k}$.

If, initially, the element is assumed to be cut free from the other elements it will contract corresponding to a strain $-\varepsilon^{E}_{i,j,k}$. During the succeeding time interval the temperature is changed from $T_{i,j,k}$ to $T_{i,j,k+1}$. For the free element this would cause a thermal strain increment denoted by $\Delta\varepsilon^{T}_{i,j,k+1/2}$ which can be calculated from the equation

$$\Delta\varepsilon^{T}_{i,j,k+1/2} = \alpha_{i,j,k+1}\left(T_{i,j,k+1} - T_o\right) - \alpha_{i,j,k}\left(T_{i,j,k} - T_o\right) \qquad (10)$$

The strain resulting, that is, the free strain is $\left(-\varepsilon^{E}_{i,j,k} + \Delta\varepsilon^{T}_{i,j,k+1/2}\right)$.

Now suppose the elements are joined together again. Due to the compatibility requirements the strain change in each element must total a strain increment $\Delta\varepsilon^{C}_{i,j,k+1/2}$ which is distributed planely over the cross section (assumption 4 above). The difference between this imposed strain and the free strain is equal to the strain after the time interval considered

$$\varepsilon_{i,j,k+1} = \Delta\varepsilon^{C}_{i,j,k+1/2} - \left(-\varepsilon^{E}_{i,j,k} + \Delta\varepsilon^{T}_{i,j,k+1/2}\right) \qquad (11)$$

The strain increment $\Delta\varepsilon_{i,j,k+1/2}$ in Fig. 17 is, therefore, equal to $\left(\Delta\varepsilon^{C}_{i,j,k+1/2} - \Delta\varepsilon^{T}_{i,j,k+1/2}\right)$.

The strain $\varepsilon_{i,j,k+1}$ will give rise to a stress equal to

$$\sigma_{i,j,k+1} = \begin{cases} E_{i,j,k+1}\,\varepsilon_{i,j,k+1} & \text{if } E_{i,j,k+1}\,\varepsilon_{i,j,k+1} \le \sigma_{y_{i,j,k+1}} \\ \sigma_{y_{i,j,k+1}} & \text{if } E_{i,j,k+1}\,\varepsilon_{i,j,k+1} > \sigma_{y_{i,j,k+1}} \end{cases} \qquad (12)$$

If n denotes the number of mesh points, there are generally n unknown strains $\varepsilon_{i,j,k+1}$ and n unknown stresses $\sigma_{i,j,k+1}$.

Furthermore, there are n strain increments $\Delta \varepsilon^{c}_{i,j,k+1/2}$ which can be represented by three unknowns, that is, a total of 2n+3 unknowns. Equation (11) gives one relation for each mesh point and so does Eq. (12), or together 2n equations. The remaining three equations to find a solution are obtained from the equilibrium conditions, that is, one equation from the equilibrium of force and two equations from the equilibrium of moments.

The formal addition of strains instead of stresses as in the previous studies[17,18] is considered to fulfill the assumptions and to simulate the physical behavior in a more correct way. A simplified example will clarify the difference between the two procedures. Consider a system as shown in Fig. 18a to be maintained at a constant elevated temperature and loaded form zero to a certain stress below the yield point. The temperature is then allowed to cool and at a lower constant temperature the specimen is unloaded. The results obtained with the two principles are shown in Fig. 18a. Since the stress was assumed to be less than the yield point of the material, the behavior must be purely elastic. The method based on an addition of stresses will result in an elastic strain remaining after unloading to zero stress which is mechanically impossible. The other principle will give zero strain after unloading. In the more general case illustrated in Fig. 18b the methods give two different answers for the stress being calculated. Here the addition of stresses happen to give a negative stress for a positive elastic strain, also mechanically impossible.

From the discussion above it might be thought that the methods will furnish results which are completely different. However, comparative calculations carried out with both methods have shown that the difference is very small, especially when the variation in elastic modulus is small from one time interval to another (that is, with short time intervals).

Figure 19 shows a short flow diagram of the computer program used for the stress computation. This program was a subroutine to the program for temperature determination.

Mechanical Coefficients

The properties of interest here are the coefficient of linear expansion α, the elastic modulus E, and the yield stress σ_y. Figures 20, 21, and 23 give the upper and lower limits of data found in the literature for carbon steels as well as the curves used in the investigation[2].

It might be well to point out that the coefficient of linear expansion normally is given as the average value in a certain temperature interval, ranging from room temperature to the considered temperature. Therefore, the thermal elongation from a temperature change between two temperatures must be computed from an equation of the type shown in Eq. (10).

The variation in α between different carbon steels is relatively small. The behavior in the transformation temperature

range is due to the gradual transformation $\gamma \rightarrow \alpha$ which is accompanied by a volume expansion. The temperature at the two discontinuity points from tests on different materials generally coincides with the A_3 and A_1 temperatures for the actual carbon contents.

The elastic modulus is normally measured by a dynamic method to minimize the effect of time-dependent influences due to creep. Figure 21 contains both "static" and "dynamic" measurements. The variation is reasonably small.

It is noted that a good representation of the actual non-linear stress-strain relationships at different temperatures and for the strain range of interest in the present application was obtained when the yield stress of the elastic-perfectly-plastic model equals the 0.2% proof stress. A comparison between the actual stress-strain relationships and the elastic-perfectly-plastic relationship based on a yield level equal to $\sigma_{0.2}$ is exemplified in Fig. 22. Fortunately, $\sigma_{0.2}$ is the stress level normally reported in the literature to represent the yield point at higher temperatures. Upper and lower limits of data from the literature are given in Fig. 23.

While time-dependent deformations have no significant influence on the $\sigma_{0.2}$ stress level at temperatures below 700-800°F, this is not true for higher temperatures. Results of some creep tests are sketched in Fig. 23. The applicable stress-strain relationship will fall between the two limits of data obtained from

tensile tests and creep tests. It should however be noted that the duration of the creep tests is 10^5h, as compared to a few minutes for the critical temperature range in the cooling process of most rolled shapes. Furthermore, the creep tests results were obtained at a constant load. However, in the application studied the stress varies and the conditions at high temperatures are in-between the creep case and the relaxation case where strain is kept constant. While it is possible for a tensile test specimen to sustain a load under continuous recrystallisation[20], zero stress would result in a relaxation test.

Approximate considerations of the time-dependent effects and the difference in behavior at constant stress versus constant strain have led to the curves shown in Fig. 23.

Results of Thermal Stress Computations on Plates

Figure 24 shows an example of the computed temperature and thermal stress behavior during cooling of a plate 24" x $3\frac{1}{2}$". It was assumed that the initial temperature was 1830°F (1000°C), uniform through the cross section, and that the surface heat transfer was free in all directions.

At the temperature of 1830°F, the material is in perfectly plastic condition, denoted by the shaded area in the first diagram of Fig. 24. The remaining diagrams show curves for constant temperature and constant stress at 10, 20, 30, and 40 minutes and

finally, at a very long time after the initial state.

After 10 minutes the temperature has cooled to about 1300 - 1500°F. The temperature is still too high to allow any stresses to be developed (Fig. 23). After 20 minutes of cooling the temperature ranges from about 1150 - 1350°F, the plate edges cooling faster than the interior of the plate. At this moment the coolest parts have entered the elastic region, but the stresses are negligible. After another 10 minutes, the temperatures being approx. 1000-1250°F, the cross section still is partly in the plastic condition although the location of the plastic region is different from that obtained at t = 20 minutes. This is due to the effects of the phase transformation.

At t = 40 minutes the temperature is about 950 - 1100°F and the entire corss section is elastic. When cooling further to ambient temperature, the thermal contraction of the central hot portion would be greater than that of the cooler surface parts. However, due to the symmetry the compatibility conditions require that the contraction is equal throughout the cross section. This will introduce tensile stresses in the central portion, balanced by compressive stresses in the regions which were cooling faster. The resulting residual stress distribution after cooling to ambient temperature is shown in the last diagram of Fig. 24. In this case the temperature differences through the cross section were large enough to cause compressive residual stresses at the yield point at the edges of the plate (shaded in the diagram). The

results exemplify the rule of thumb that the portions of the cross section to cool faster will be left in a state of compressive residual stress.

Figures 25 through 28 give the results obtained for four different plate sizes: 6" x $\frac{1}{2}$", 20" x 1", 12" x 2", and 24" x $3\frac{1}{2}$". Three curves are shown for each plate: the distribution of residual stress in the plate surface, in the mid-plane, and the average across the thickness. The four different plates represent two thin plates (less than, or equal to, 1 inch) and two thick plates. In the $\frac{1}{2}$" plate (Fig. 25) the maximum variation across the thickness is less than 3 ksi, whereas the same variation in the thickest plate ($3\frac{1}{2}$ inches) is approx. 15 ksi.

It can also be noted from a comparison of the data in the diagrams, that there is a trend of increasing magnitude of the stresses with increasing size of the plates. The average residual stress at the plate edge is -10, -13, -21, and -31 ksi, respectively, and the average tensile stress in the center of the plates is approx. 3, 2, 8, and 9 ksi, respectively, for plates of increasing size.

The distribution of residual stress through the thickness is generally close to a parabolic shape. The distribution across the width is of a similar shape, and colser to a parabola with smaller width/thickness ratios.

For increasing thickness of the plate, the magnitude of residual stresses at both center and edge will increase as well as the extension of the compressive stress region into the plate. This is illustrated in Fig. 29. The influence of plate width on the residual stress distribution is more complex as shown in Fig. 30. Note that the dimension of width is shown non-dimensionalized. In actual scale, the extension of the compressive stresses in a wide plate is larger than in a smaller plate. Finally, the effect of the "size factor", when keeping the width/thickness ratio constant, is indicated in Fig. 31. The difference in the center part of the diagram are very small in this specific case, the deviation being less than 1 ksi, whereas the stress magnitude in the area close to the edges is a function of the plate size.

Results of Thermal Stress Computations on H-Shapes

Figure 32 shows an example of the computed temperature and thermal stress behavior during cooling of a shape HE 200 B. (Compare with Figs. 11 through 13). The initial temperature was assumed to be 1830°F, uniform over the cross section. The material is in the perfectly plastic condition, denoted by the shaded area in the first diagram of Fig. 32. The succeeding diagrams show contour lines for equal temperature and equal stress at 2, 4, 8, 16 minutes and finally, at a very long time after the initial state. After 2 minutes the temperature has cooled down to about 1400-1525°F, but still no stresses have been formed. After 4 minutes of cooling, the temperature ranging roughly between 1250 and 1350°F, the coolest parts, that is, the flange tips and the web, have entered the

elastic condition. The stresses are still negligible. After another 4 minutes the entire cross section is elastic and remains so for the rest of the cooling. The sign of the stresses at 8 minutes reflects the fact that the temperature differences through the section have increased from t = 4 min to t = 8 min. This is due to the phase transformation; see Fig. 12. At 16 min from the initial stage, the temperature gradients have decreased, giving increased stress gradients. Finally, after a very long time the ambient temperature is approached and the thermal stress distribution is then equal to the residual stress distribution. The parts to cool fastest, that is, the flange tips and the web, are left with a compressive residual stress which is balanced by tensile residual stresses at the junction between flange and web.

A comparison between the residual stress diagram and the temperature diagram in the range where the material changes from the plastic to the elastic-plastic condition reveals a similarity between these patterns. Figure 33 illustrates this further. The thermal stress for three points of the cross section is compared with the corresponding yield stress, with time as a parameter.

It is noted that the thermal stresses are elastic except for a short interval in the beginning of the cooling. This can be observed in Figs. 24, 32, and 33. The change of the material from the plastic to the elastic-plastic condition is a function of temperature. These facts imply that the temperature differences at the time when this particular temperature region is passed are of

primary importance for the formation of residual stresses. This point was intuitively realized by Mathar (see the Introduction) and suggests that a two-step analysis considering only the temperature distribution at the critical temperature region and the uniform temperature after finished cooling can be used to give a qualitative estimation of the cooling residual stresses. An analogous method has been proposed for the estimation of welding residual stresses, where the initial temperature distribution is assumed equal to the maximum temperature envelope during welding.[19]

Some examples of the effect of different assumptions for initial temperature and material properties on the residual stress distribution are given in Fig. 34. The various assumptions for the material properties were chosen according to the curves in Figs. 7, 8, 9, 20, 21, and 23. The effect is shown to be negligible for most cases illustrated here. This means that realistic predictions of residual stress can be based upon a nominal initial temperature distribution and average curves for the variation of material properties with temperature, especially when a comparative study of geometry, etc. is to be made. On the other hand, if constant coefficients were chosen for all material properties, this would result in inaccurate description of the physical behavior. The most important assumptions are the relationships for the yield stress and the coefficient of linear expansion. In Fig. 34, the yield stress curve used for the comparison (curve 2 in Fig. 23) was chosen to give the maximum deviation from the first case.

Figure 35 illustrates the results obtained for two shapes which are geometrically similar, one being the shape HE 200 B, the other, a hypothetical shape with dimensions twice those of the HE 200 B. All other variables are exactly the same. Figure 36 gives another comparison between an HE 200 B shape and a shape of the same dimensions except that the width was 4" instead of 8". The results show that the dimensions and the size of the shape is a significant variable.

So far it was assumed that the heat transfer is free in all directions. Figures 37 and 38 give examples of the possible influence of different cooling conditions on the residual stress distribution.

In the first case (Fig. 37) the heat transfer from the web surfaces was reduced to a certain percentage varying between 100 and 30%. This will simulate very schematically the conditions when the shape is placed with the web in vertical position during cooling and with adjacent shapes reducing the possible heat transfer. The results show that the distribution in the web is completely reversed as compared to the distribution to be expected from free cooling. Instead of compressive stresses in the central part of the web, there are high tensile stresses. The type of distribution obtained in the flange is similar for both cases although the position of the zero line in the forced heat-transfer case has shifted, resulting in higher compressive stresses to balance the tensile stresses in the web.

Residual stress distributions of this forced heat-transfer type have been measured in some cases; for instance, see the distribution obtained by Mathar, Fig. 4. The H-shapes of Figs. 37 and 4 are very similar, and the residual stress distributions exhibit a good resemblance.

Figure 38 illustrates further the effect of various cooling conditions. Results were obtained for three different assumed heat-transfer conditions: free heat transfer, heat transfer reduced by 50% on all surfaces except the outer sides of the flanges, and finally heat transfer reduced by 50% only on these outer flange surfaces. Schematically, the three different cases can be considered simulating different arrangements during the cooling, that is, a member cooling separately, a member cooling with the web in a vertical position and adjacent members on both sides, and a member cooling with the web in a horizontal position and adjacent members on both sides. As can be seen in Fig. 38, the residual stress distribution in the web is very sensitive to the cooling conditions. Stresses in the flange are also different for the three cases although the stresses at the flange tips are all at the same level.

It is expected that the extreme cases illustrated in Figs. 37 and 38 represent limit conditions for normal manufacturing practice of small to medium-size shapes. For prediction of the behavior of most such shapes the assumption of free heat transfer appears reasonable since a main part of the critical temperature range is passed before the shape arrives to the cooling bed. For heavy shapes,

however, the actual cooling conditions must be considered for accurate predictions.

While the variation of residual stress across the thickness is very small for thin components of the shape, this is not true for heavy shapes. Figures 39 and 40 give the computed residual stress distribution for a heavy rolled shape 14WF426. The diagrams shown are based on the assumptions of free cooling and reduced heat transfer from the inner surfaces (the same assumptions as cases a and b, Fig. 38). The variation through the thickness of the flanges is quite considerable. Also, the stresses are higher than was encountered in the calculations for smaller shapes.

The heaviest shape rolled in today's practice is a "jumbo" shape 14WF730. Figures 41 and 42 illustrate the distribution of residual stresses in this shape, as obtained in computations based upon the same assumptions as in Figs. 39 and 40, that is, free cooling, and reduced heat transfer, respectively. The computed stresses in the jumbo shape are very high in both cases considered, and equal the yield stress in the outer portions of the flanges.

While the magnitude and distribution of residual stresses in general plays a role, the residual stresses at the flange tips are of primary importance in determining the buckling strength of centrally loaded compressed members.[9] It is evident that the high compressive stresses predicted in the heavy columns would be detrimental to column strength. Figure 43 shows computed column curves,

based upon the tangent modulus load concept and the actual distribution of predicted residual stresses for a 14WF730 shape. Figure 44 gives a comparison between the tangent modulus load and the ultimate strength, both curves computed for weak axis buckling and the free heat transfer type of residual stress (Fig. 41). The ultimate strength curve was obtained assuming the initial out-of-straightness to be a sine curve with a mid-height deflection of 0.001L. Also shown in Fig. 44 is the Basic Column Curve developed by the Column Research Council from research on small rolled shapes.[21] The column curves based upon the predicted thermal residual stresses in the 14WF730 fall far below the Basic Column Curve. However, in the practical range of slenderness ratios of such heavy columns in buildings, that is, at KL/r = 20 to 50, the reduction in strength is not as severe as for slender columns.

The compressive residual stress at the flange tips obtained in a number of computations is plotted in Fig. 45 against a geometrical parameter $\frac{b/t}{d/w}$. This parameter had been suggested to describe the variation of measured residual stresses at the flange tips of different shapes.[7,8] The computations shown in Fig. 45 were obtained from a systematic variation of the four dimensions of the shape, and assuming free heat transfer.

The results of these computations show a clear tendency of increasing residual stress with increasing value of the parameter. This was also noted previously from the experimental results.[7] In Fig. 45 there appears to be a wide scatter, and the scatter was

still larger in the experimental values. A closer examination of the points in Fig. 45 would, however, reveal that there is a regular pattern in that the upper points are for the heavier shapes and the lower points are for lighter shapes.

From the computations plotted in Fig. 45 and from a considerable number of additional computations[2] it was noticed that all calculations furnished results in a region within two limiting boundary lines and that most heavy shapes will fall in the upper part of this region and most small shapes in the lower part. This has been illustrated in Fig. 46.

Comparison With Experimental Results

While it can not be expected that all experimental results will correlate well with computations based on nominal shape dimensions, average material properties and certain assumptions on the heat transfer in cooling, some comparisons between computed and measured residual stresses will be made here to give an idea of the applicability of the method. The experimental results were obtained from the literature as referred to for each specimen. The diagrams shown are for average residual stress through thickness, except for the 14WF730 shape.

Figure 47 shows comparisons between experimental and computed residual stresses in universal-mill plates of three different sizes,

6" x $\frac{1}{4}$", 10" x $\frac{1}{2}$", and 20" x 1". The computed distributions were obtained using the free heat-transfer assumption. For the larger plate there are results of two independent measurements on different specimens.[22,23] The agreement between experimental and theoretical results is satisfactory, the maximum deviation being of the same order as the experimental accuracy, except for one of the 20" x 1" plates.

Figures 48 through 55 give some examples of the correlation between experimentally obtained residual stresses and computed results for shapes ranging from a small I-shape IPE200 to a 14WF730 shape. All computations were based on the free heat-transfer assumption, except for the 14WF426 shape, Fig. 54, where comparative results are given based on the alternative assumption of reduced heat transfer from inner surfaces of the shapes.

It should be borne in mind that the computations can simulate only the "average" behavior. For the small and medium-size shapes, computations based on the free heat-transfer assumption appear to predict the actual measured residual stress distribution fairly well as could be expected (see the discussion on heat transfer in the previous section). In deep shapes the magnitude of the residual stress in the center of the web approaches the yield point of the material (assumed as 31 ksi in the computations). Since the yield stress of the web material in the deep test shapes apparently was higher than the value assumed in the computations, closer correlation

would be obtained for these shapes applying the actual yield stress level.

For the 14WF426 shape (Fig. 54) the seemingly crude assumption of forced heat transfer indeed predicts the residual stresses better than the free-cooling assumption, most experimental points falling in between the two calculated distributions and closer to the solution based on the forced heat-transfer assumption. As was stated earlier, detailed agreement for a heavy shape specimen can be obtained only if the actual cooling conditions are known and applied in the calculation.

In Fig. 55, the measured residual stress distribution in the 14WF730 shape shows little resemblance to the thermal residual stress distribution that was predicted. While the distribution in the left part of the measured diagram is qualitatively similar to the predicted distribution, the right part is completely different. It is believed that this id due to the cold-straightening operations after cooling in the mill. The mill scale of the test specimen showed clear evidence of cold-bending yield lines. Further studies would be needed to determine the general significance of either type of distribution in "jumbo" shapes manufactured according to today's practice. However, as for the strength of the columns in the lower slenderness ratios, the measured residual stress distribution of Fig. 55 appears to be as unfavorable as the predicted thermal stress distribution.[27]

SUMMARY AND CONCLUSIONS

The investigation described in the paper has been concerned with the thermal residual stresses existing in hot-rolled plates and H-shapes after cooling. A method was developed to calculate these particular stresses considering the complete temperature and stress history during cooling. The temperature calculation is based on a solution of the Fourier heat conduction equation, taking into account the actual boundary conditions at the surface of the shape. The thermal stress is computed from the temperature distribution throughout the cooling process using an elastic-perfectly-plastic model for the material behavior. The final thermal stresses after cooling to ambient temperature are the residual stresses.

Calculations were carried out using a finite-difference method and an electronic computer and simulating the actual conditions, including variable material coefficients. The principal objective was to investigate the influence of different factors on residual stresses. At the same time, a better understanding of the formation of cooling residual stress was achieved. The method can be employed for prediction of thermal residual stresses in rolled plates and H-shapes.

The results of the computations indicate that small variations in the material coefficients have generally only a small influence on the computed residual stress; the yield stress in the temperature

range where this stress is small and approaches zero is the most important material property in this respect. For calculations with an accuracy which is satisfactory for most practical purposes it is sufficient to base the computations on average curves for the different coefficients and the actual type of material. Upper and lower limits of data found in a literature survey for carbon steels, as well as the average curves for these coefficients as used in the study are given in the paper. Computations employing constant coefficients for all relevant material properties will give only a qualitative description of the actual temperature and thermal stress behavior.

The principal factors which influence the distribution and magnitude of thermal residual stresses are shape geometry and cooling conditions. A few cases of different assumed cooling conditions were studied. It was found that the residual stress distribution in the web is extremely sensitive to the cooling conditions. This may explain the apparantly erratic results for the web obtained in experimental residual stress measurements by different investigators. The distribution in the flange is less dependent but the magnitude varies to a certain extent. The computations also indicate that the conditions on the cooling bed will have a major influence in the critical temperature range only for relatively heavy shapes. For small shapes a main part of the cooling will occur during the conveyance of the shape from the finishing stand to the cooling bed. The assumption of free cooling appears to be reasonable for the conditions during the transport to the

cooling bed and consequently, this assumption should generally result in good predictions for at least small shapes. For large shapes the free-cooling assumption may or may not give valid results, and for an accurate prediction the actual cooling conditions on the cooling bed should be considered.

Several computations were carried out for plates and H-shapes with a systematic variation of the dimensions as well as for a number of commercially available H-shapes. These computations were based on the free-cooling assumption. Practically all computations for shapes resulted in a residual stress distribution with compression at the flange tips and in the web, and tension at the junction between flange and web. Correspondingly, the edges of the UM plates are in compression, balanced by tension in the center. However, the stress magnitude varies considerably between different cross sections. The variation of computed residual stress through the thickness direction is negligible for very thin elements, but for thick elements is almost as pronounced as across the width direction.

One of the important details of the residual stress distribution in an H-shaped member under compressive load is the residual stress region at the flange tips. The computed residual stress at the flange tip for all H-shapes considered ranged between -0.7 and -31 ksi in compression, corresponding to

2 and 100% respectively of the assumed yield stress at room temperature. There is a clear trend of increasing stress at the flange tips of H-shapes with increasing value of a geometric parameter, relating the width to thickness ratio of the flange and web components. This parameter, $\frac{b/t}{d/w}$, was suggested previously from results of experimental residual stress measurements, which showed the same general relationship between residual stress and the parameter.

It was also noted in the study reported in this paper that there is a tendency of increasing magnitude of the residual stresses with increasing size of the member. This is an important conclusion, implying that the column strength characteristics obtained in previous research on small rolled shapes would not be completely applicable to the heaviest shapes rolled today. For thick universal-mill plates and heavy shapes, the magnitude of the predicted residual stresses is very high and can approach the yield stress. The column strength of a heavy rolled shape is detrimentally affected by these high residual stresses, and more so than smaller rolled shapes with smaller residual stresses. Similarly, for a welded H-shape built up of thick universal-mill plates, the high compressive stresses at the plate edges would lower the column strength.

The computed temperature distribution during cooling and the computed residual stresses were compared with experimental

results. The agreement between computed and experimental data is good in most cases, indicating that predictions with reasonable accuracy can be obtained using the analysis developed.

Future research topics concerning residual stresses in hot-rolled plates and shapes could include an experimental study of residual stresses applying statistical sampling methods. Some hypotheses could be formulated with the information from this investigation. Further studies should be directed towards the possibility of reducing thermal residual stresses by rational manufacturing techniques. Controlled cooling procedures and cold-straightening operations should prove useful in this respect.

The method as described in this paper was applied to members cooling in the atmosphere. The computer program can be utilized also for predicting residual stresses which are the result of different thermal treatments, for instance, the tempering process employed for ASTM A514 steel sections. Analogous analyses can also be used for studies of temperatures and residual stresses in flame-cutting and welding. The use of finite-difference methods provides a possibility of making realistic assumptions on the geometry, the actual arrangement of heat sources, the boundary conditions, and the material properties.

ACKNOWLEDGMENTS

The study reported in this paper was a phase of an investigation into residual stresses and their influence on the strength of structural elements; this investigation was carried out at the Institution of Structural Engineering and Bridge Building at the Royal Institute of Technology, Stockholm, Sweden. The investigation was conducted under the sponsorship of the Swedish Technical Research Council. The author is greatly indebted to Dr. Georg Wästlund, Head of the Institution of Structural Engineering and Bridge Building, for his continuing encouragement and constructive criticism during the progress of the work. Mrs. Nan Stråât and Mr. Toivo Tagél assisted in the preparation of the computer programs for H-shapes and plates, respectively. Their cooperation is gratefully acknowledged. Dr. Bertil Aronsson, the Swedish Institute for Metal Research, reviewed the original dissertation and his suggestions were incorporated in the paper.

Certain aspects of the study were continued at Fritz Engineering Laboratory, Lehigh University, Bethlehem, Pennsylvania, under a general research project "Residual Stresses in Thick Welded Plates", sponsored by the National Science Foundation. Dr. Lynn S. Beedle, Director of Fritz Engineering Laboratory, encouraged the international cooperative nature of the study. Dr. Lambert Tall, Principal Investigator of the research project at Lehigh University, reviewed the paper and made a number of valuable suggestions. His interest and encouragement in its preparation is sincerely appreciated. This

research is under the technical guidance of Column Research Council Task Group 1, of which Mr. John A. Gilligan is Chairman.

Special thanks are also due to Miss Joanne Mies for typing the report and to Mrs. Sharon Balogh for preparing the drawings.

NOMENCLATURE

Symbols and Units

A	= area	(in^2)
E	= modulus of elasticity	(ksi)
L	= length	(in)
P	= load	(kips)
Q	= generated heat energy	(Btu/ft^3-hr)
T	= temperature	(°F)
b	= width	(in)
c_p	= specific heat	(Btu/lb-°F)
d	= depth	(in)
H	= surface coefficient of heat transfer	(Btu/ft^2-h-°F)
k	= thermal conductivity	(Btu/hr-°F-ft)
n	= coordinate normal to surface	(in)
r	= radius of gyration	(in)
t	= time; flange thickness	(hr; in)
w	= web thickness	(in)
x	= Cartesian coordinates	(in)
y		(in)
z		(in)
α	= coefficient of linear expansion	$(°F)^{-1}$
ε	= strain	
ν	= Poisson's ratio	

ρ	= density	(lb/ft^3)
σ	= stress	(ksi)

Subscripts:

C	= compressive
R	= residual
atm	= atmosphere
cr	= critical
f	= flange
i	= mesh point in x direction
j	= mesh point in y direction
k	= order of time interval
w	= web
x	= Cartesian coordinate
y	= Cartesian coordinate; yield
z	= Cartesian coordinate

Superscripts:

C	= compatibility
E	= elastic
P	= plastic
T	= thermal

FIGURES

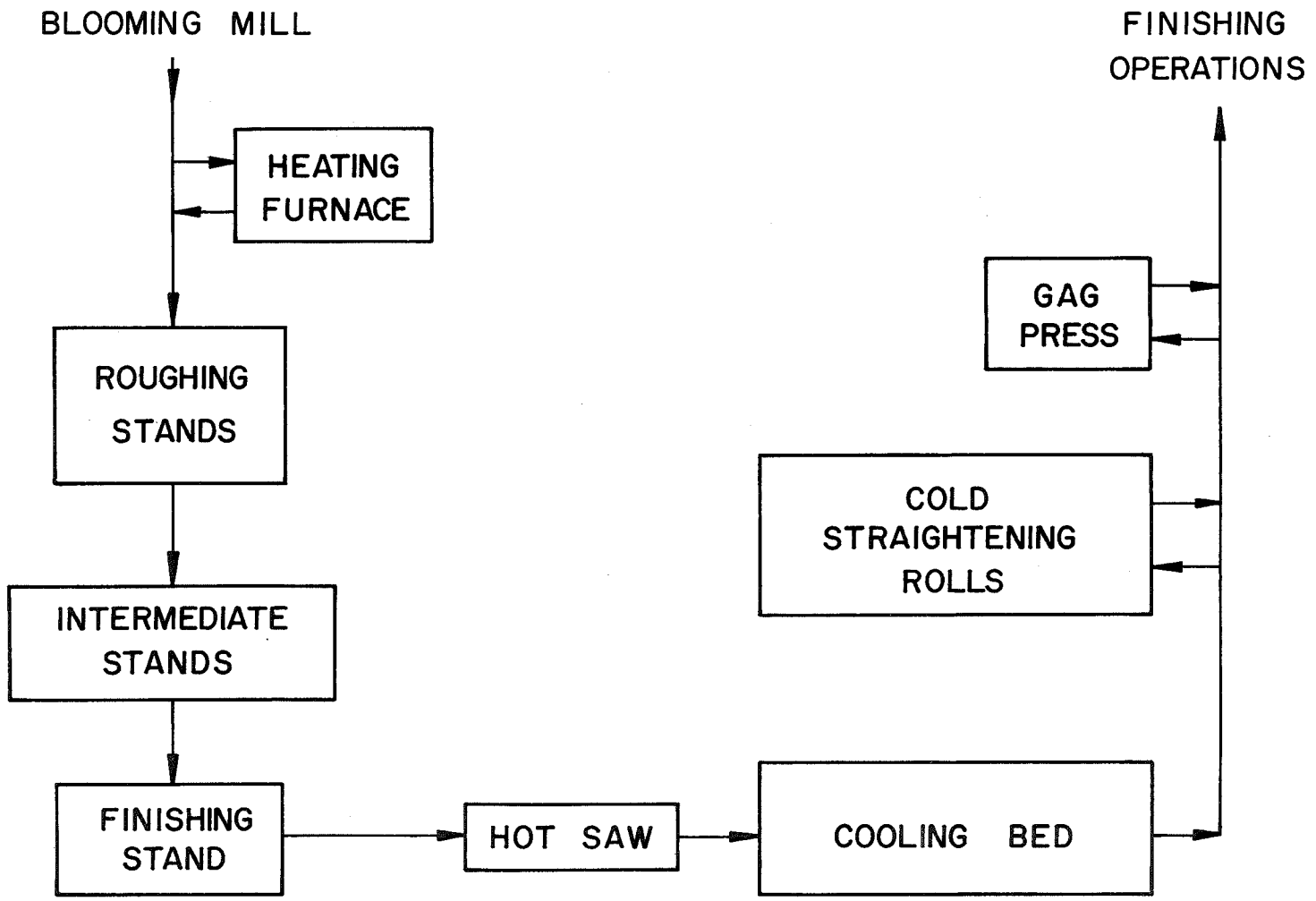

Fig. 1 Schematic arrangement of a typical mill for rolling structural shapes

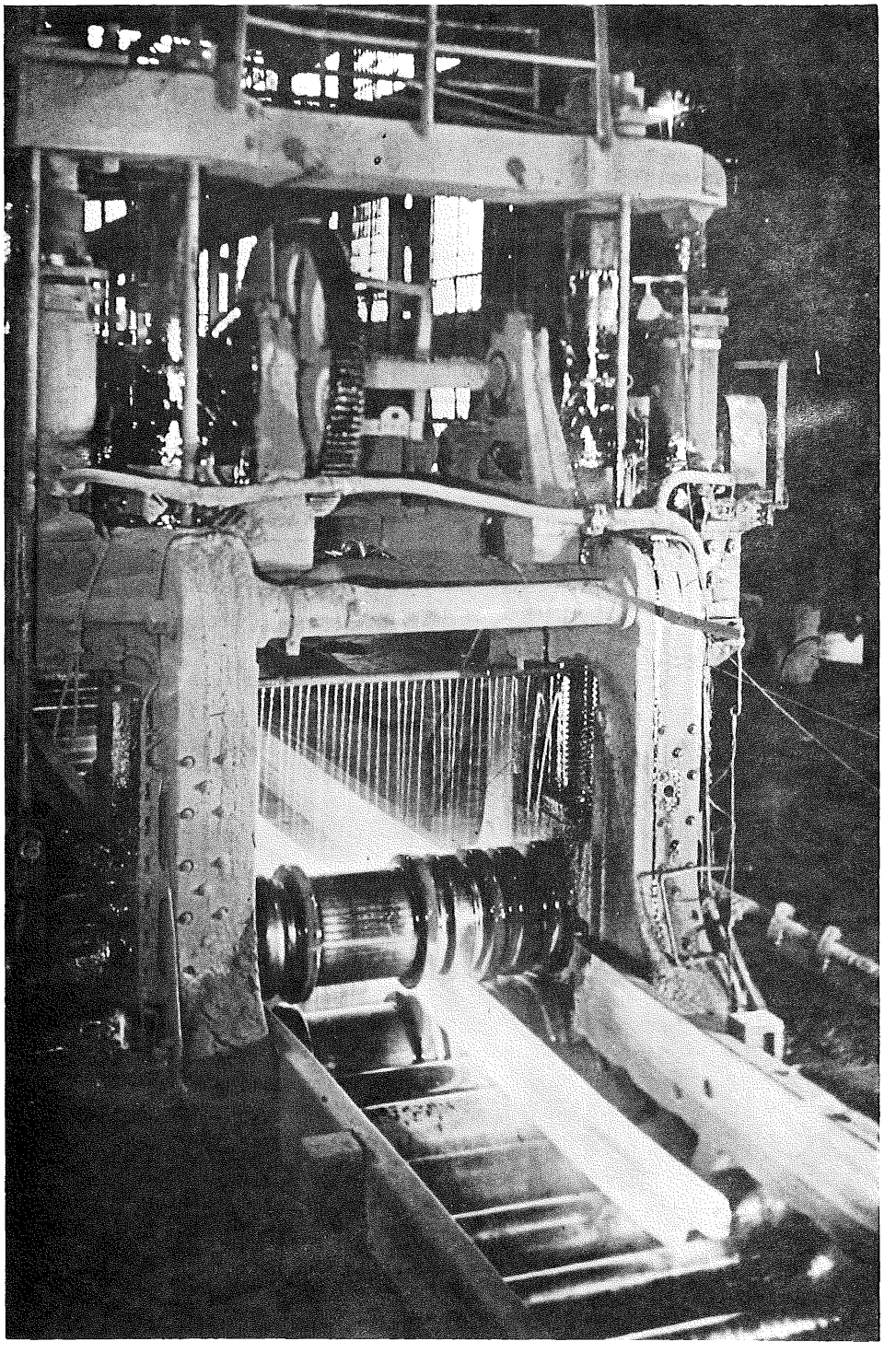

Fig. 2 Rolling of a structural H-shape (Courtesy Bethlehem Steel Corporation)

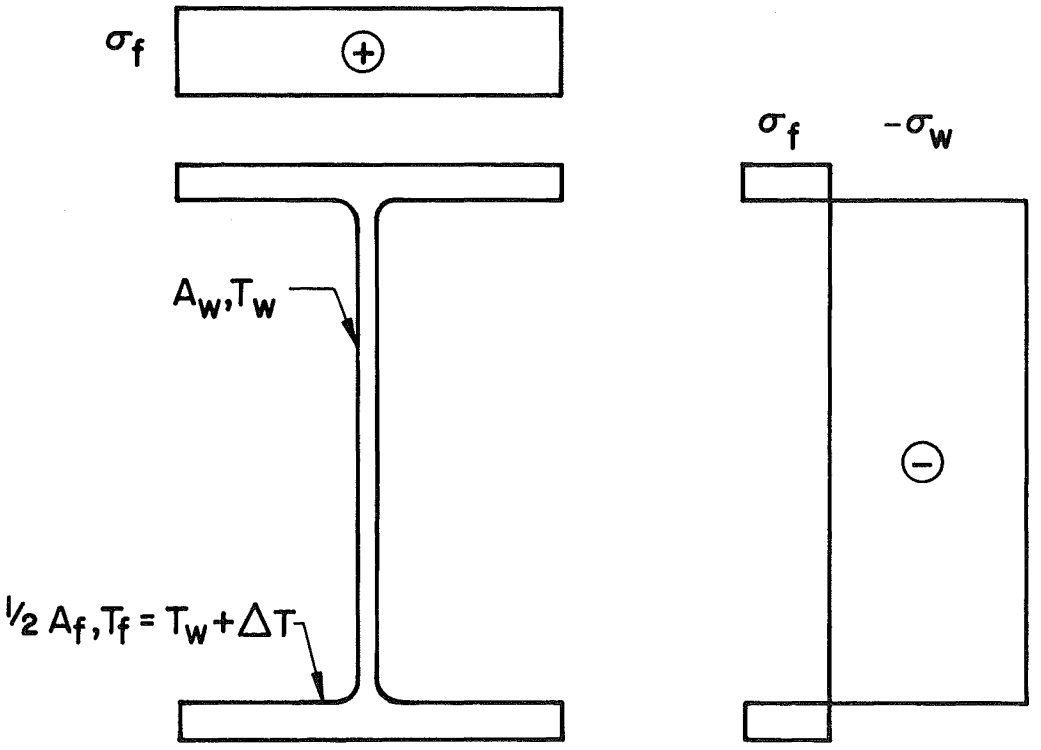

$$\begin{cases} \sigma_f \cdot A_f + \sigma_w \cdot A_w = 0 \\ \sigma_f - \sigma_w = E\,\alpha\,\Delta T \end{cases}$$

Fig. 3 Predicted residual stresses in a hot-rolled H-shape. After Roš[3].

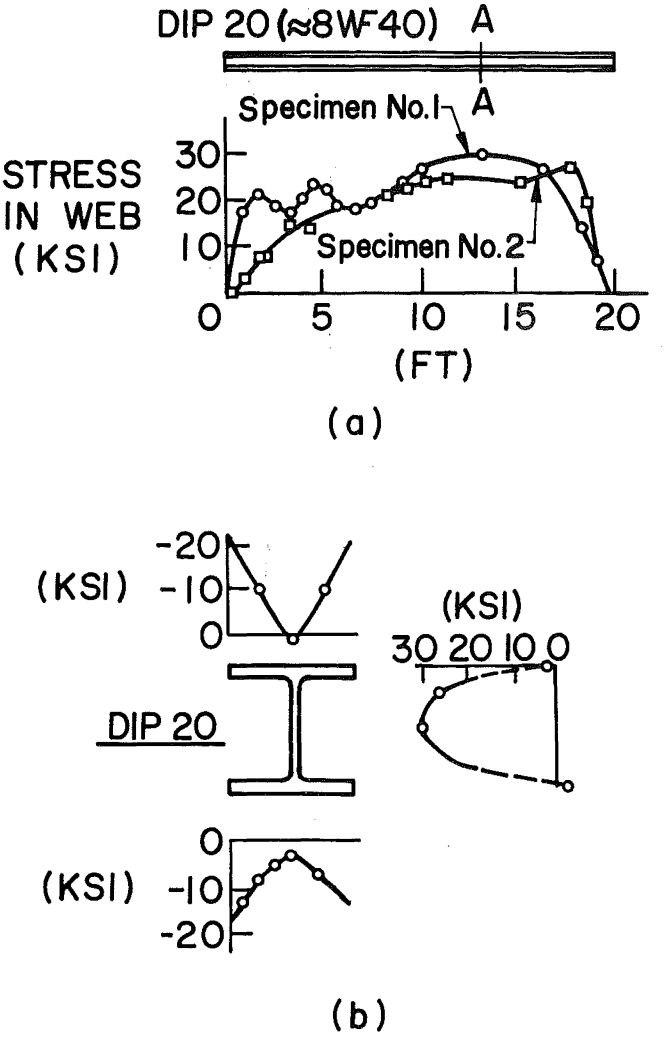

Fig. 4 Measured residual stresses in a hot-rolled H-shape DIP20 (nearest American equivalent 8WF40). After Mathar[4].

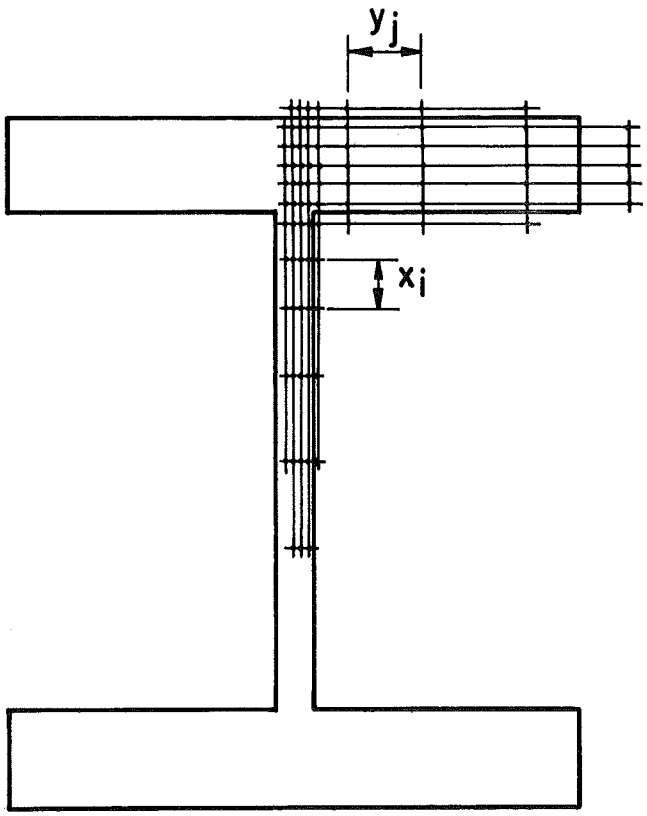

Fig. 5 Subdivision of an H-shape into a mesh for finite-difference calculations

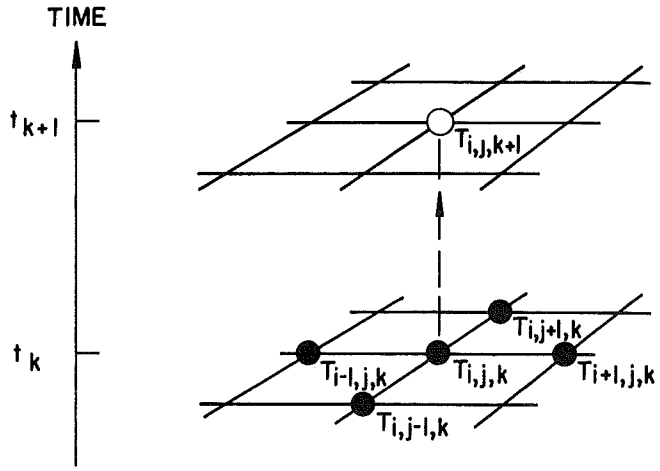

EXPLICIT FINITE-DIFFERENCE METHOD

(a)

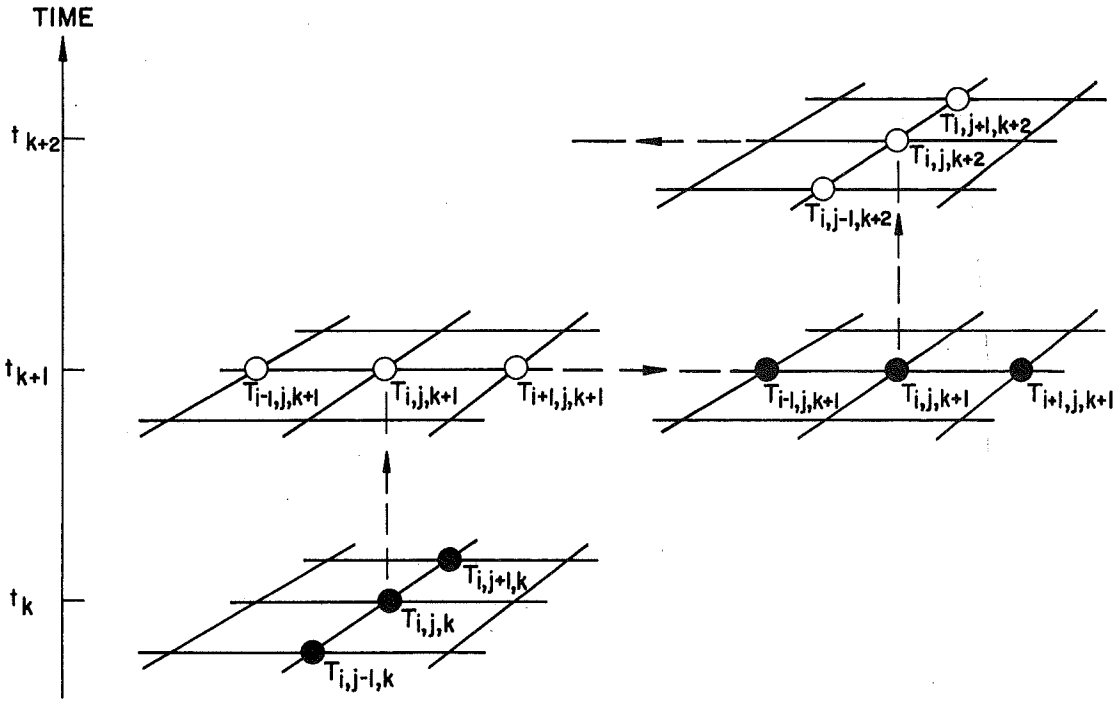

IMPLICIT ALTERNATING DIRECTION (IAD) METHOD

(b)

Fig. 6 Principles of finite-difference methods for the solution of the Fourier Equation

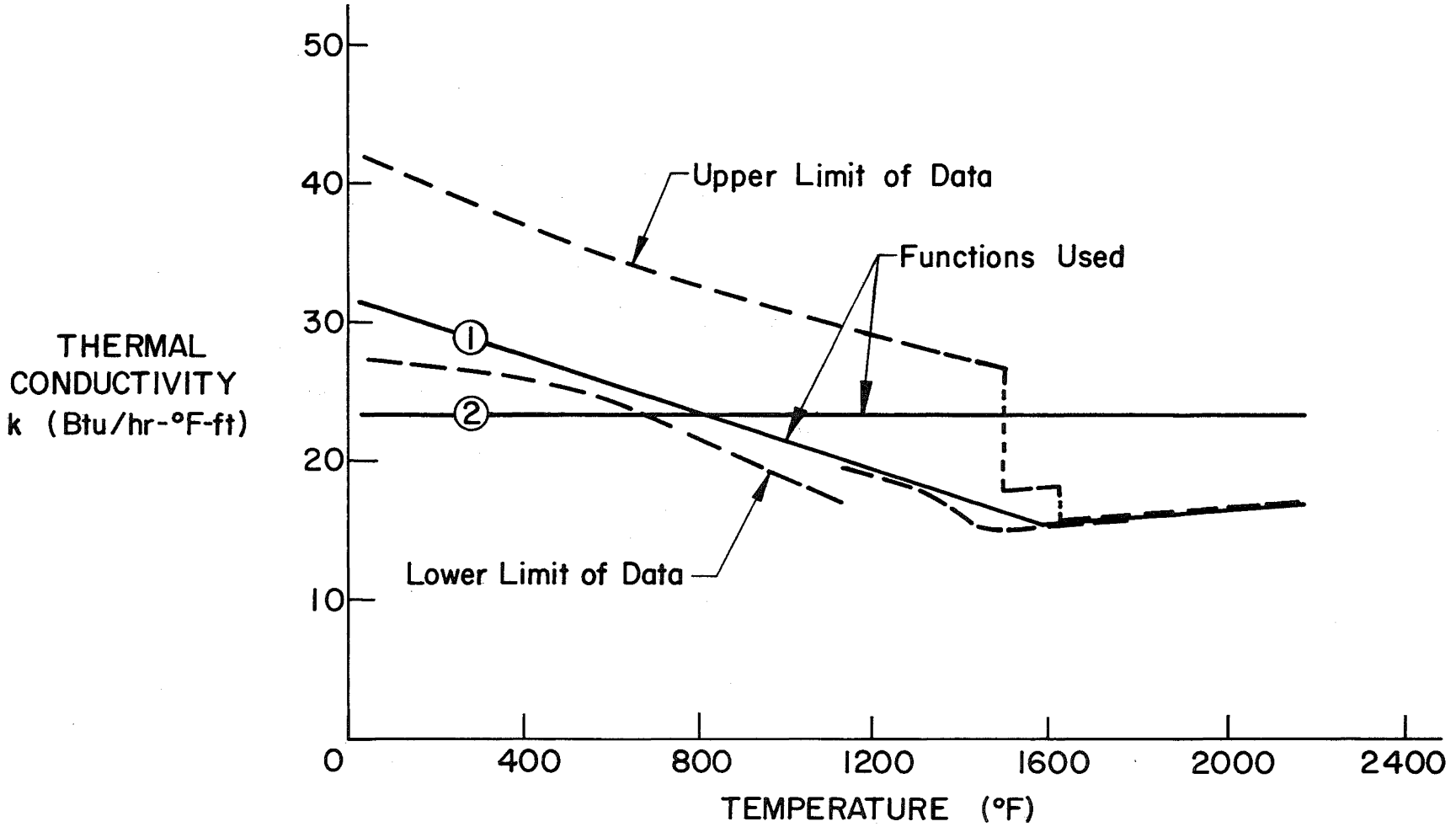

Fig. 7 Thermal conductivity k of carbon steels

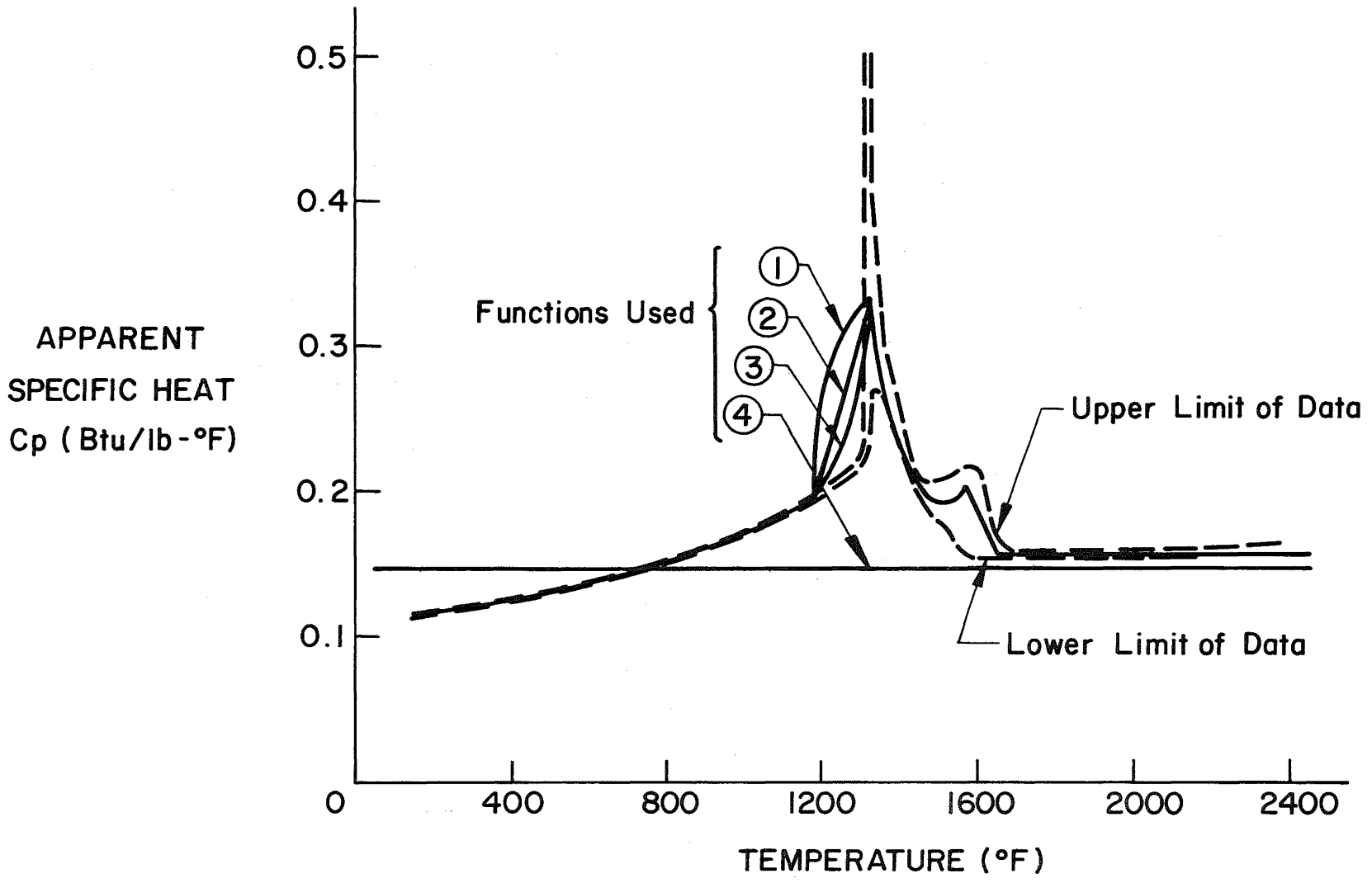

Fig. 8 Specific heat c_p of carbon steels

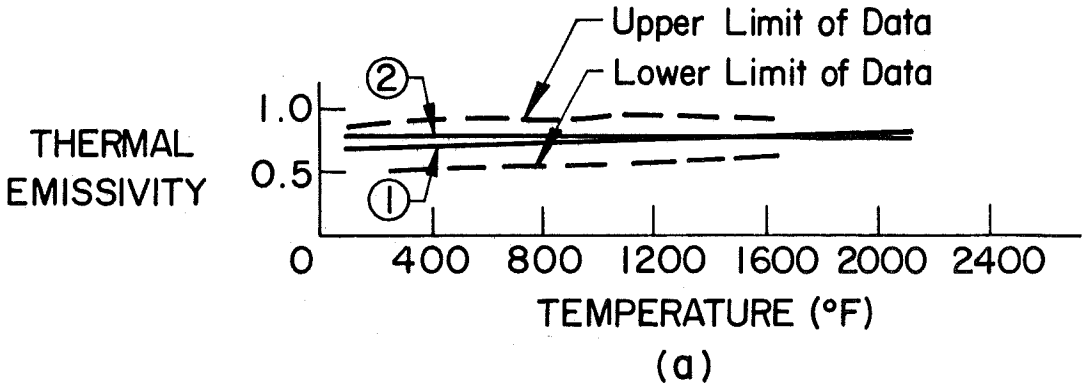

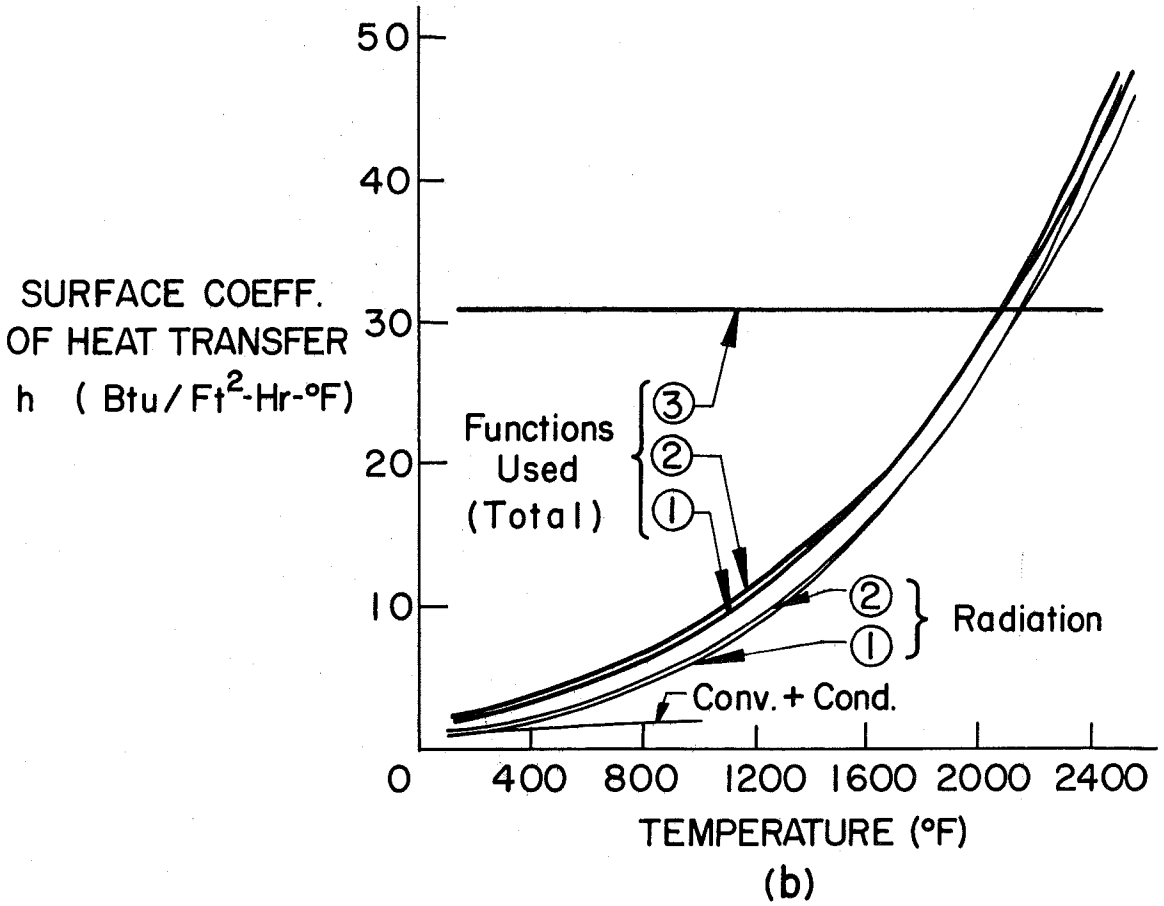

Fig. 9 Surface coefficient of heat transfer h for carbon steels

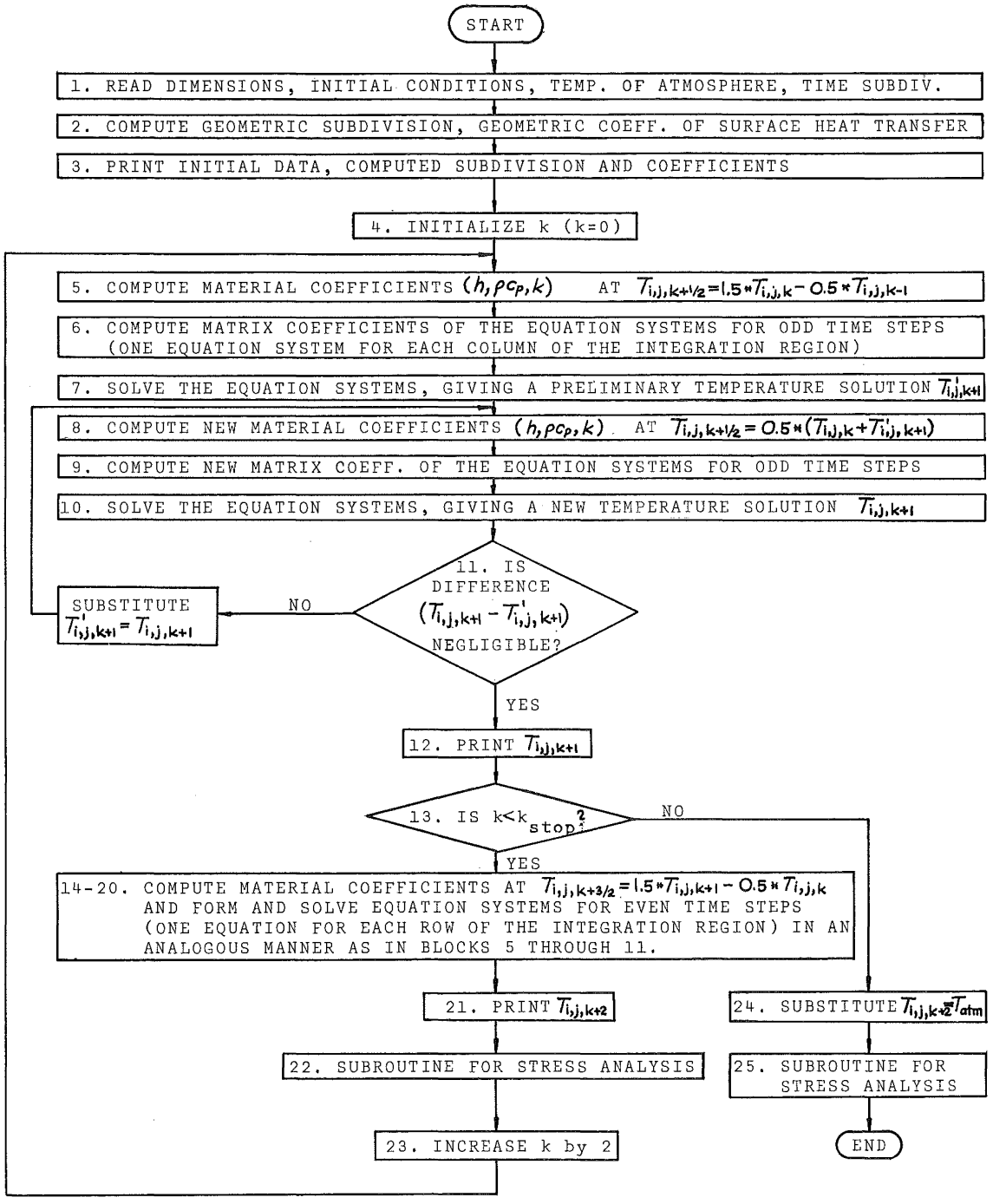

SUBSCRIPTS: i,j DENOTE GEOMETRIC LOCATION OF MESH POINTS,

k DENOTES ORDER OF TIME INTERVAL

Fig. 10 Short flow diagram of the computer program for temperature analysis

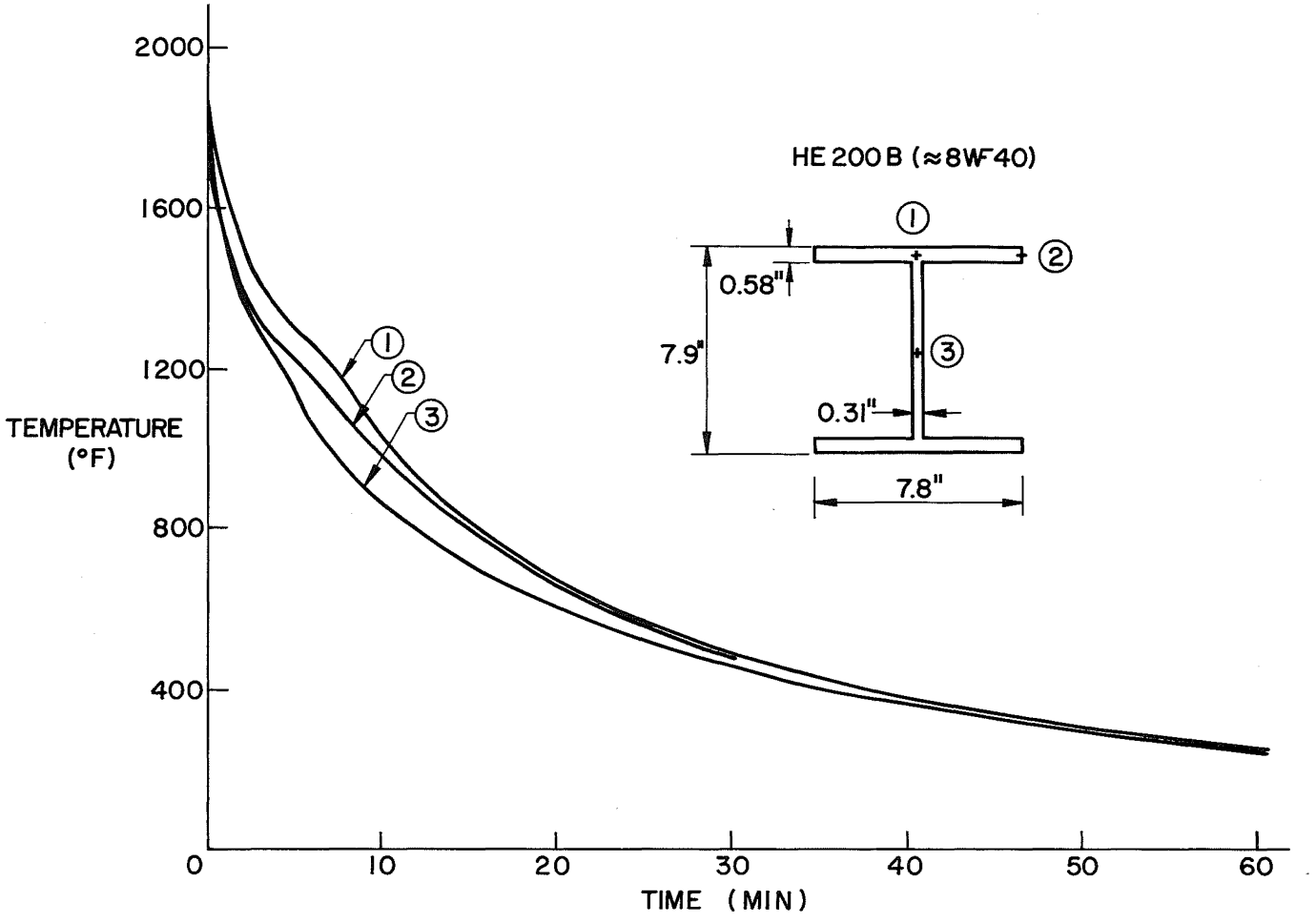

Fig. 11 Computed cooling curves for a European shape HE 200 B. Initial temperature 1830°F, uniform through the cross section.

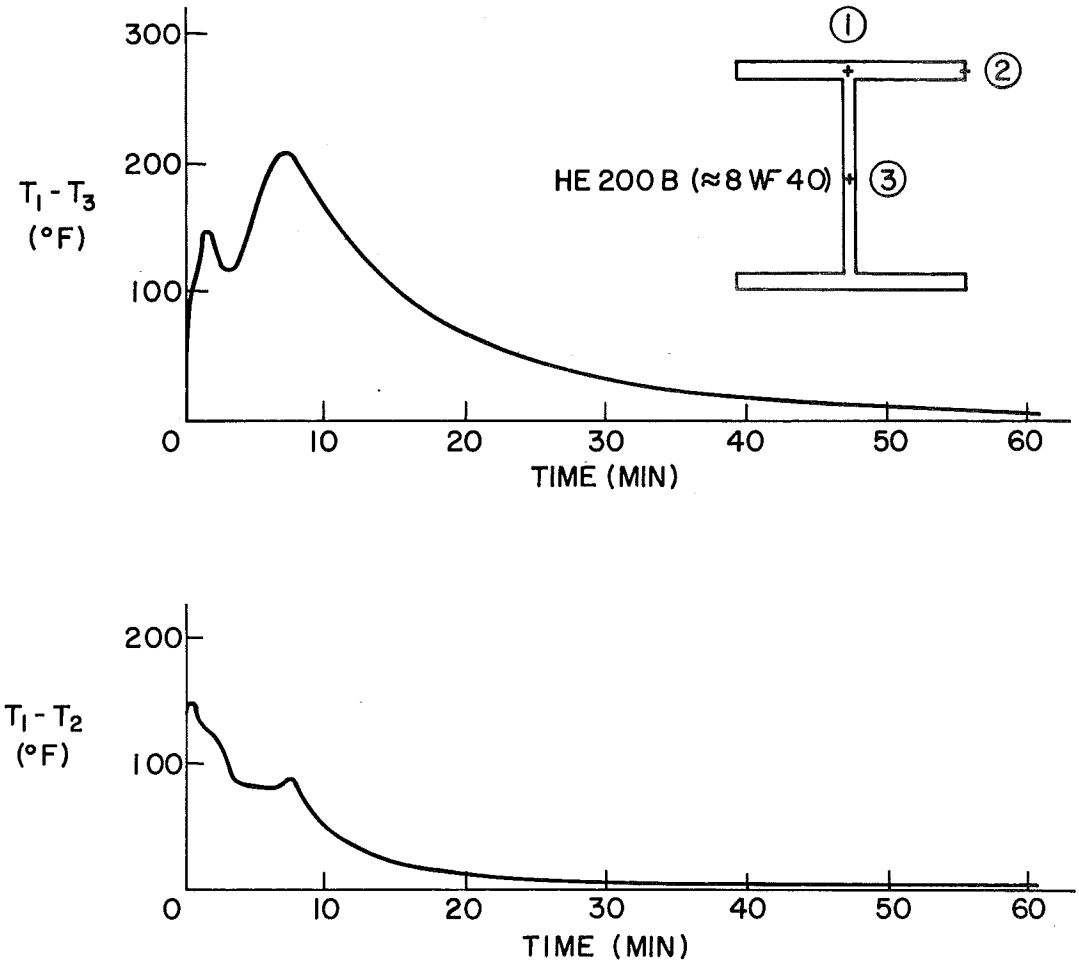

Fig. 12 Temperature differences as a function of cooling time. Same computations as in Fig. 11.

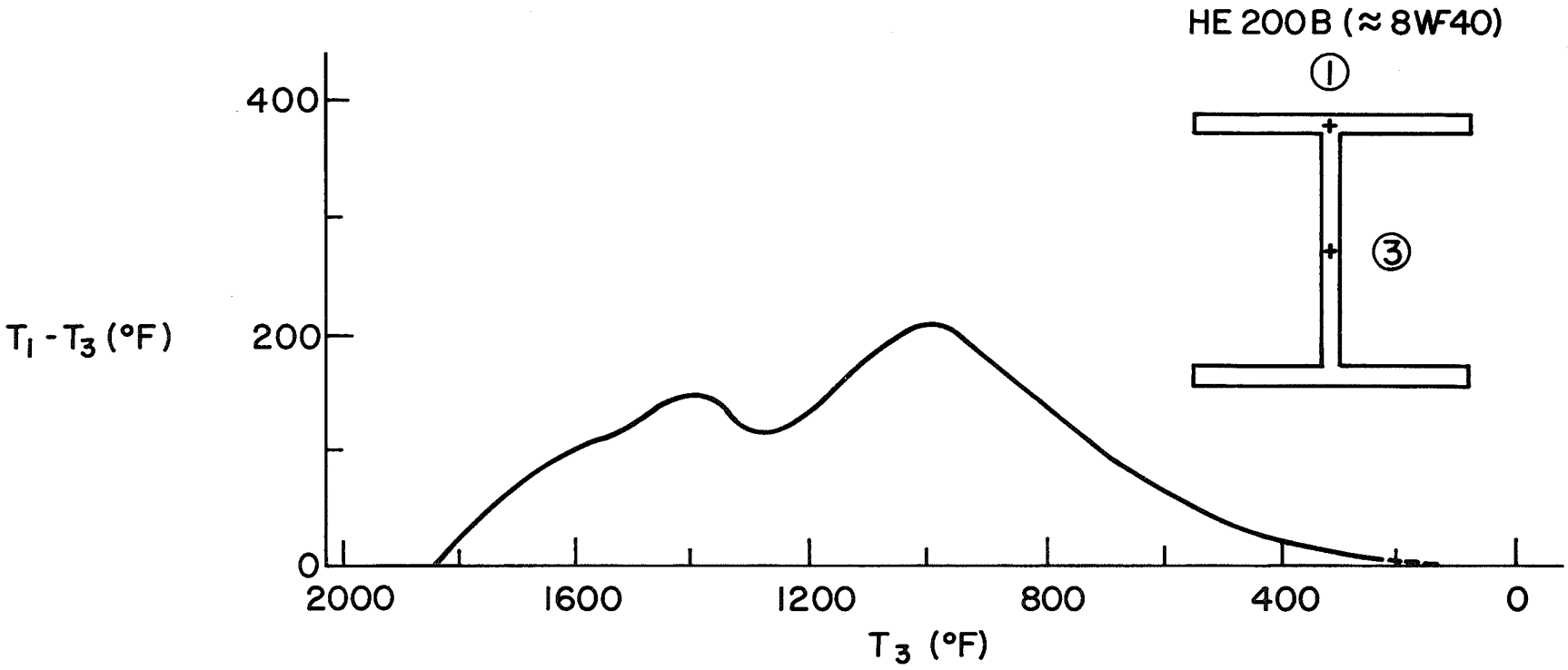

Fig. 13 Temperature difference as a function of temperature in the web center. Redrawn from the upper diagram of Fig. 12.

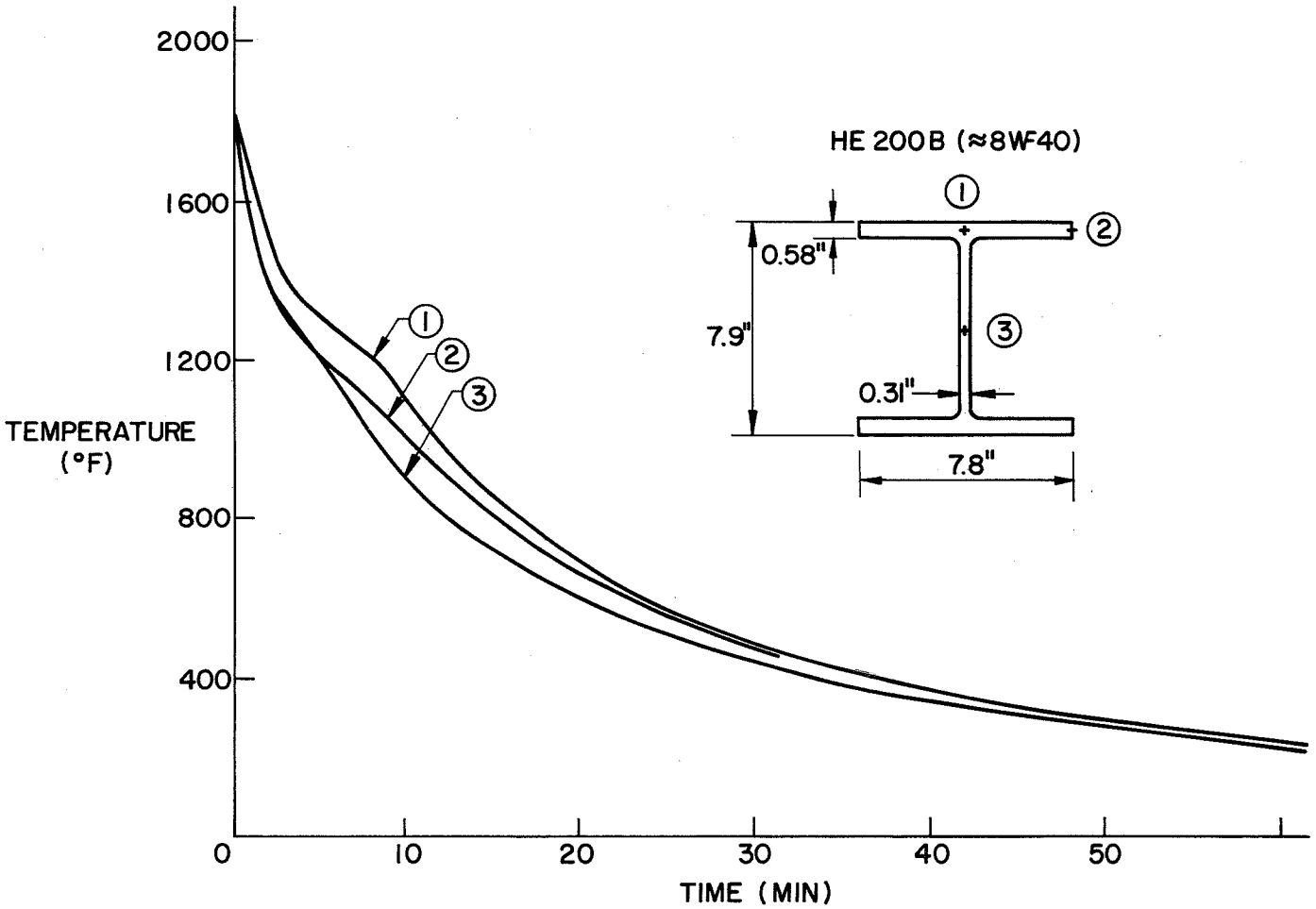

Fig. 14 Experimental cooling curves for the HE 200 B shape. Initial temperature 1830°F, uniform through the cross section.

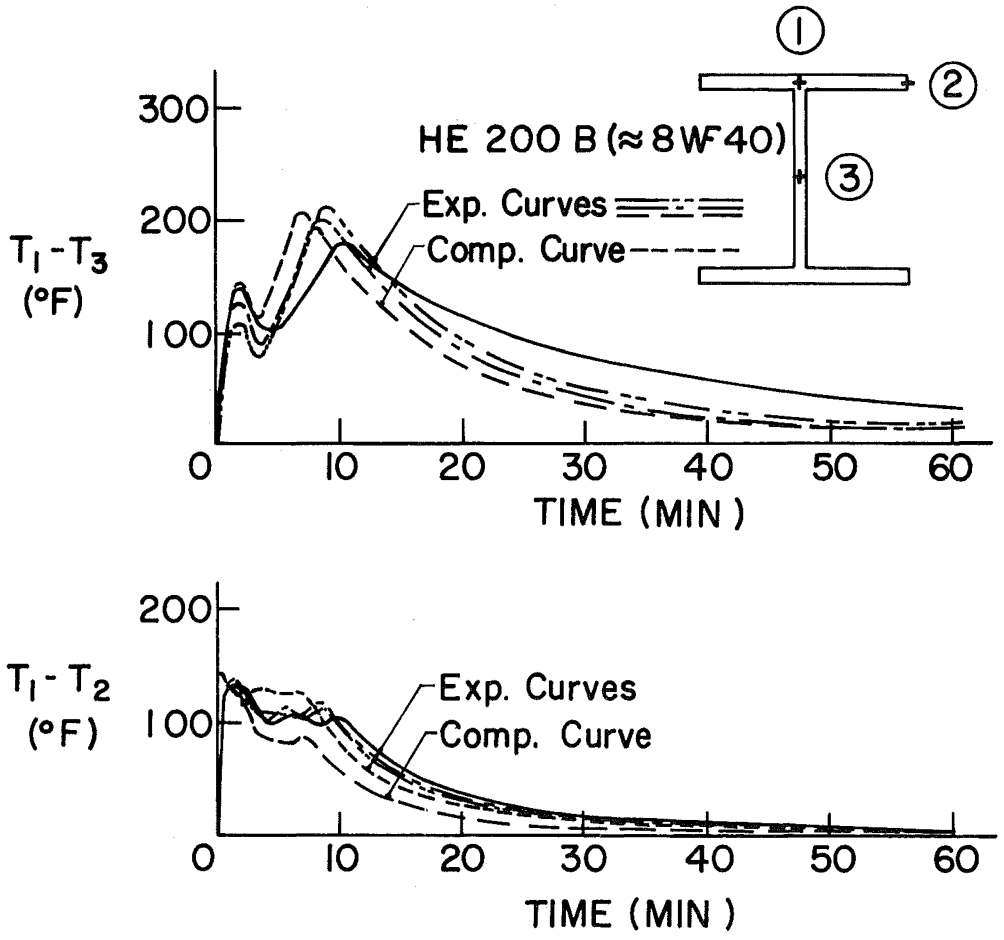

Fig. 15 Temperature differences as a function of cooling time from four repeated tests, one of which is the test shown in Fig. 14

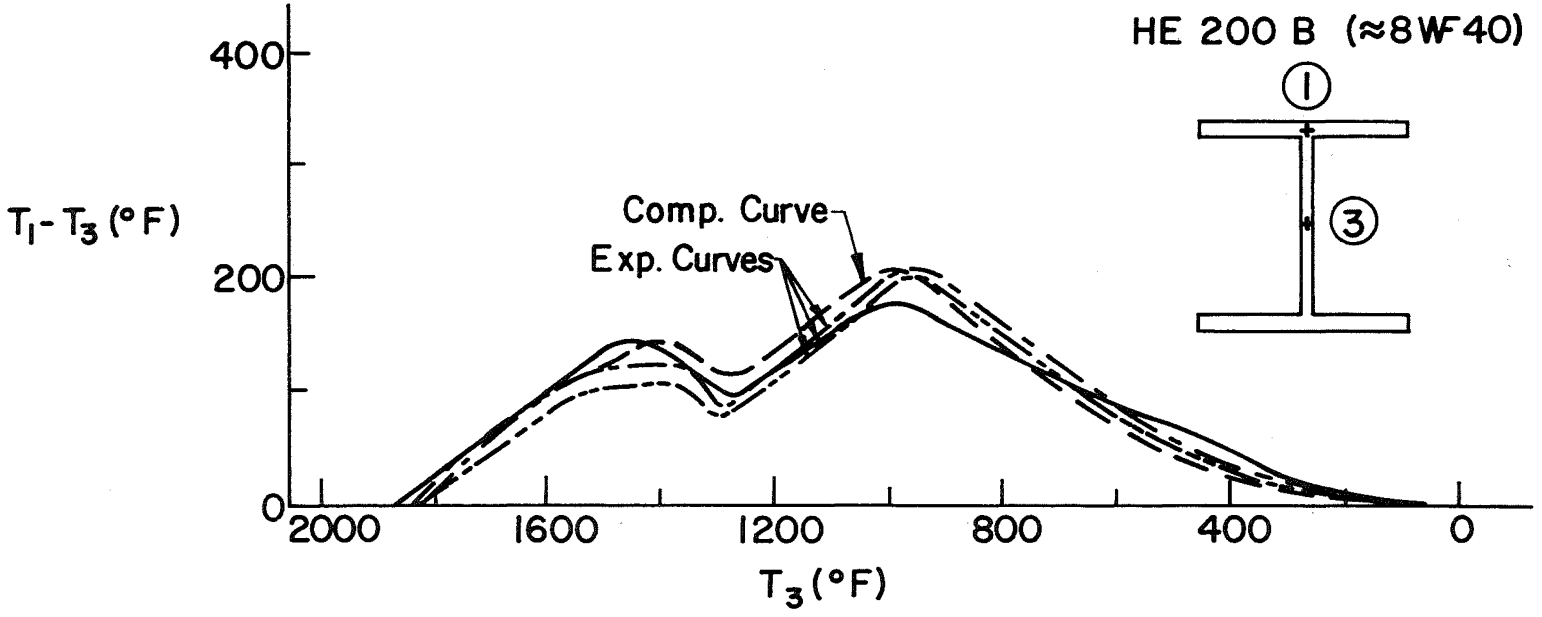

Fig. 16 Measured temperature difference between flange-web junction and web center as a function of temperature in the web center. Redrawn from the upper diagram of Fig. 15.

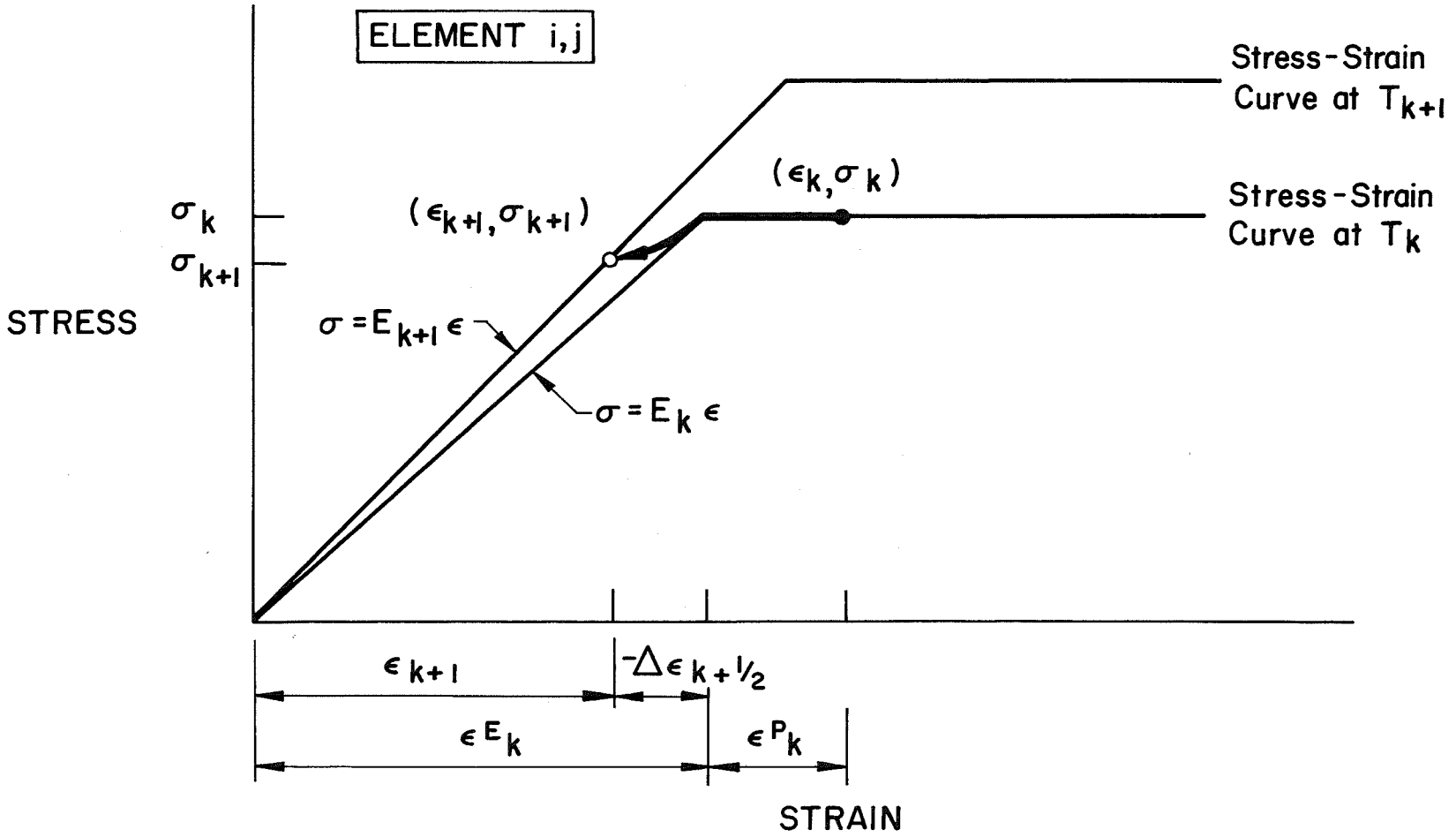

Fig. 17 Procedure for calculation of thermal stresses in an element (i,j) by a finite-difference method, for "unloading" ($\Delta\epsilon_{k+1}/\epsilon_k<0$), and when $\epsilon_k>\epsilon_{y,k}$

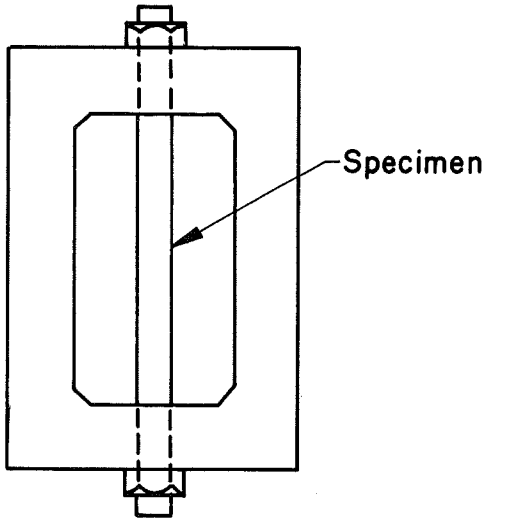

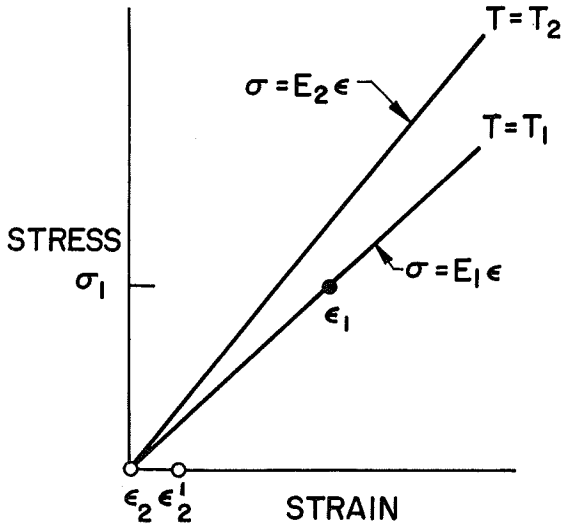

PROCEDURE

1. The system is maintained at a constant elevated temperature T, and the specimen is loaded to a stress σ_1.
2. Allow the system to cool to $T_2 < T_1$, then remove the load on the specimen.

Calculate the remaining elastic strain considering the conditions before and after moment 2.

A. Adding Stresses

Before: $\sigma = \sigma_1$; $\epsilon_1 = \frac{\sigma_1}{E_1}$

After : $\sigma = 0$; $\epsilon'_2 = \frac{\sigma_1}{E_1} - \frac{\sigma_1}{E_2} > 0$

B. Adding Strains

Before: $\sigma = \sigma_1$; $\epsilon_1 = \frac{\sigma_1}{E_1}$

After : $\sigma = 0 = E_2 \left(\frac{\sigma_1}{E_1} - \Delta\epsilon \right)$

$$\epsilon_2 = \frac{\sigma_1}{E} - \Delta\epsilon = 0$$

Fig. 18a Comparison between principle using a summation of incremental strains and principle using a summation of incremental stresses for a simplified example

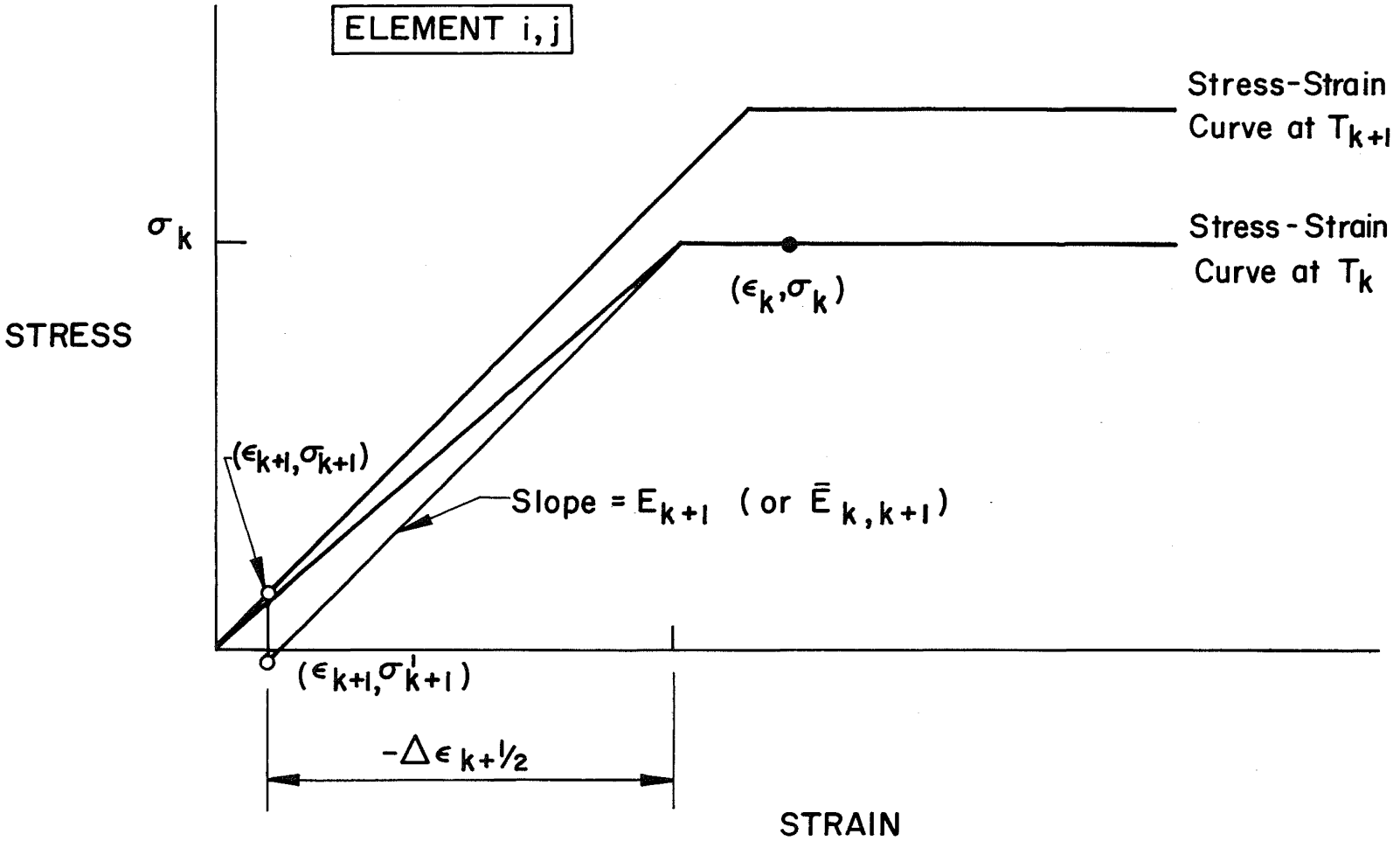

Fig. 18b Comparison when strain increments are large

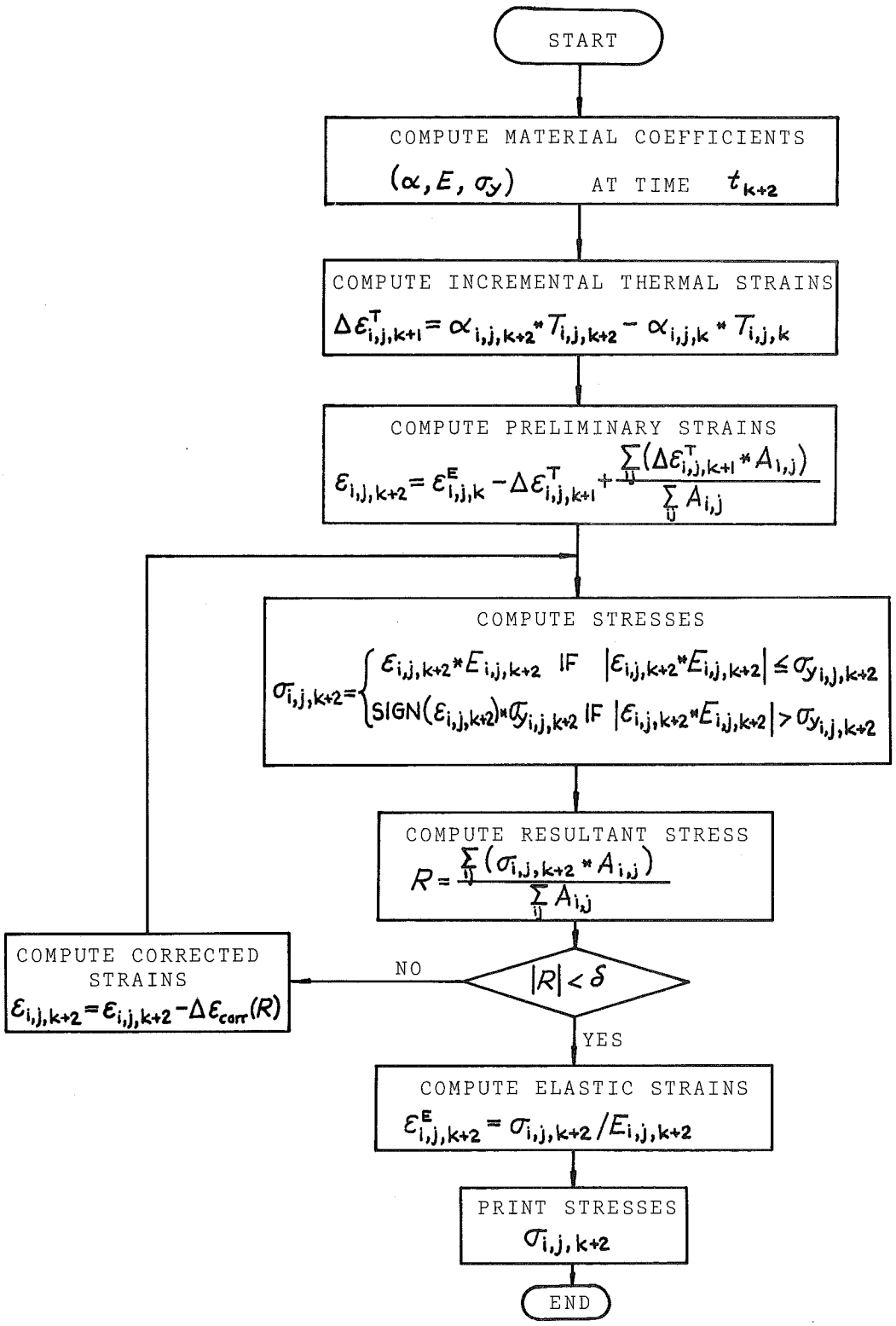

Fig. 19 Short flow diagram of the subroutine for thermal stress analysis

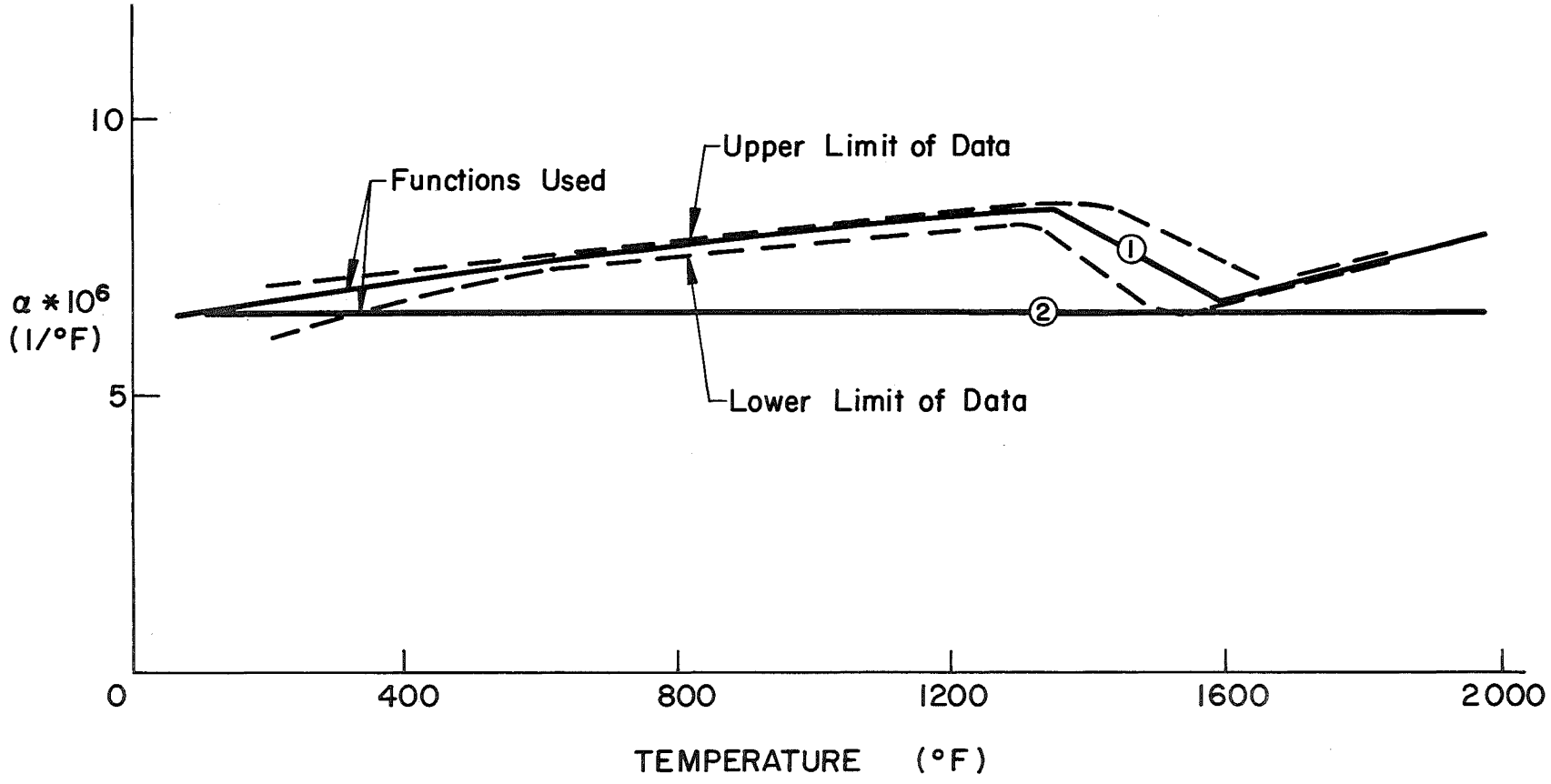

Fig. 20 Coefficient of linear expansion α for carbon stress

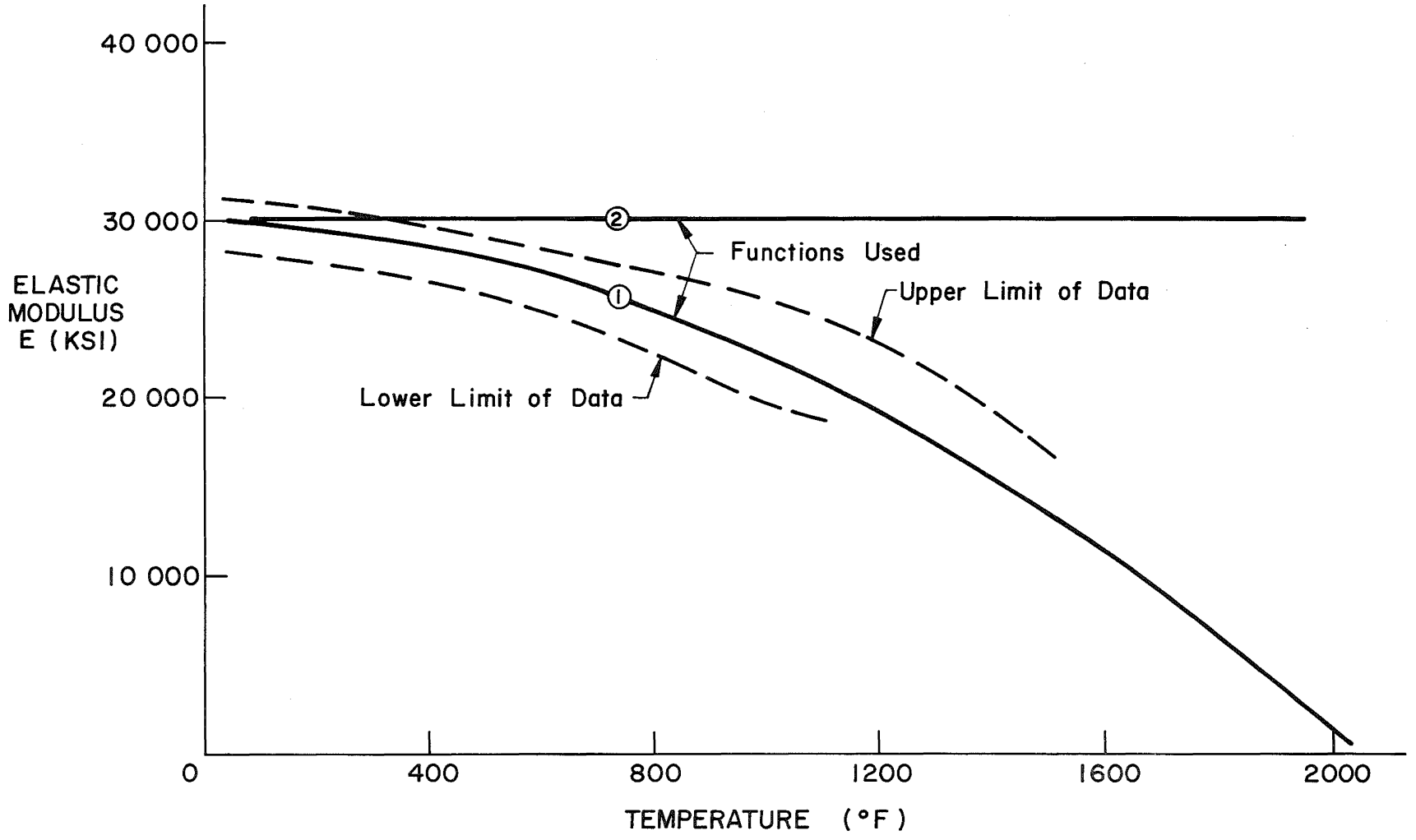

Fig. 21 Modulus of elasticity E for carbon steels

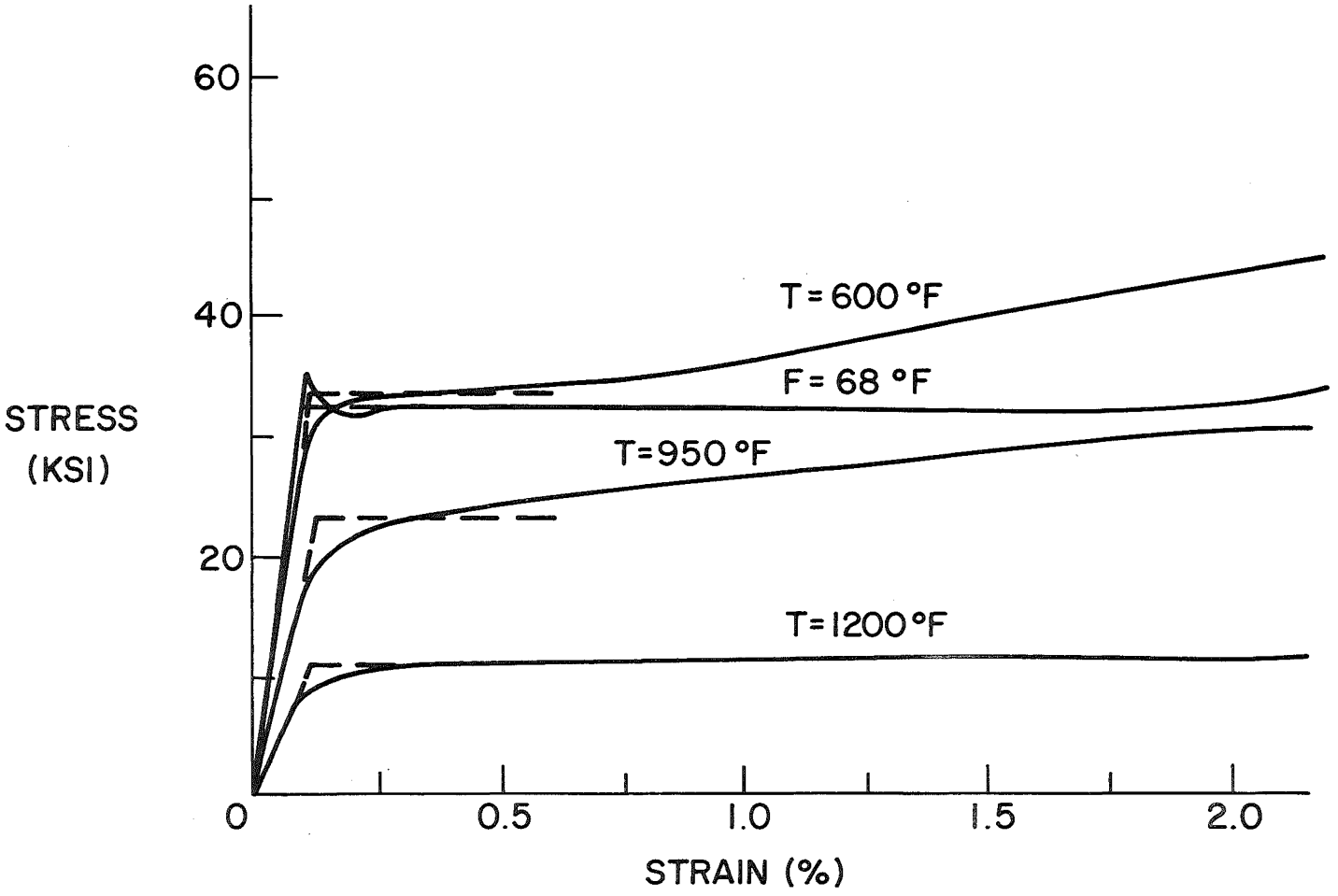

Fig. 22 Schematic comparison between stress-strain curves and the corresponding elastic-perfectly-plastic relations with yield stress level equal to $\sigma_{0.2}$

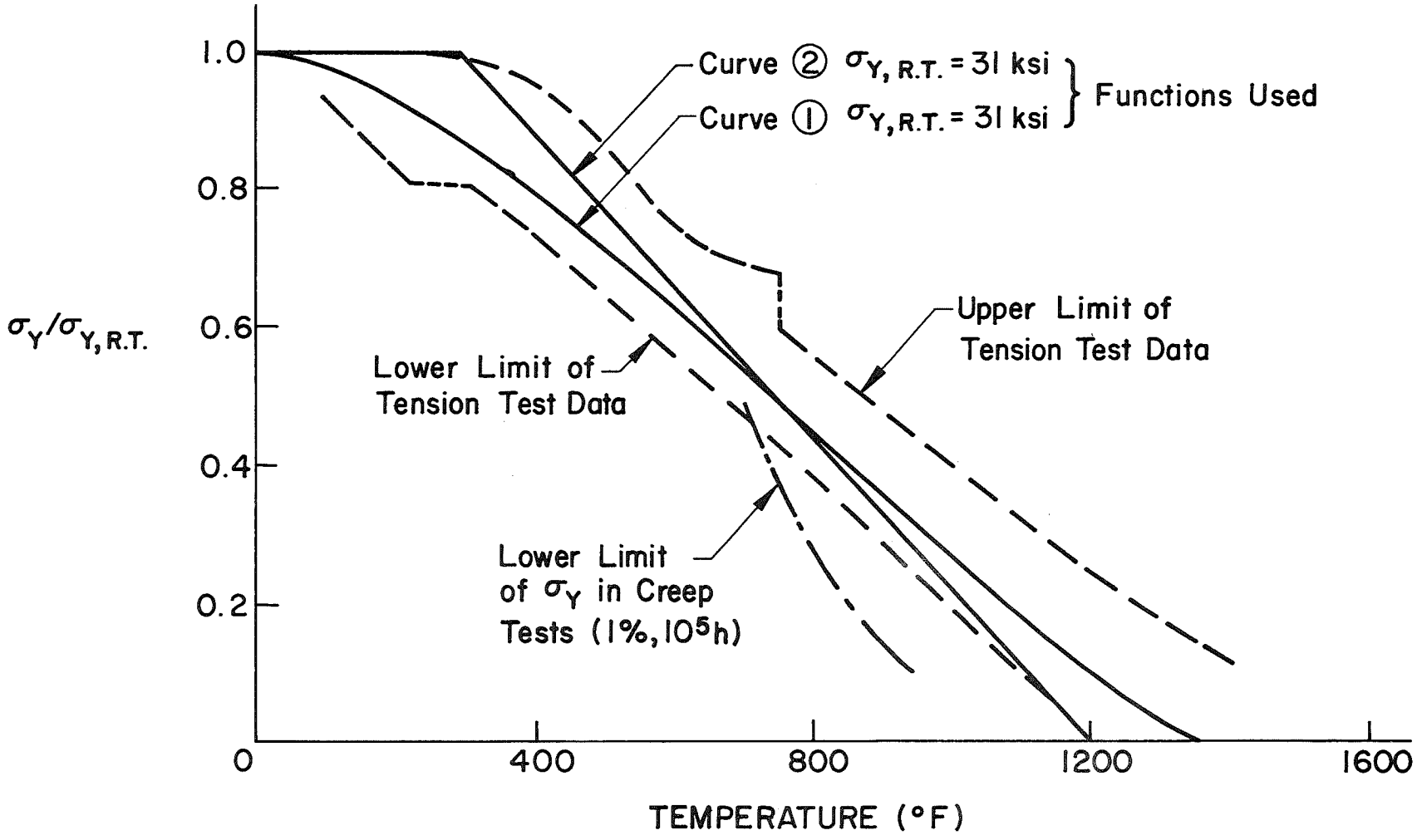

Fig. 23 Yield stress σ_y for carbon steels

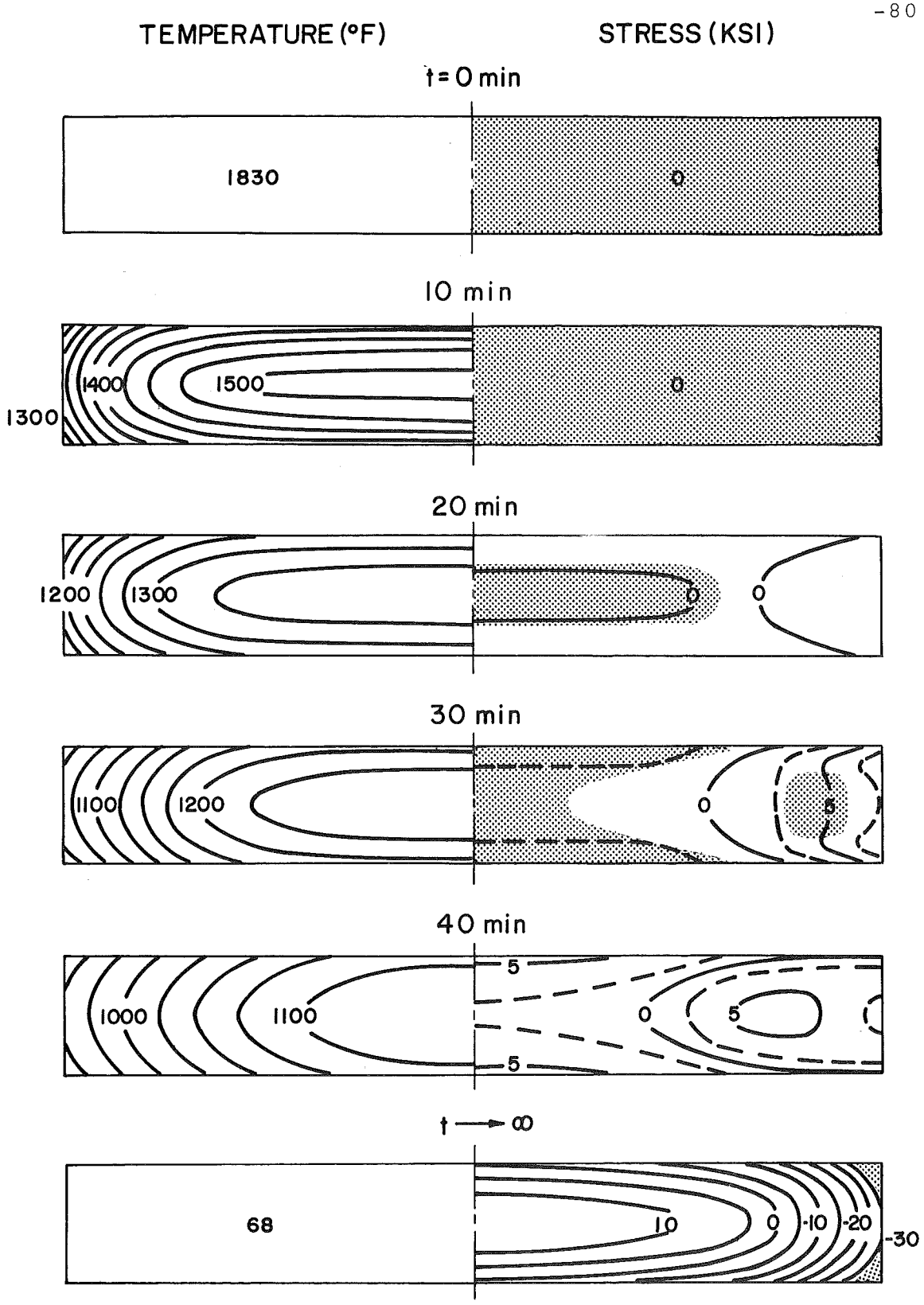

Fig. 24 Computed temperature and thermal stress behavior during cooling of a universal-mill plate 24"x3½"

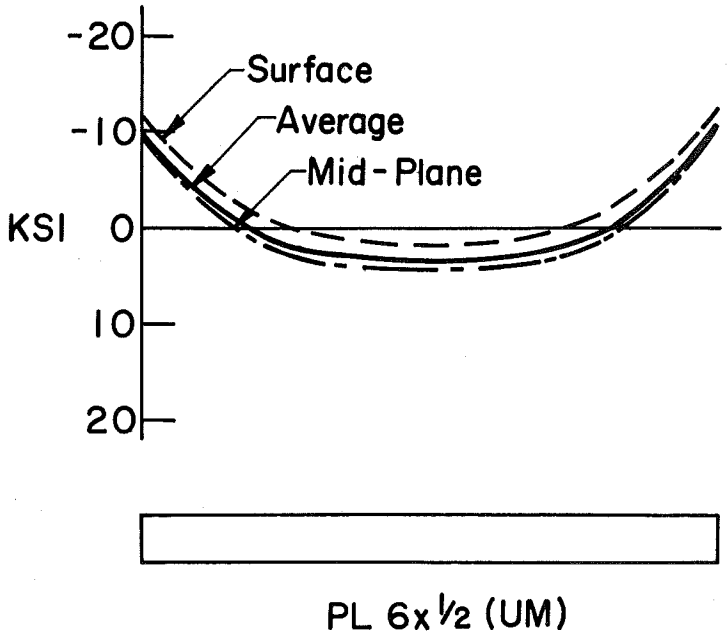

Fig. 25 Computed residual stresses in a universal-mill plate 6"x½"

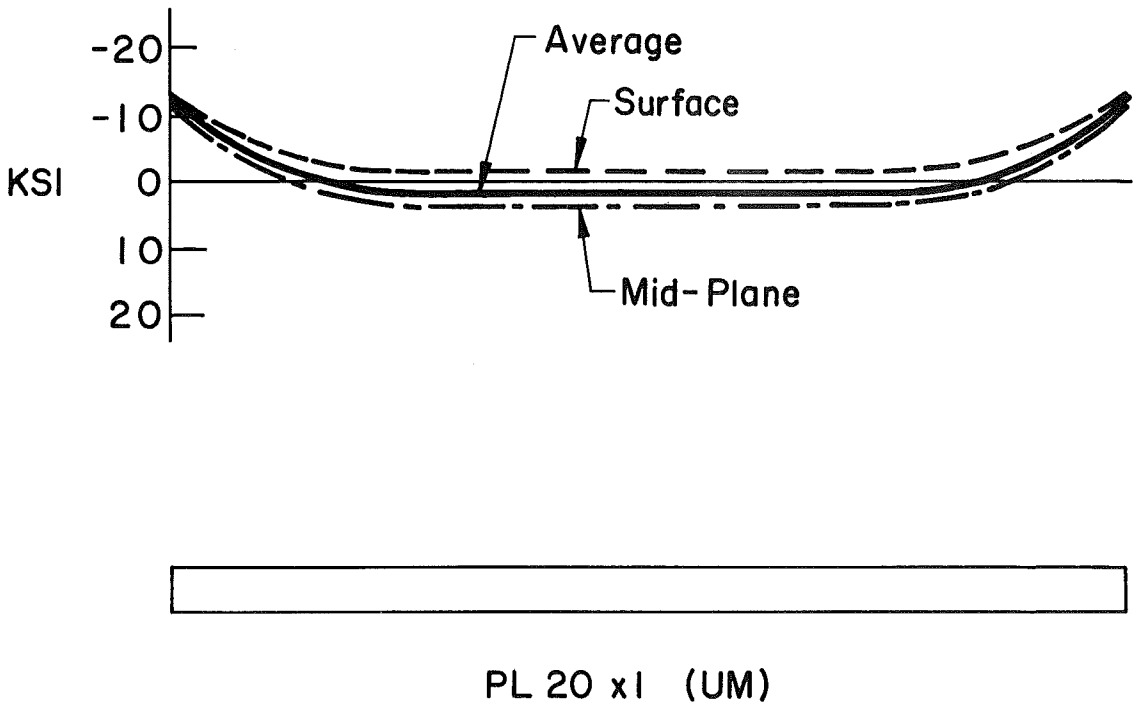

Fig. 26 Computed residual stresses in a universal-mill plate 20"x1"

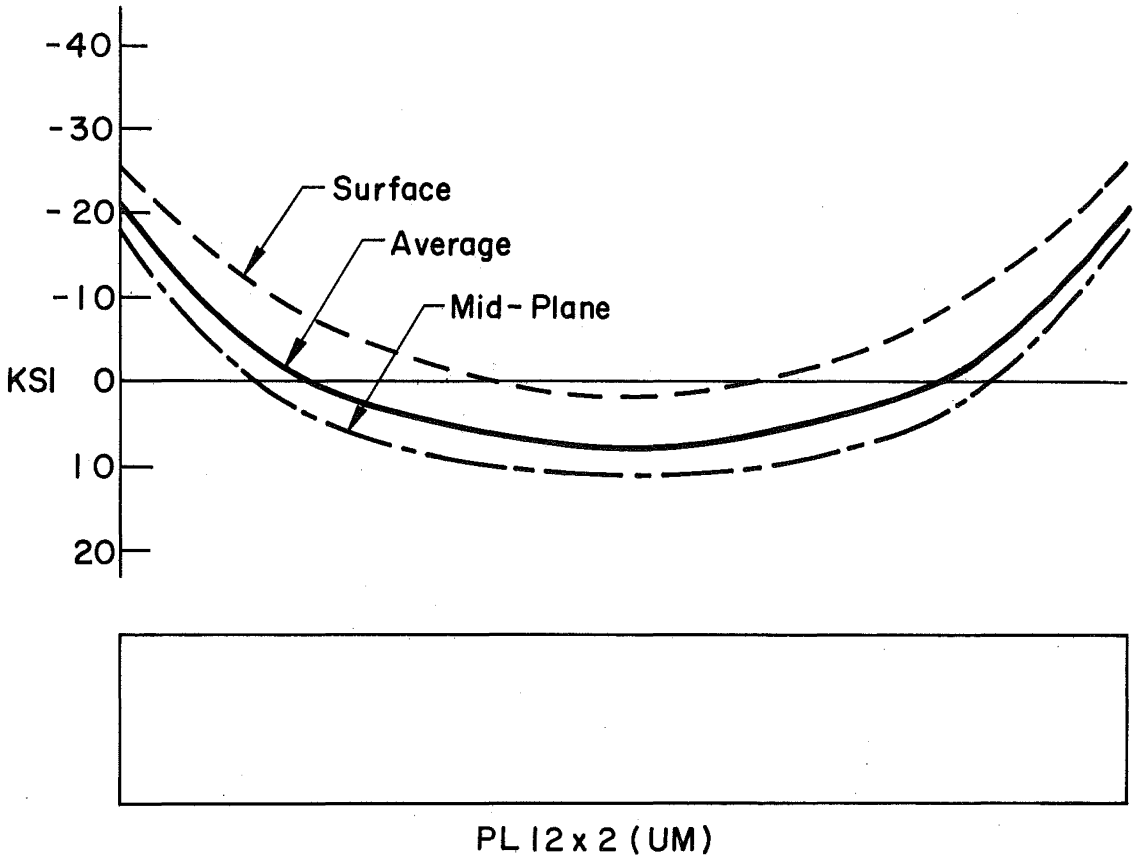

Fig. 27 Computed residual stresses in a universal-mill plate 12"x2"

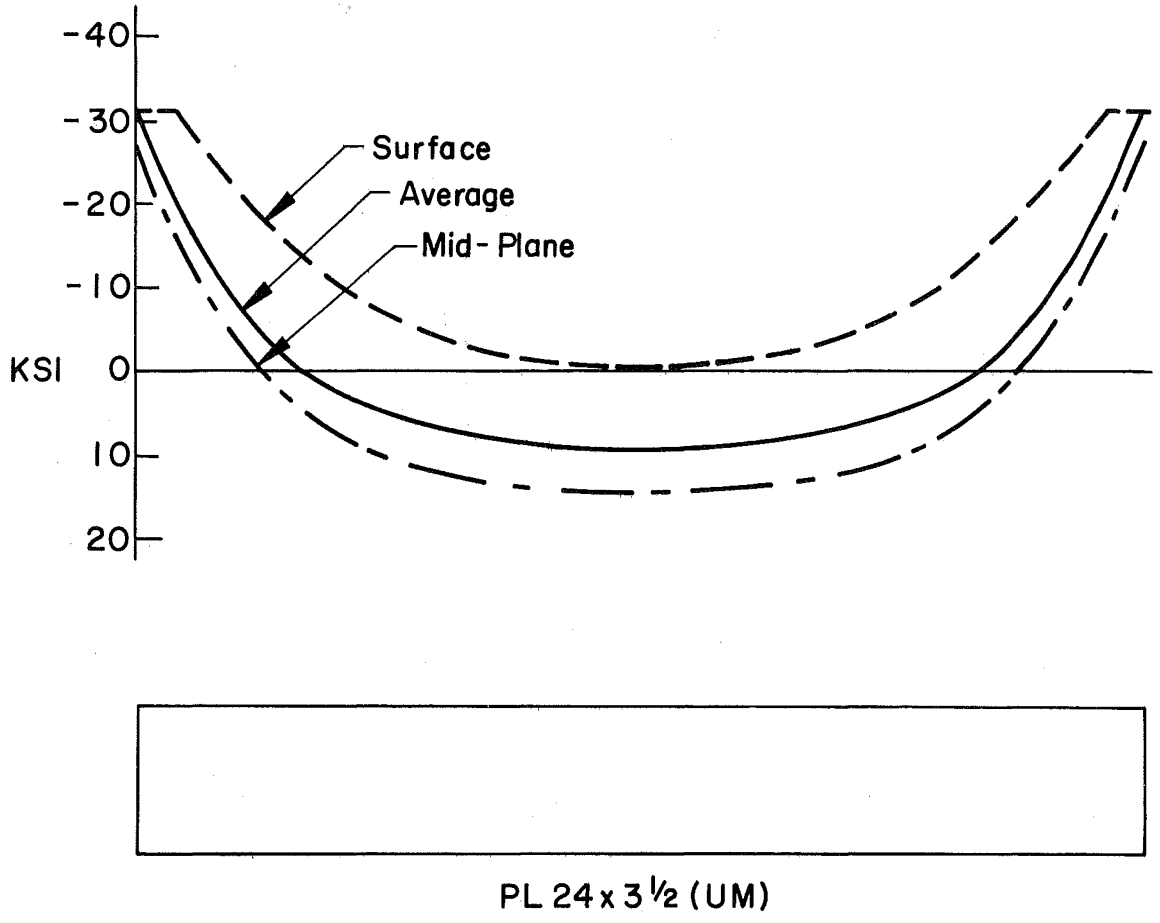

Fig. 28 Computed residual stresses in a universal-mill plate 24"x3½"

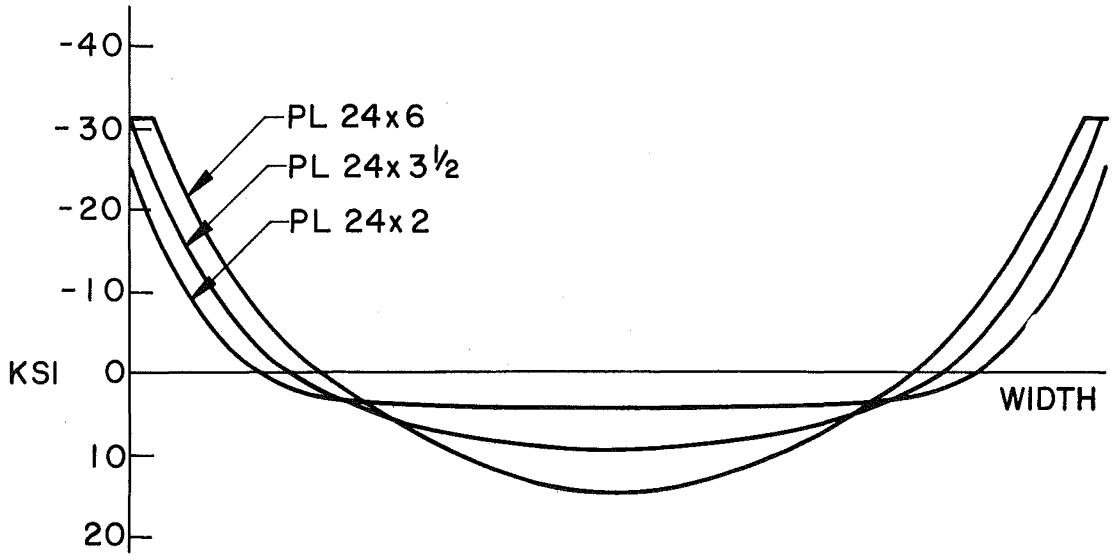

Fig. 29 Average residual stresses across thickness for three universal-mill plates with different thickness

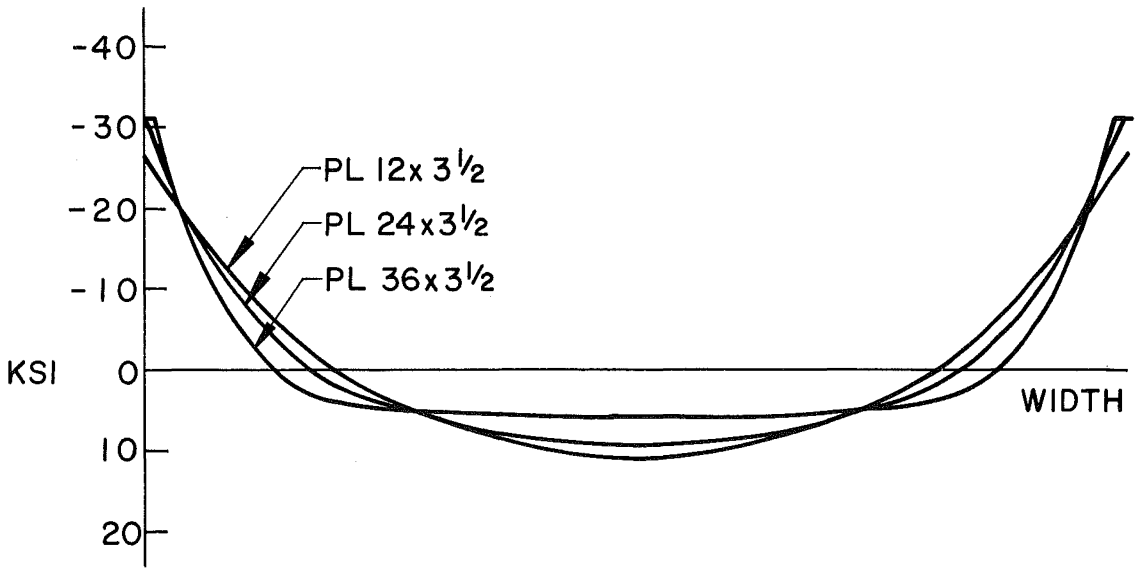

Fig. 30 Average residual stresses across thickness for four universal-mill plates with different width

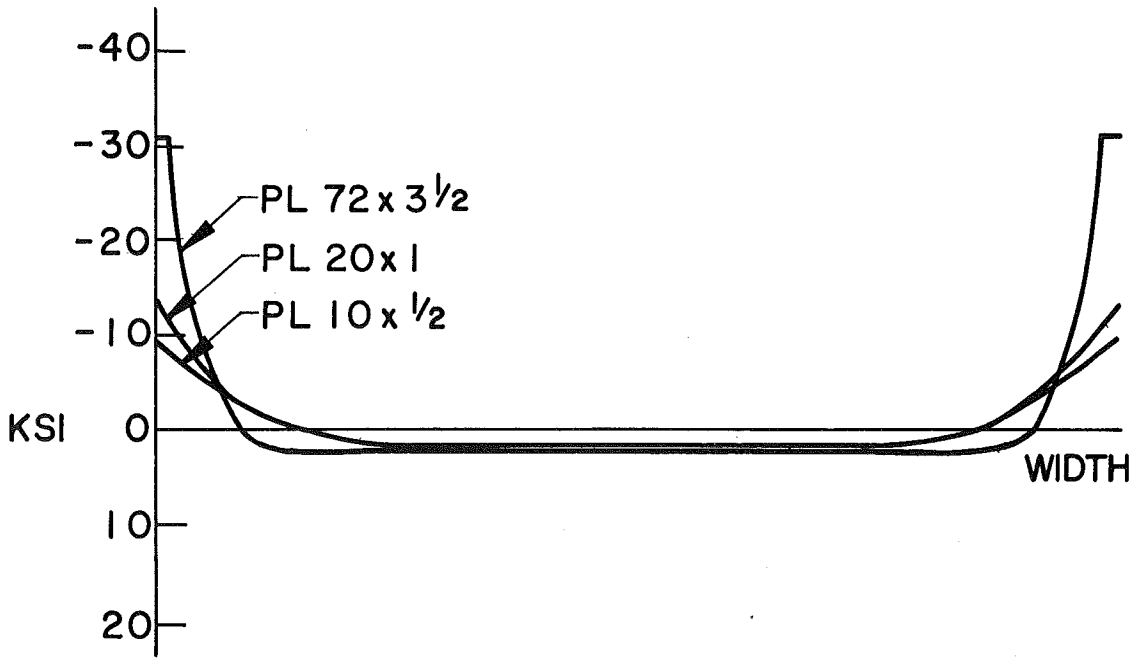

Fig. 31 Average residual stresses across thickness for three plates with approx. same width/thickness ratio

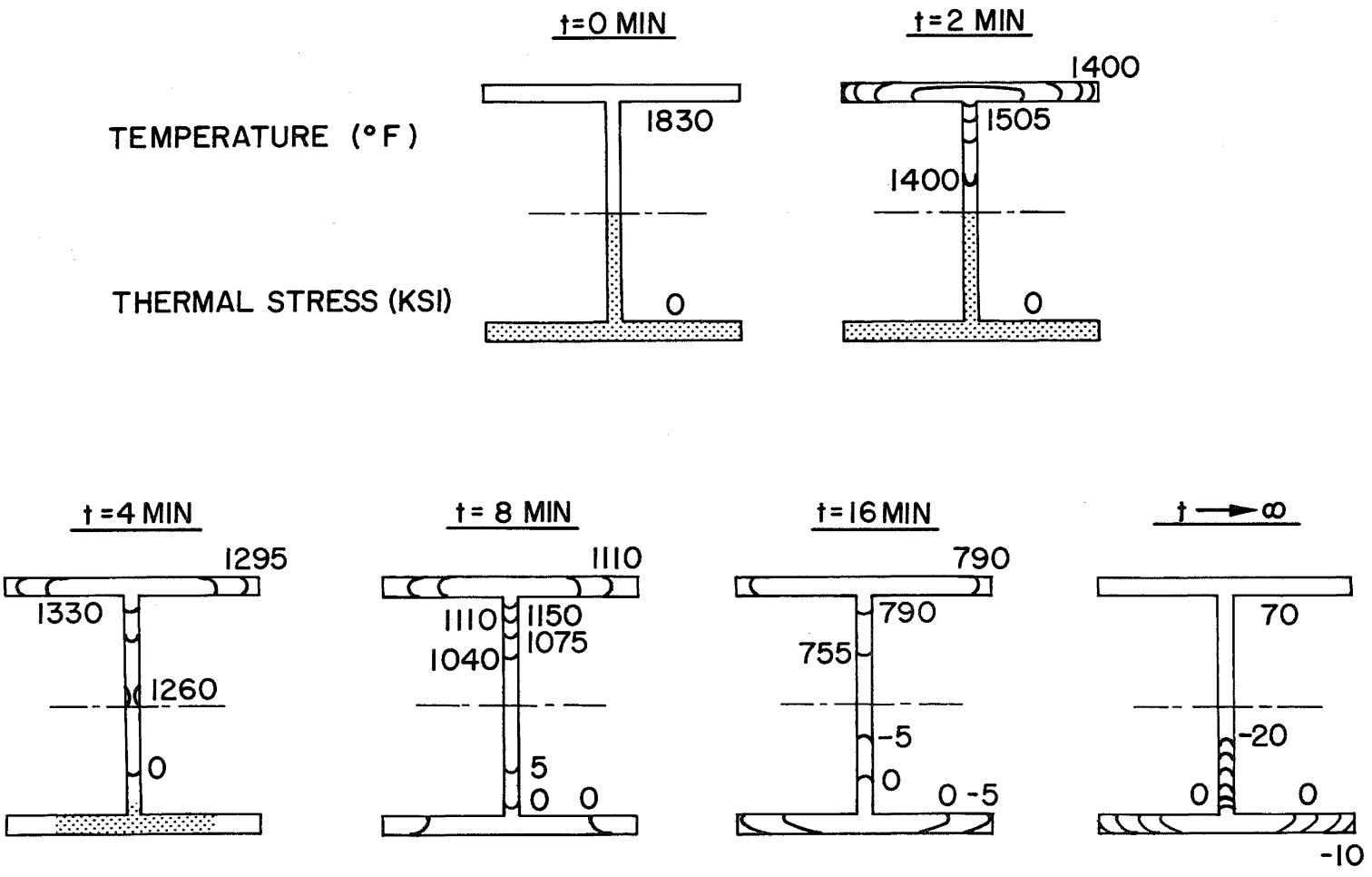

Fig. 32 Computed temperature and thermal stress behavior during cooling of an HE 200 B shape

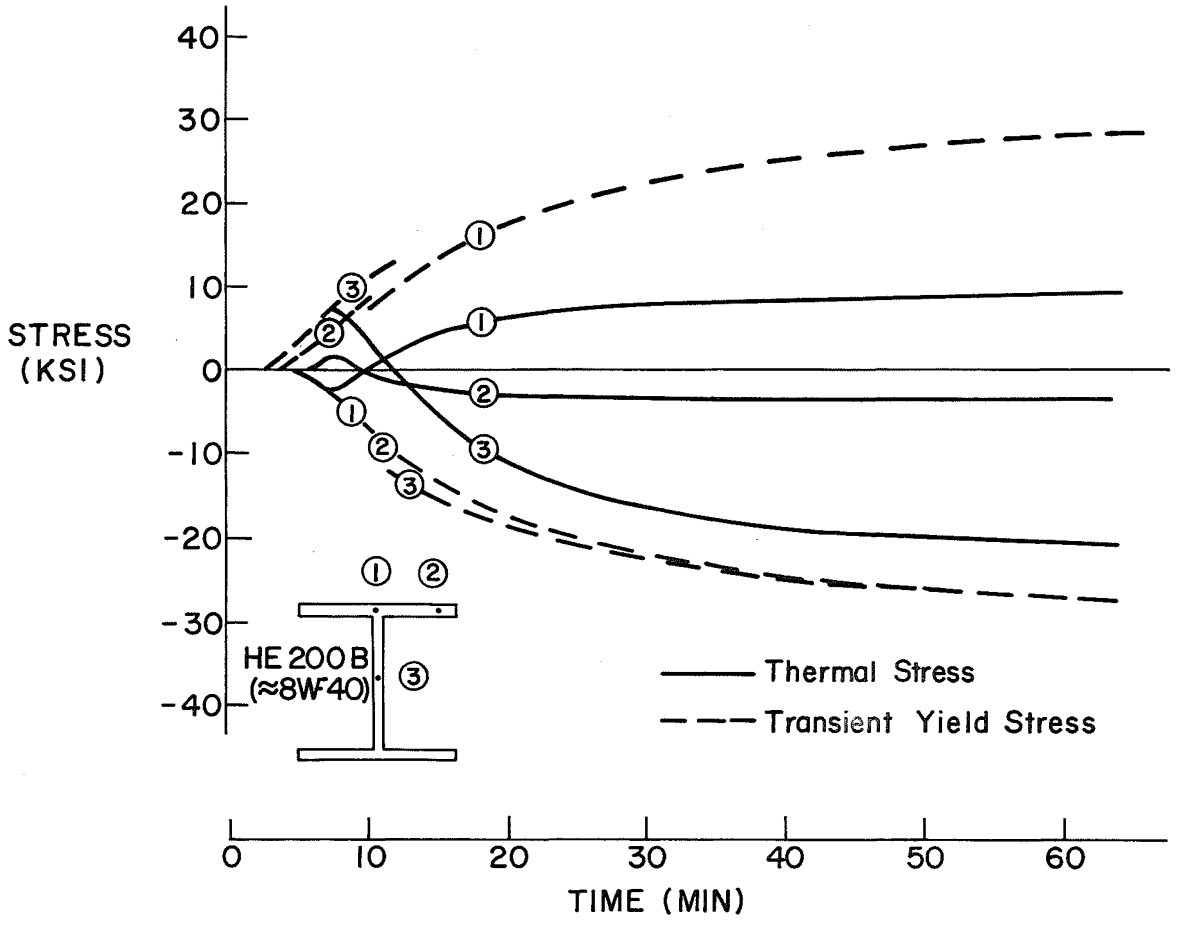

Fig. 33 Thermal stresses at three points of the cross section as a function of temperature. Same computation as in Fig. 32.

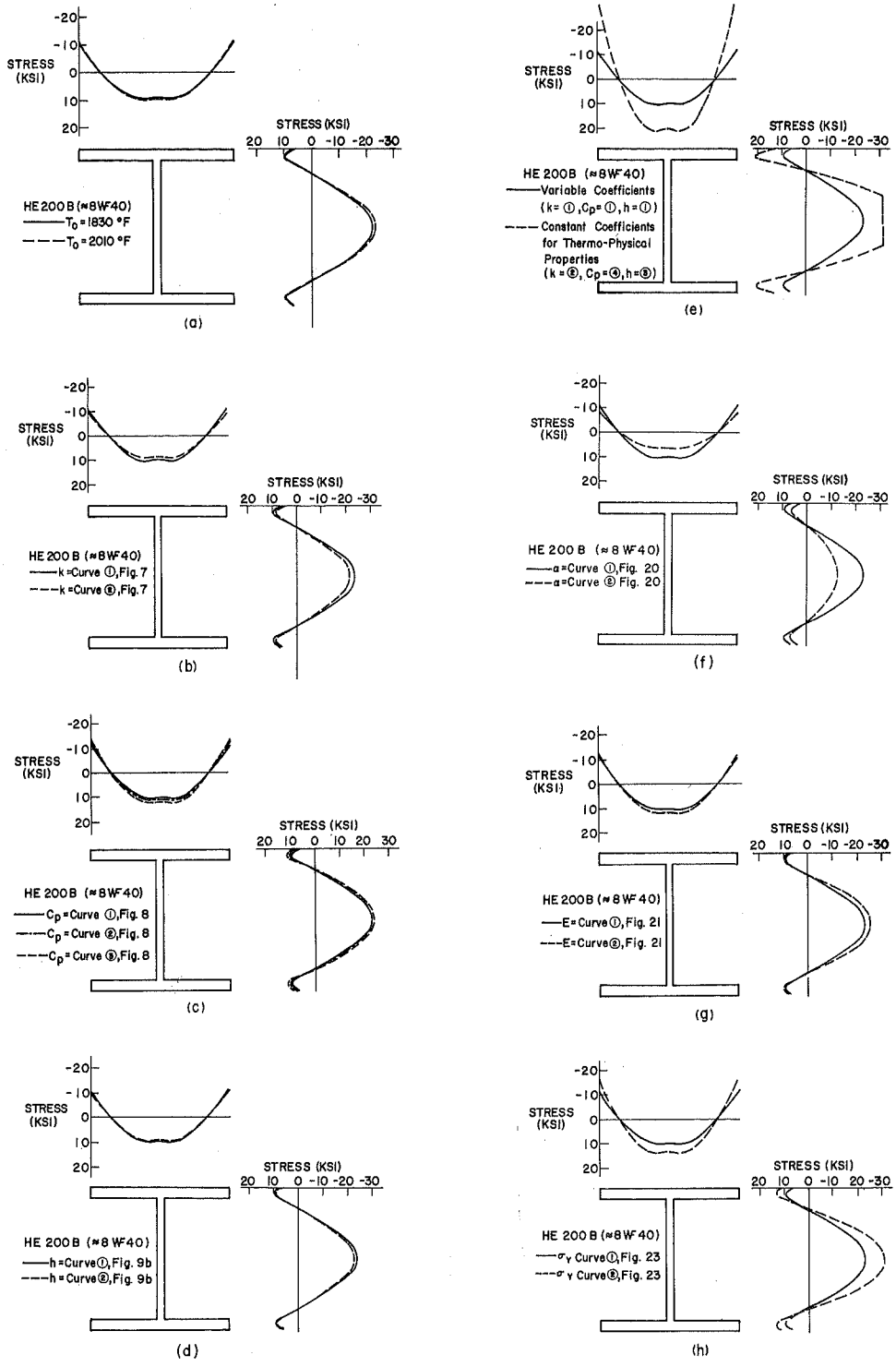

(a) initial temperature
(b) thermal conductivity, k
(c) specific heat (incl. latent heat), c_p
(d) surface coefficient of heat transfer, h
(e) constant thermo-physical coefficients (k, c_p, and h)
(f) coefficient of linear expansion, α
(g) modulus of elasticity, E
(h) yield stress, σ_y

Fig. 34 Influence of different assumptions on computed residual stresses. Shape HE 200 B (≈8WF40). Stresses in the mid-planes of flange and web.

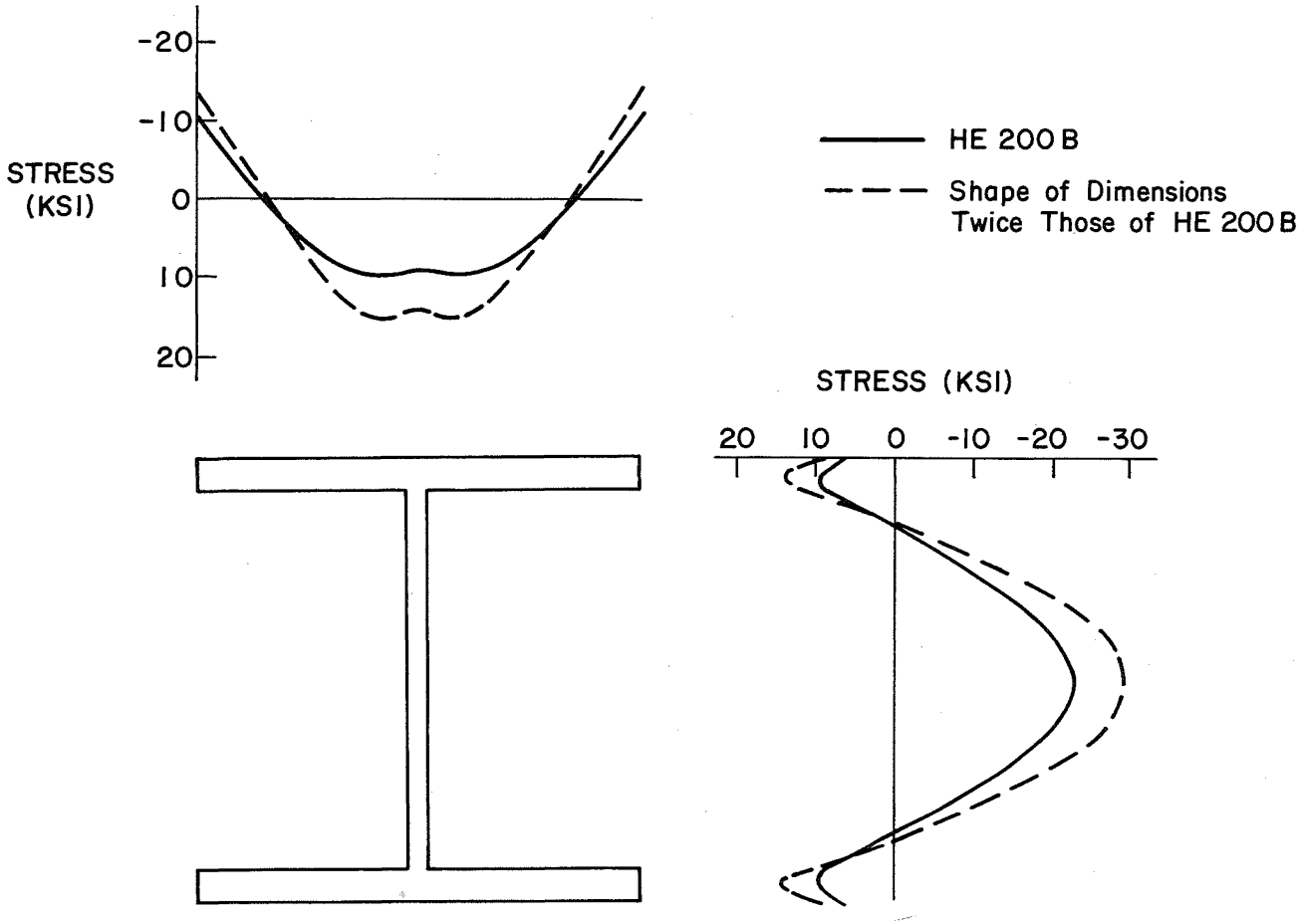

Fig. 35 Comparison of residual stress distributions in two shapes which are geometrically similar. Stresses in the mid-planes of flange and web.

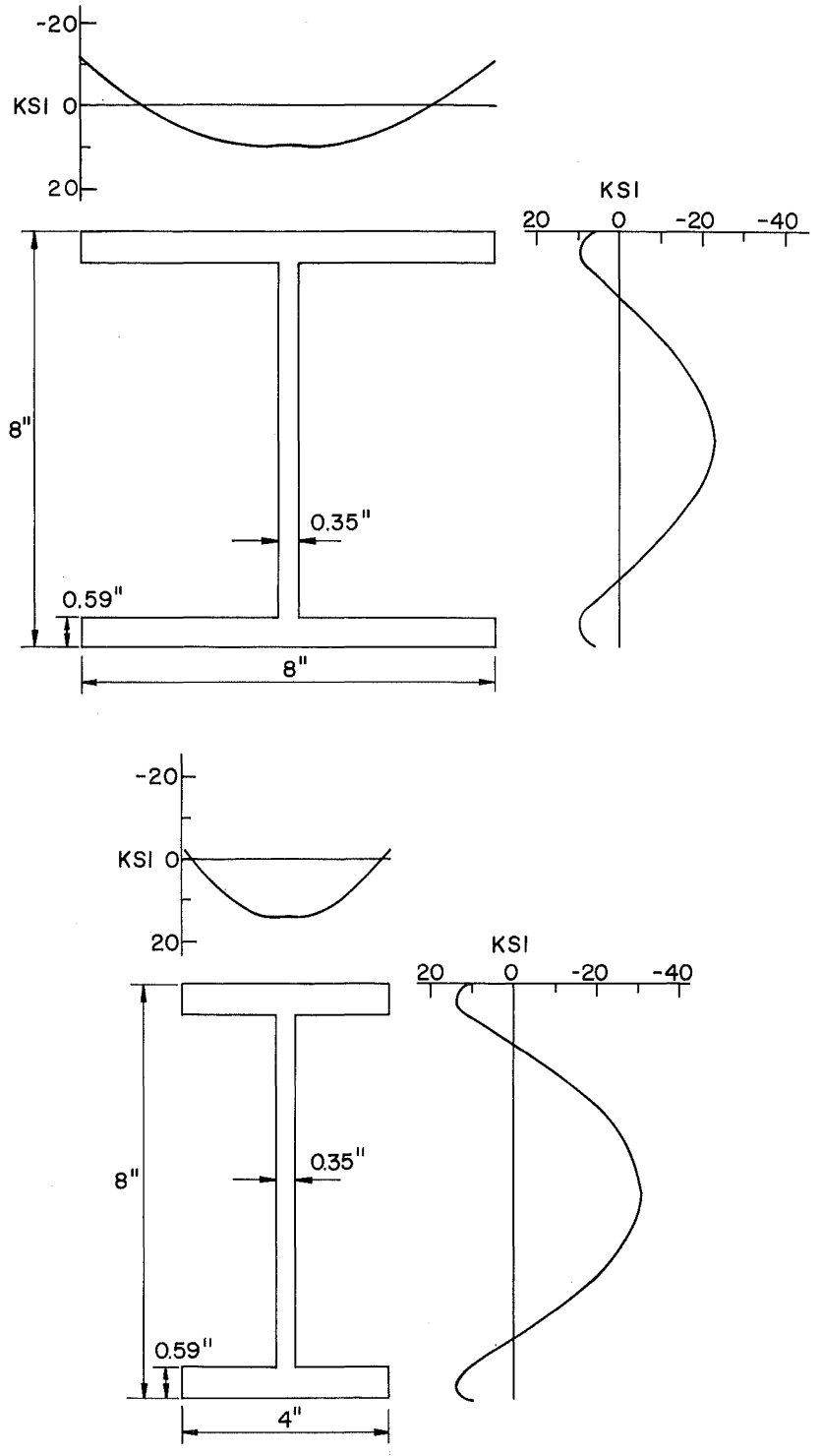

Fig. 36 Comparison of residual stress distributions in the HE 200 B (≈8WF40) shape and a shape with the same geometry except that width is 4" instead of 8".

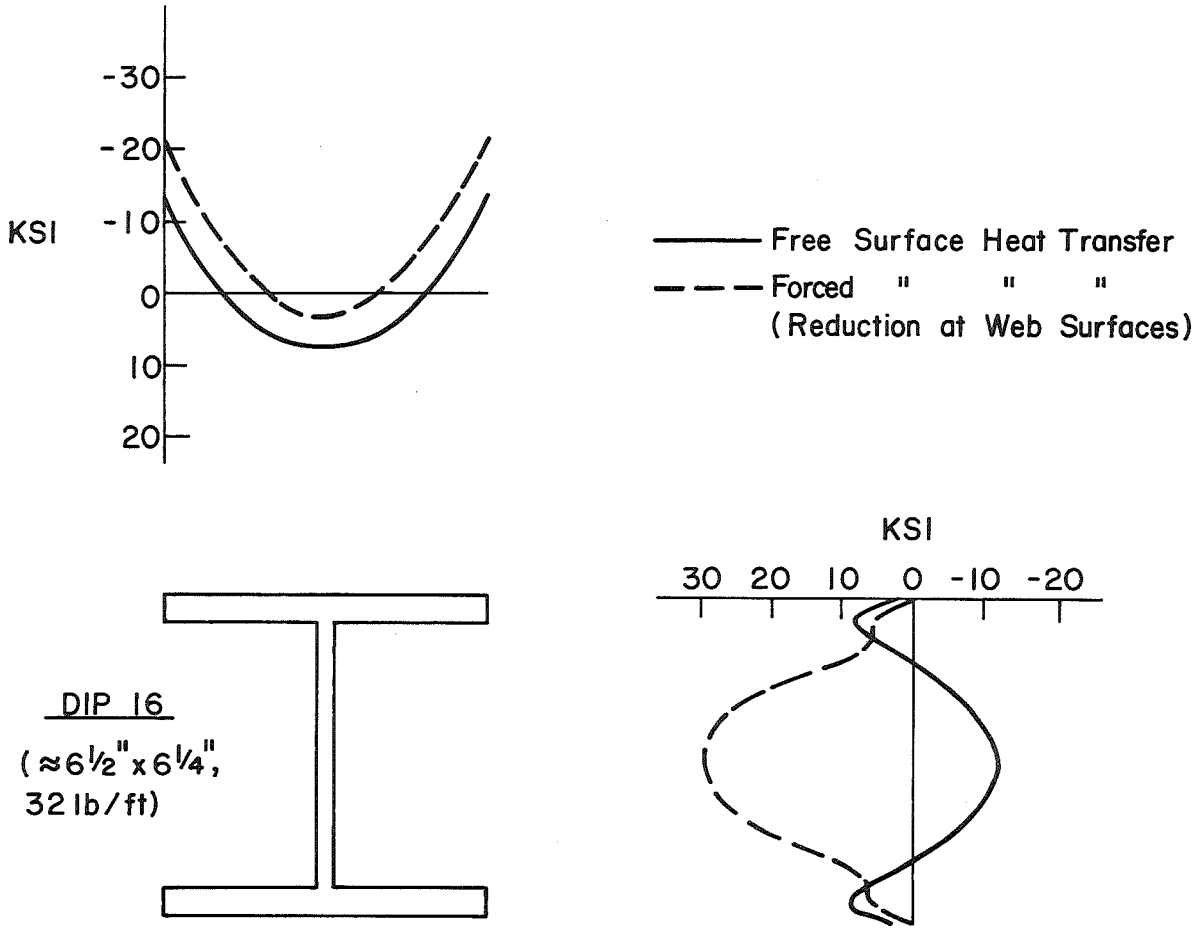

Fig. 37 Computed residual stress distribution in a shape DIP16 when the heat transfer from the web surface is reduced to 30-100%.

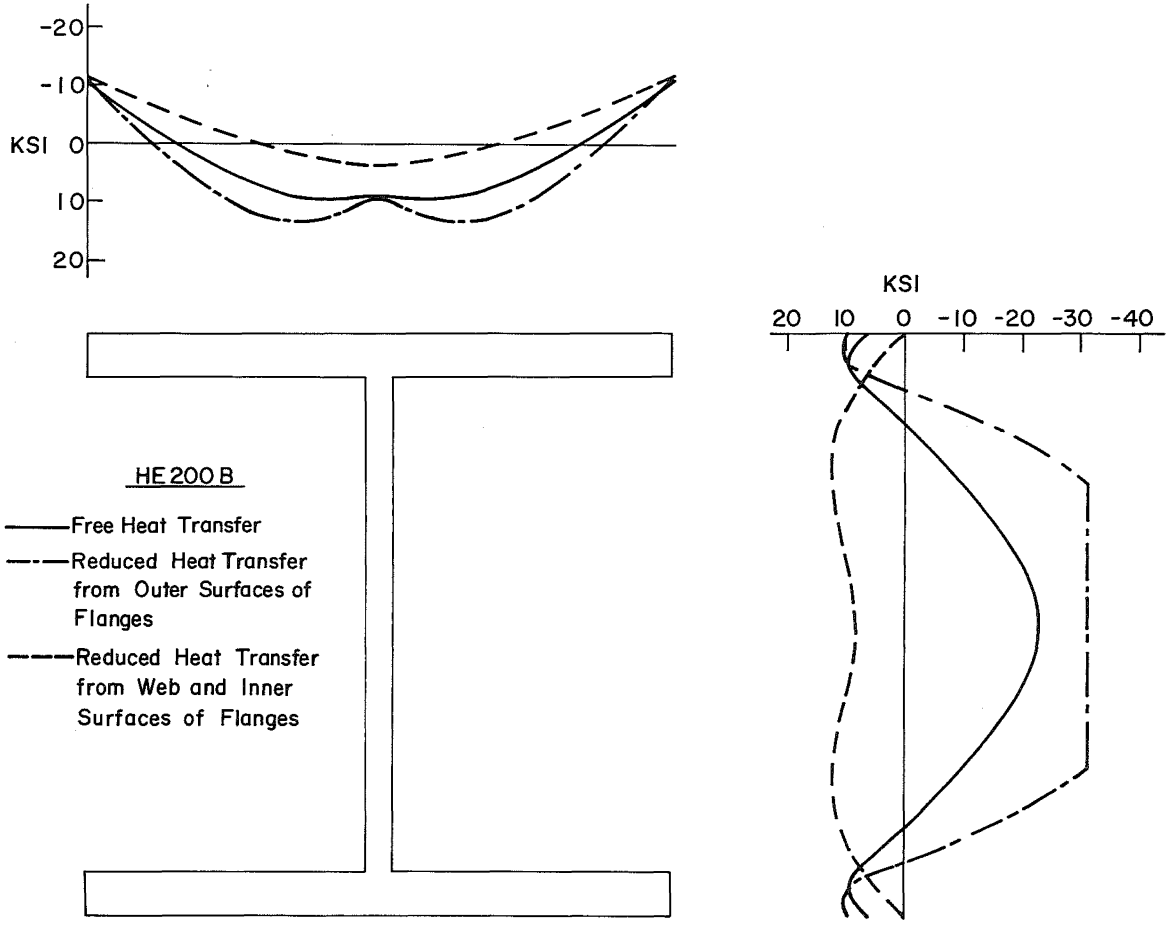

Fig. 38 Computed residual stress distribution in a shape HE 200 B ($\approx$8WF40) with different heat-transfer assumptions

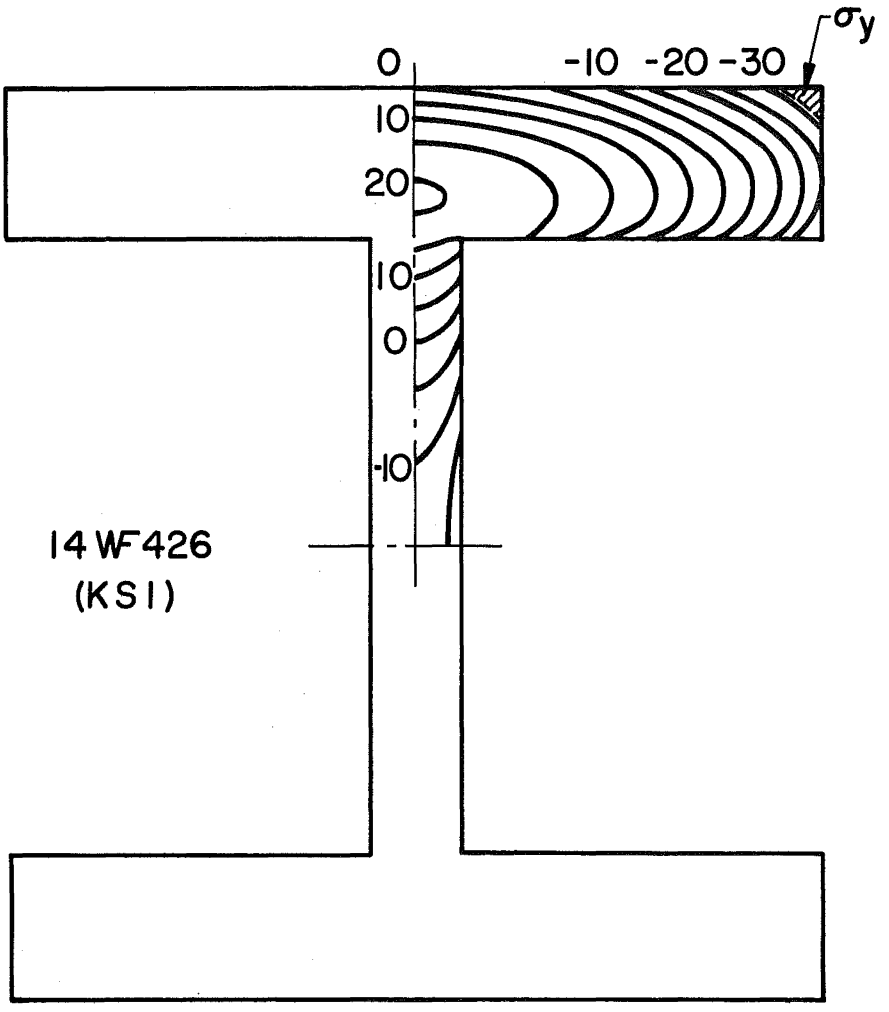

Fig. 39 Computed two-dimensional variation of residual stress in a 14WF426 shape--free heat transfer

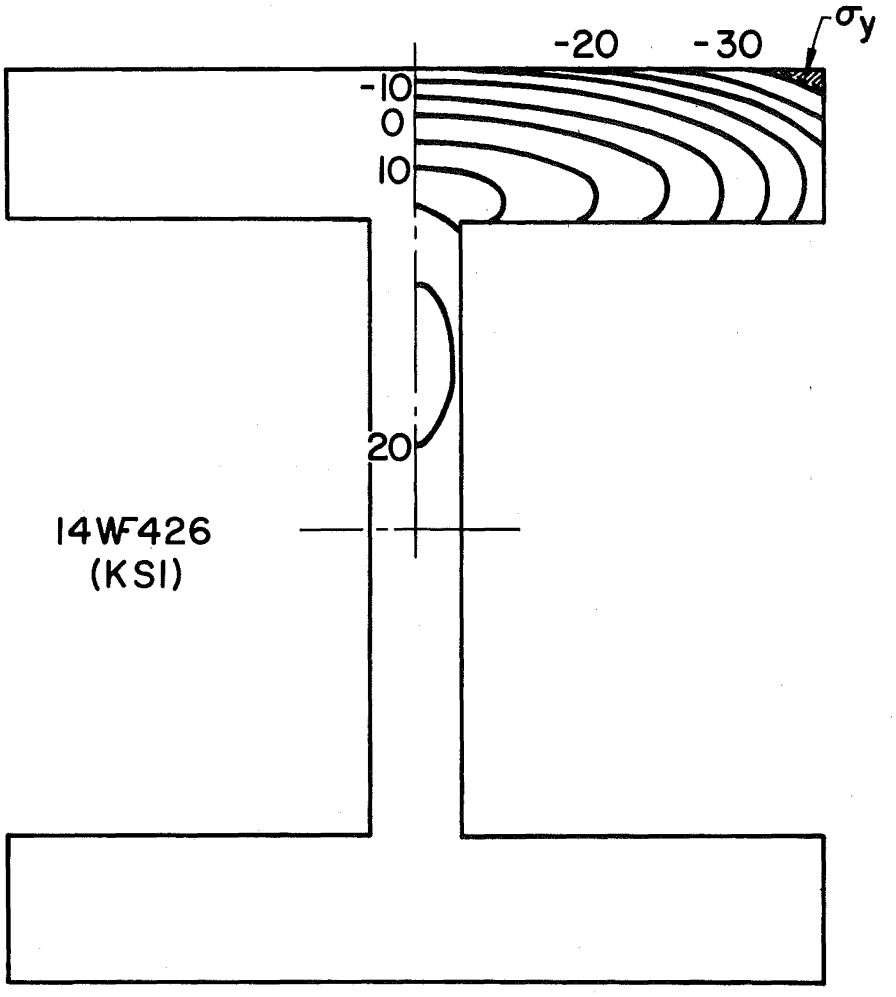

Fig. 40 Computed two-dimensional variation of residual stress in a 14WF426 shape--heat transfer reduced by 50% from inner surfaces

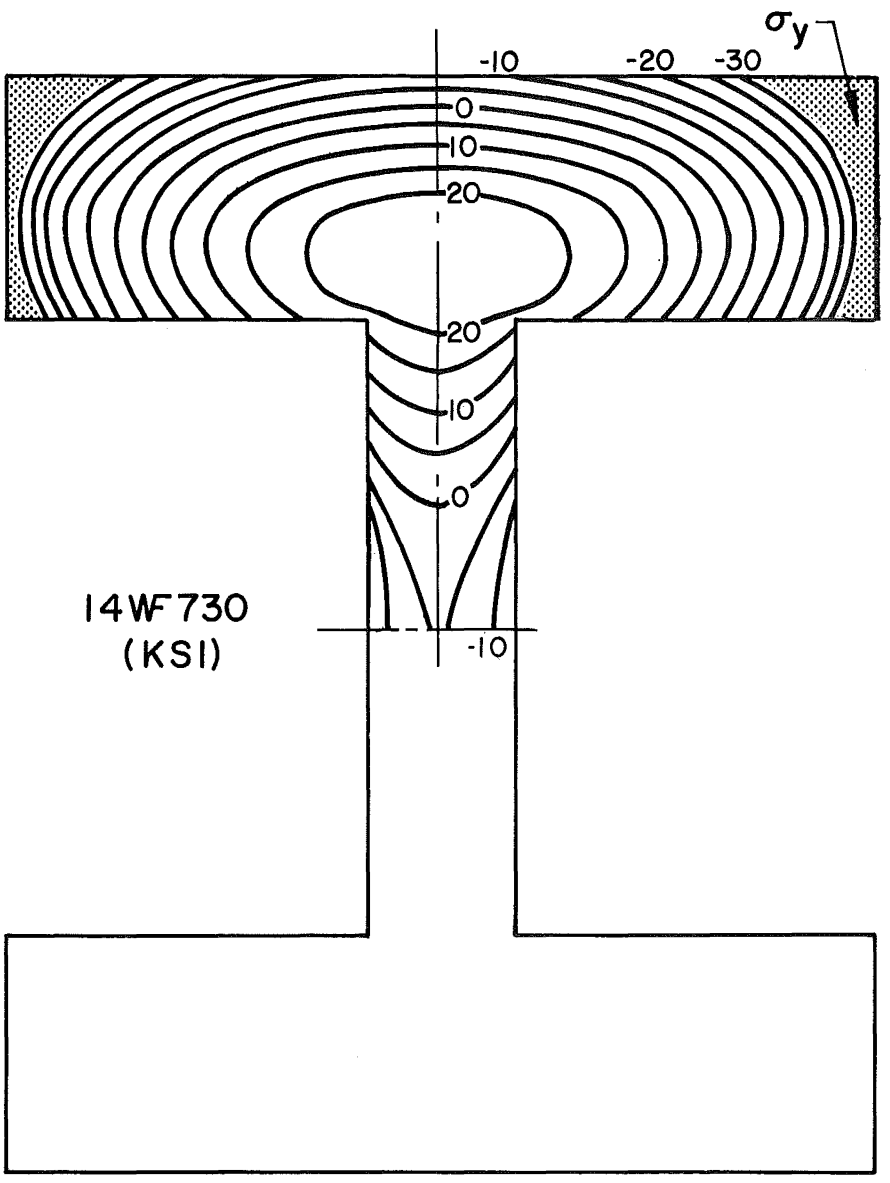

Fig. 41 Computed two-dimensional variation of residual stress in a "jumbo" shape 14WF730--free heat transfer assumed

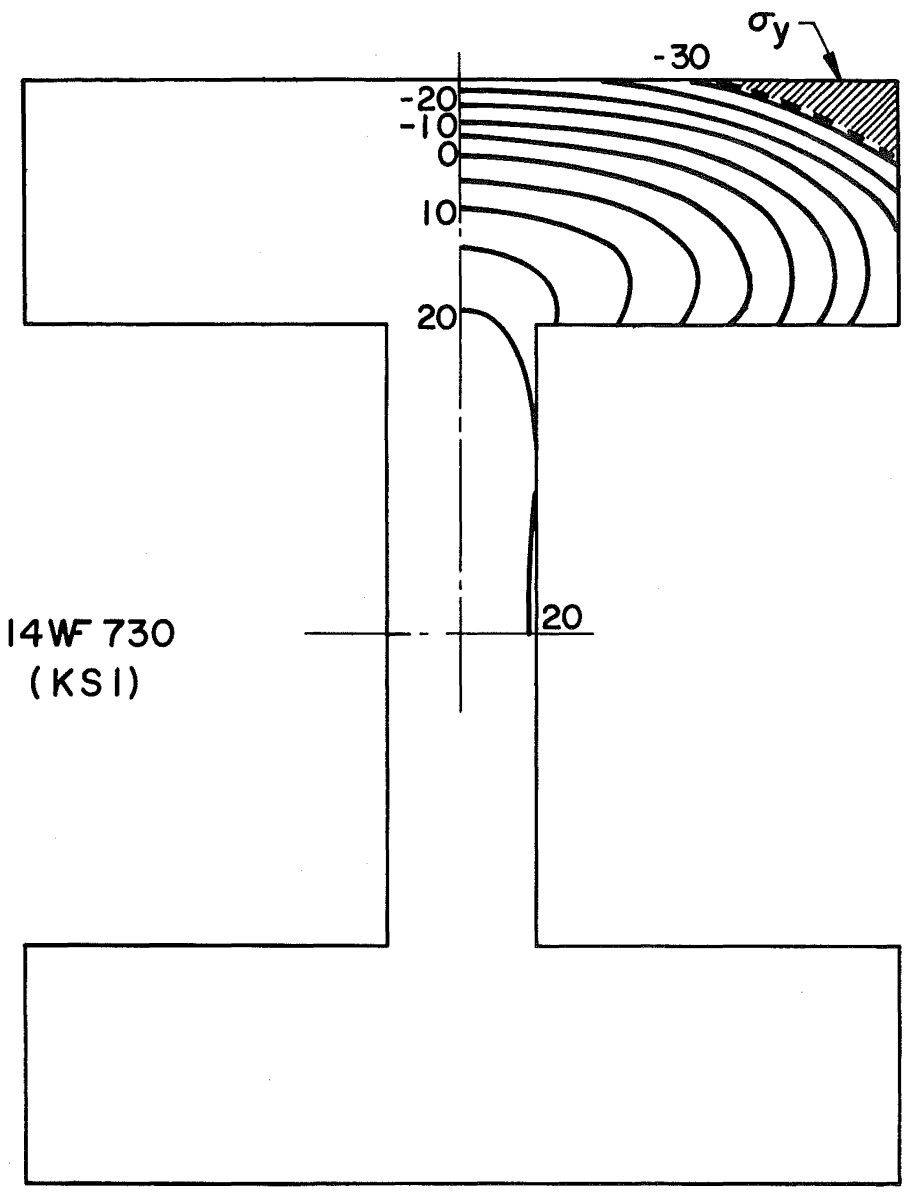

Fig. 42 Computed two-dimensional variation of residual stress in a "jumbo" shape 14WF730--heat transfer reduced by 50% from inner surfaces

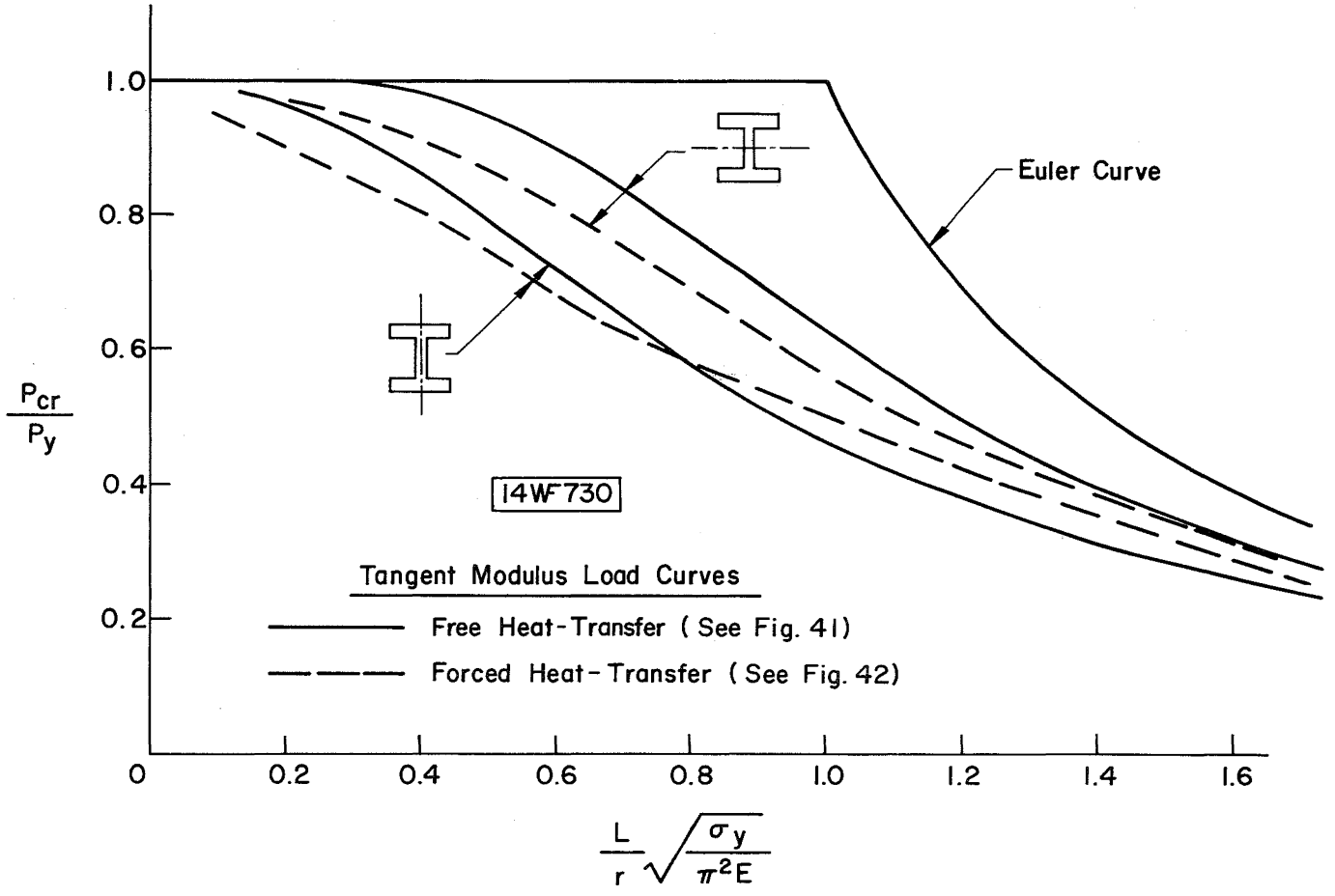

Fig. 43 Column curves for the "jumbo" shape 14WF730. Tangent modulus load based on the residual stress distributions of Figs. 41 and 42.

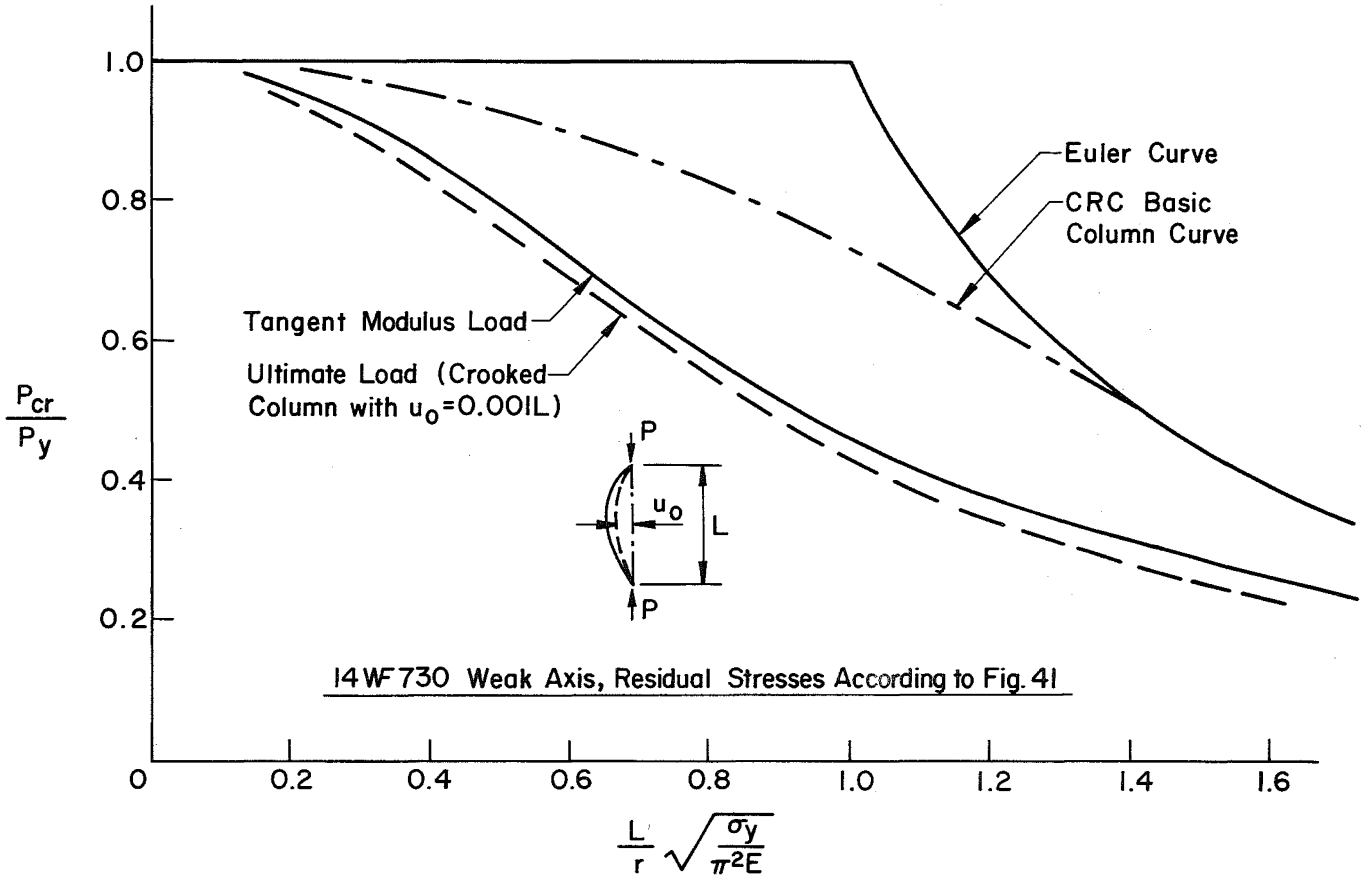

Fig. 44 Comparison between tangent modulus load and ultimate strength of the 14WF730 shape with residual stresses according to Fig. 41.

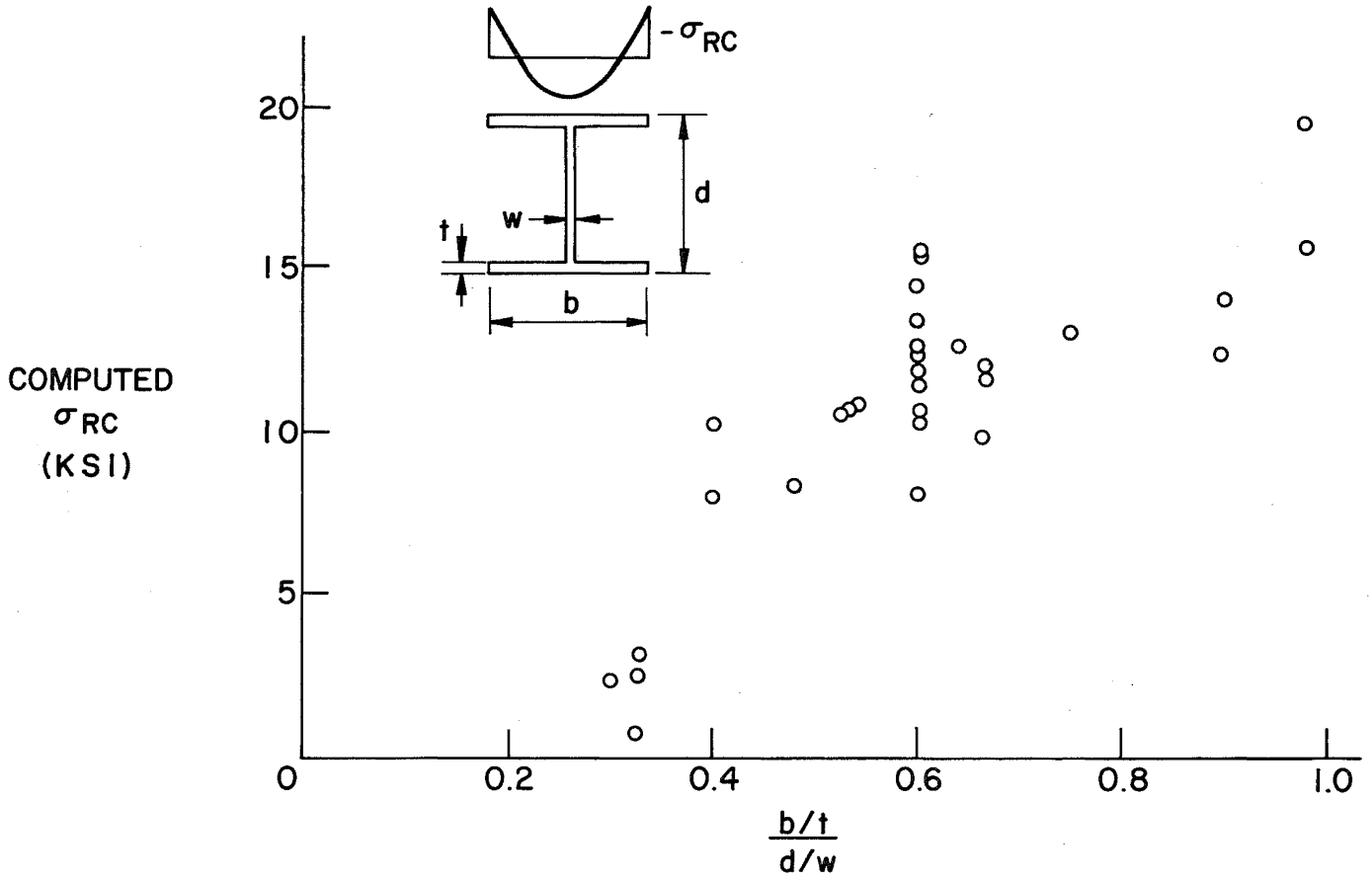

Fig. 45 Average residual stress at flange tips of H-shapes, plotted against a geometrical parameter $\frac{b/t}{d/w}$

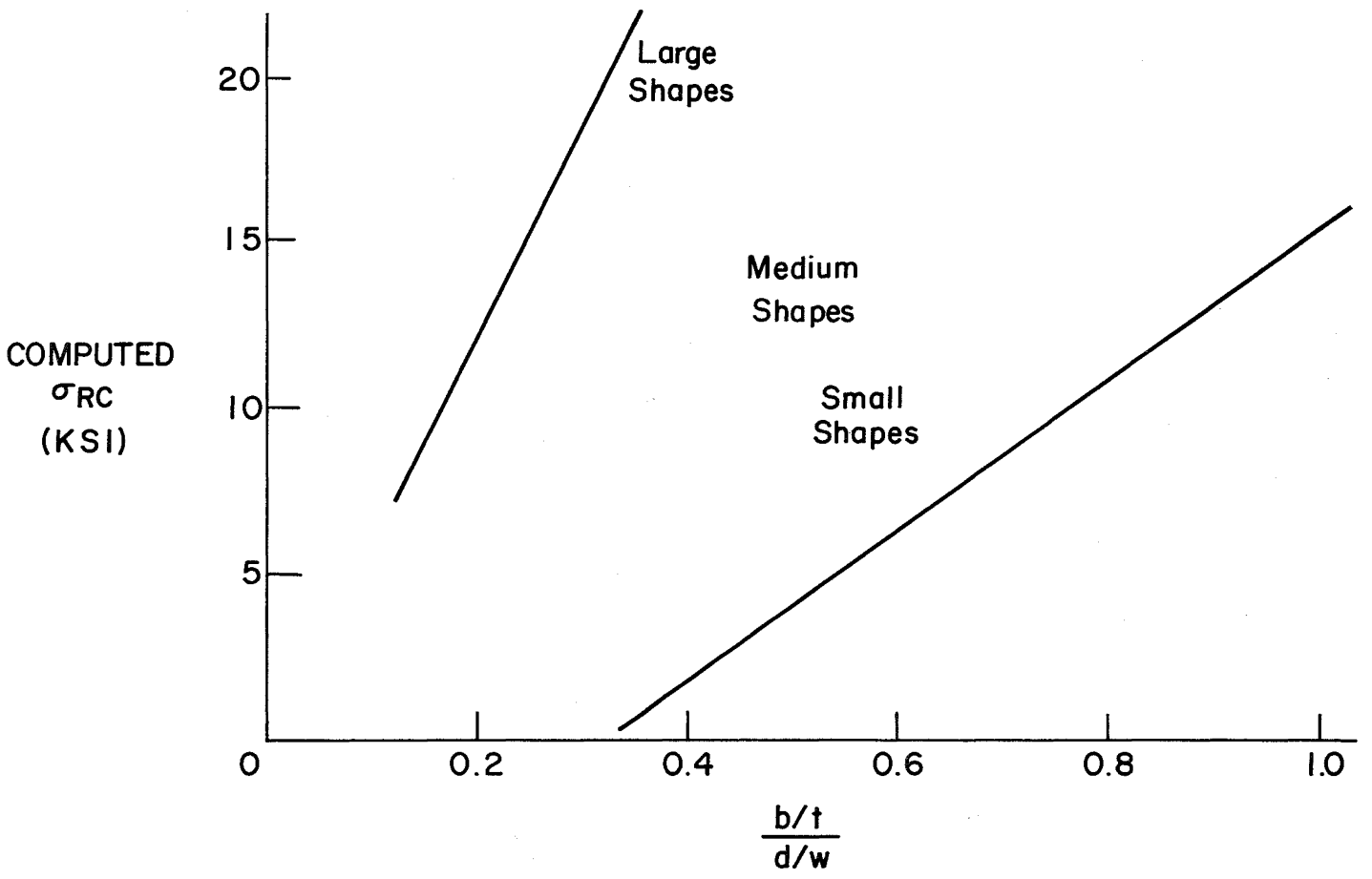

Fig. 46 Schematic diagram showing the principal influence of shape geometry upon residual stresses at flange tips of H-shapes

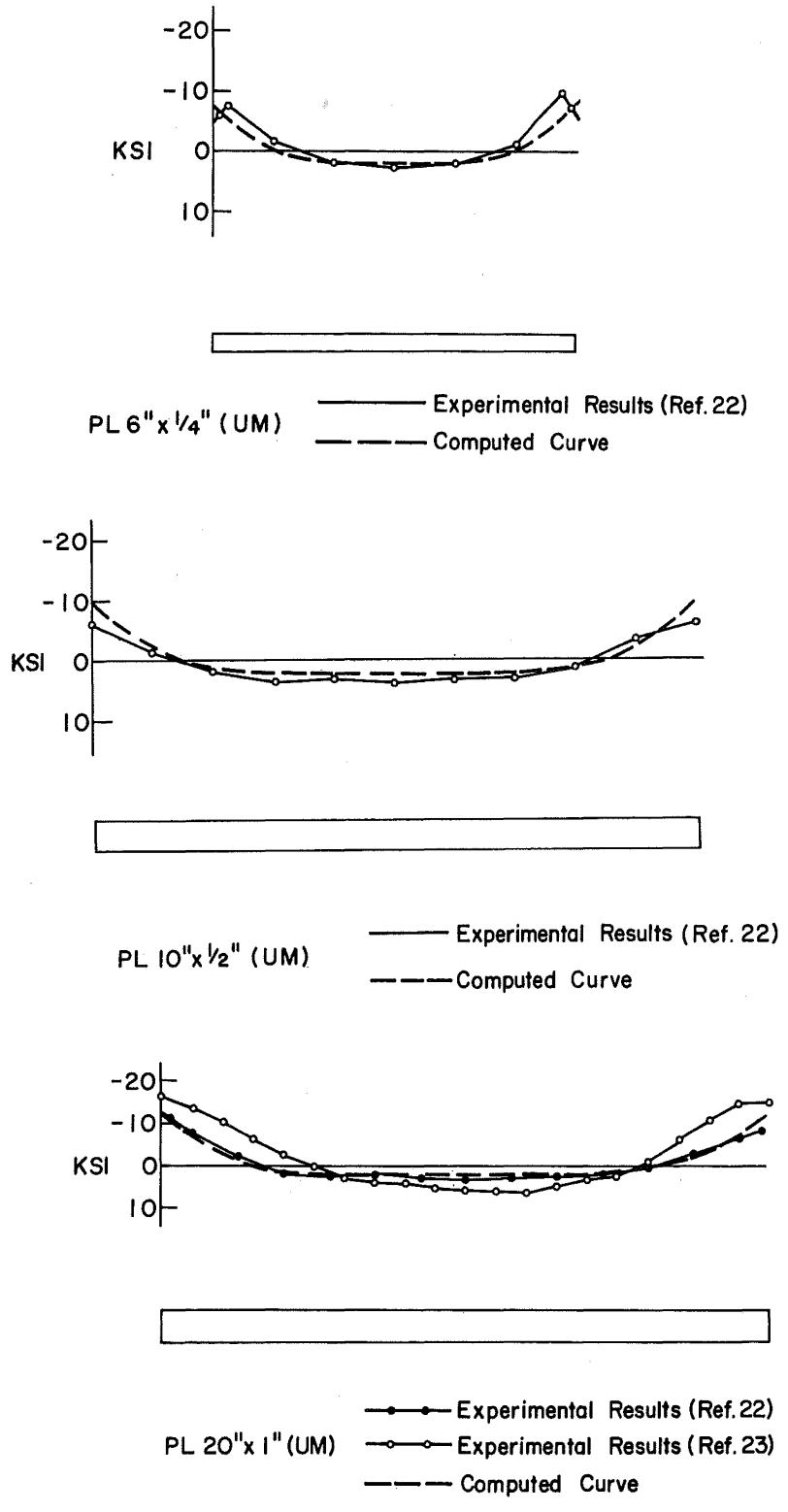

Fig. 47 Comparison between computed residual stresses and experimentally measured residual stresses for universal-mill plates

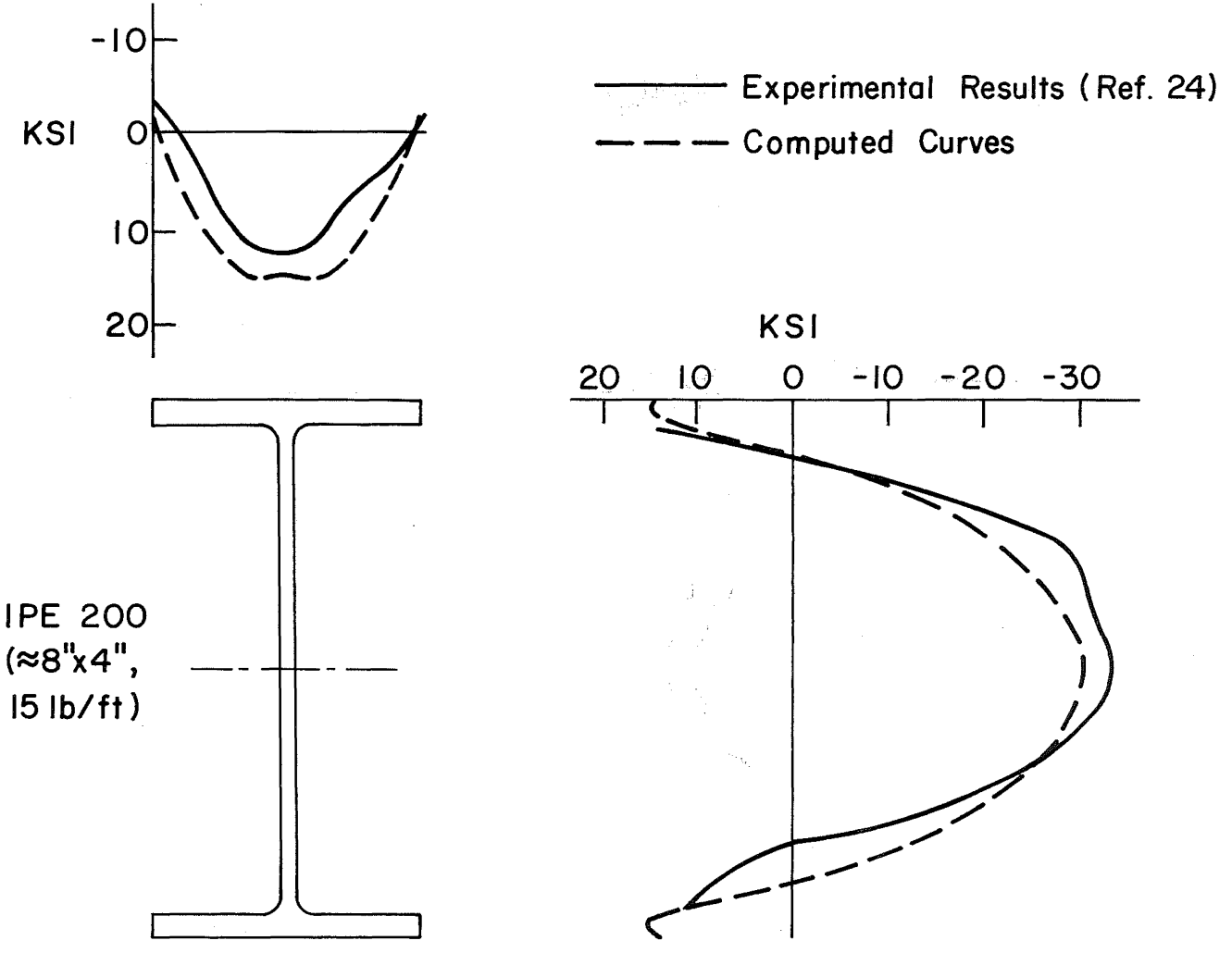

Fig. 48 Residual stresses in a European I-beam IPE200

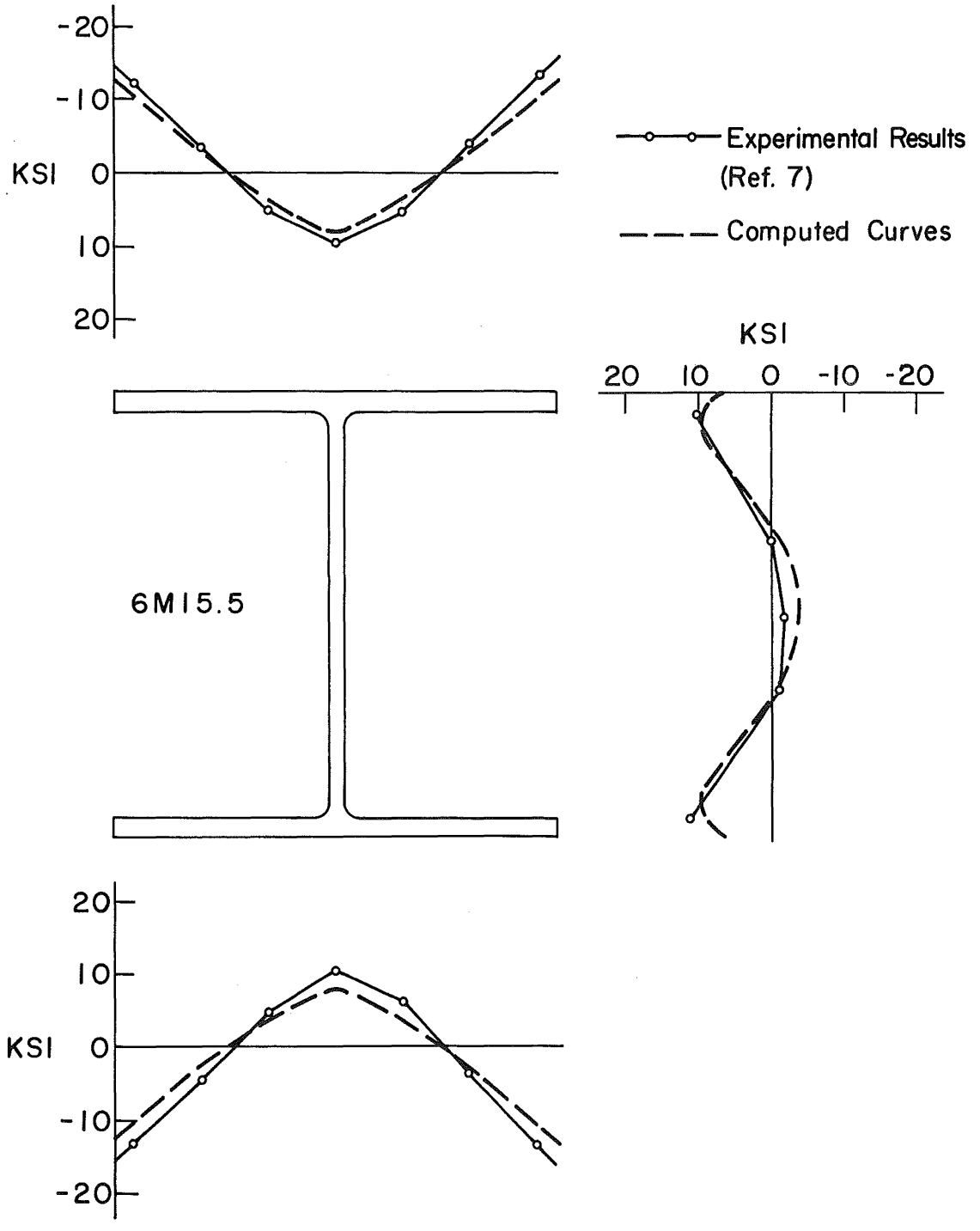

Fig. 49 Residual stresses in a 6M15.5 shape

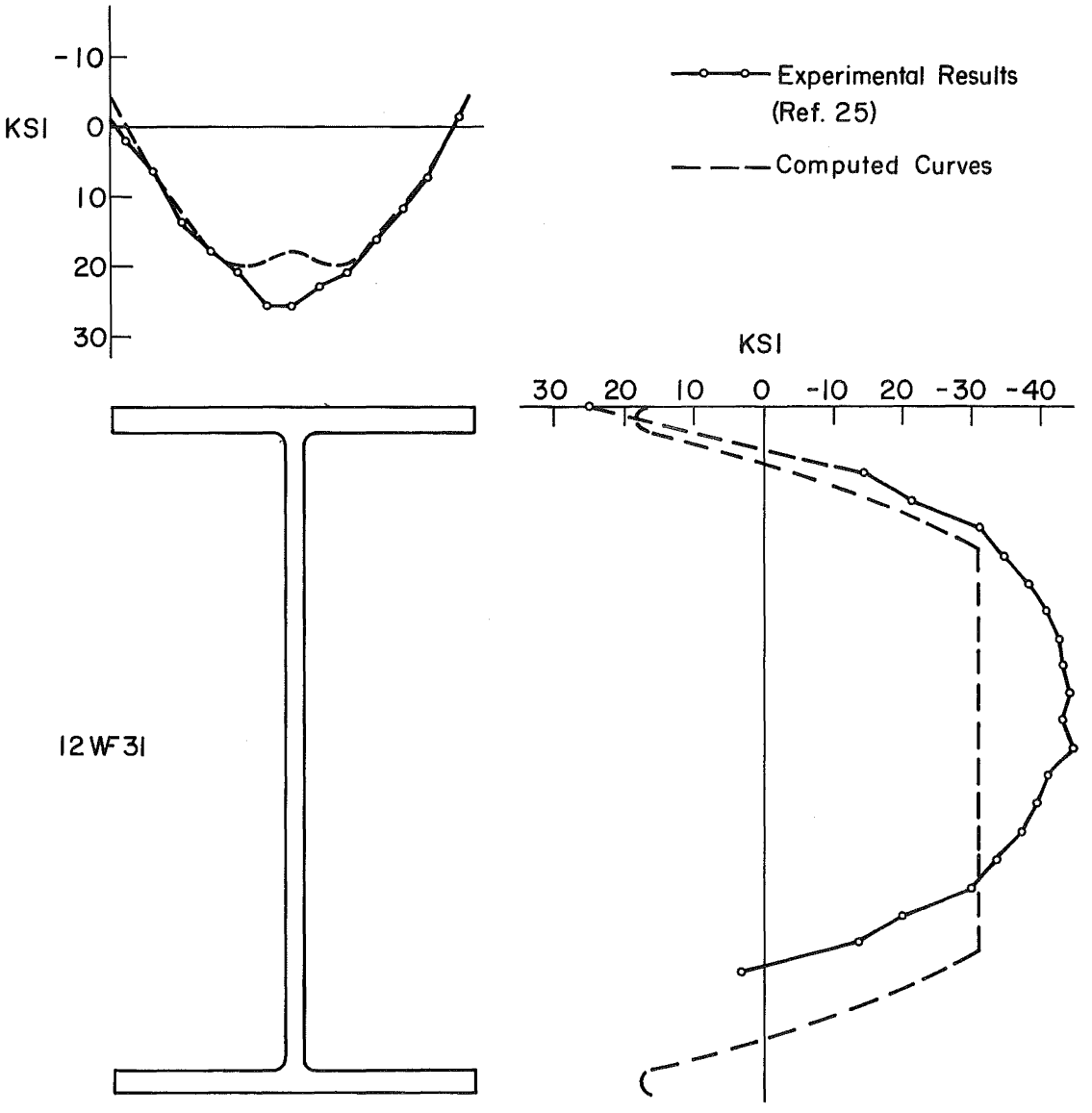

Fig. 50 Residual stresses in a 12WF31 shape

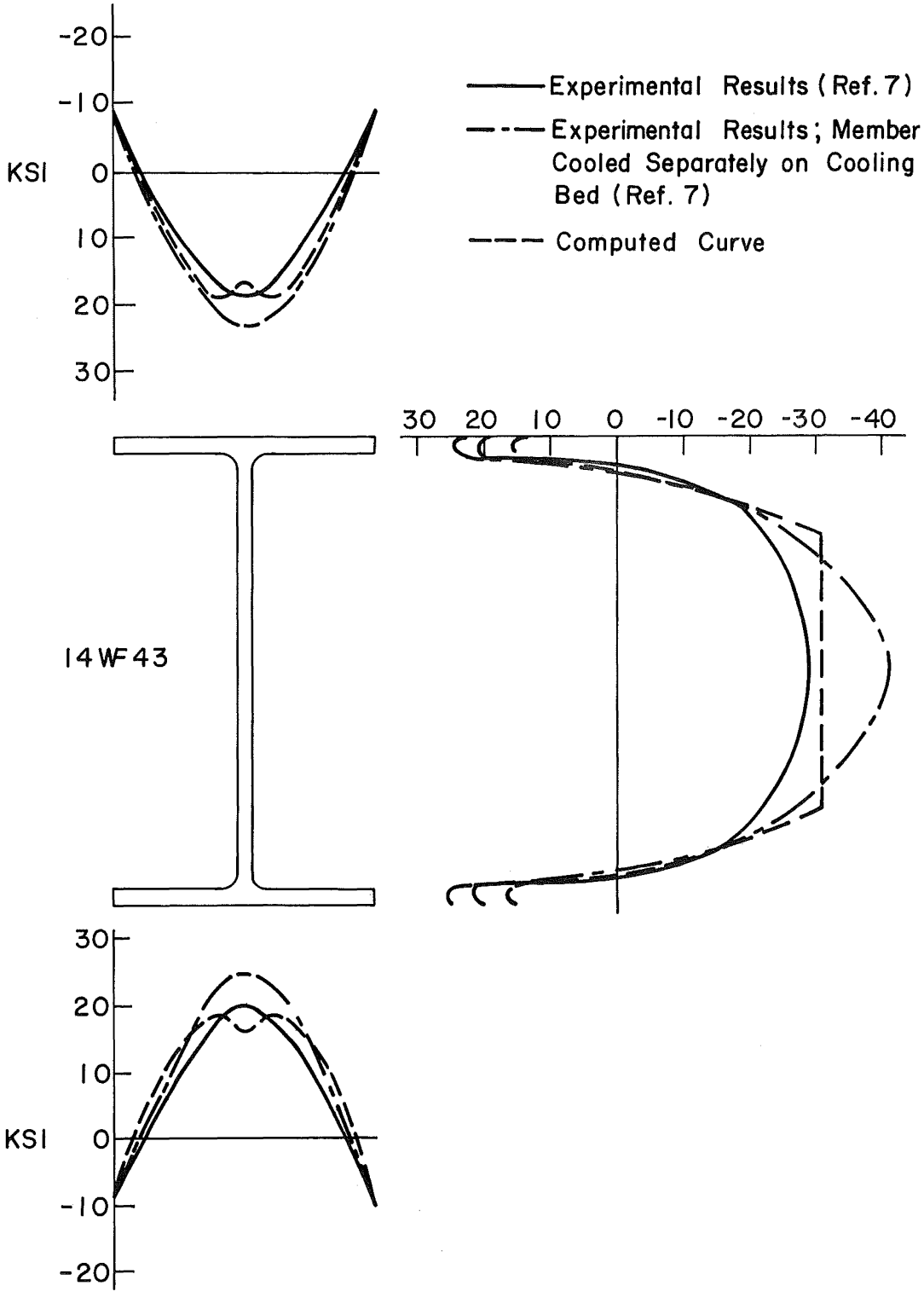

Fig. 51 Residual stresses in a 14WF43 shape

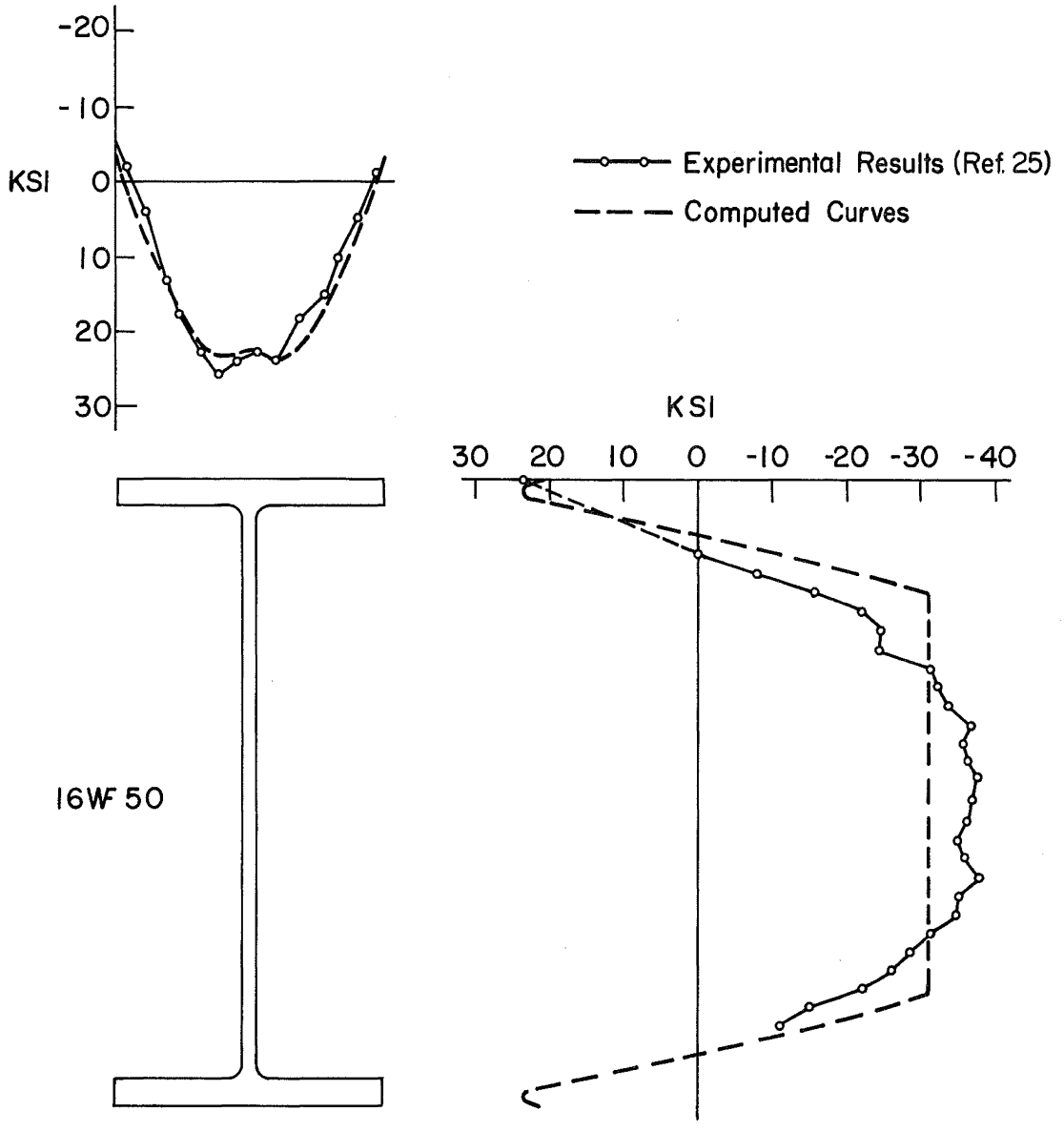

Fig. 52 Residual stresses in a 16WF50 shape

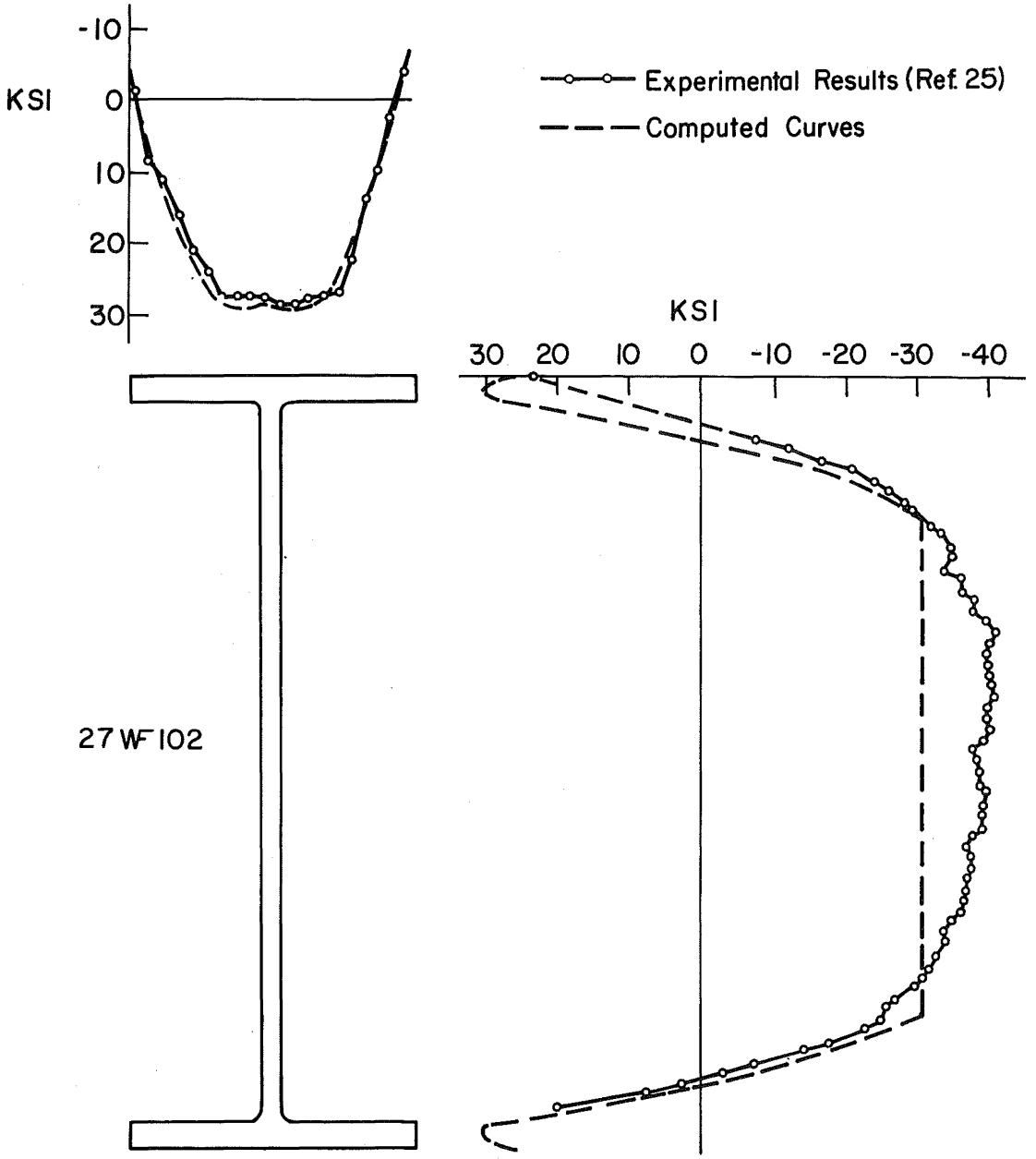

Fig. 53 Residual stresses in a 27WF102 shape

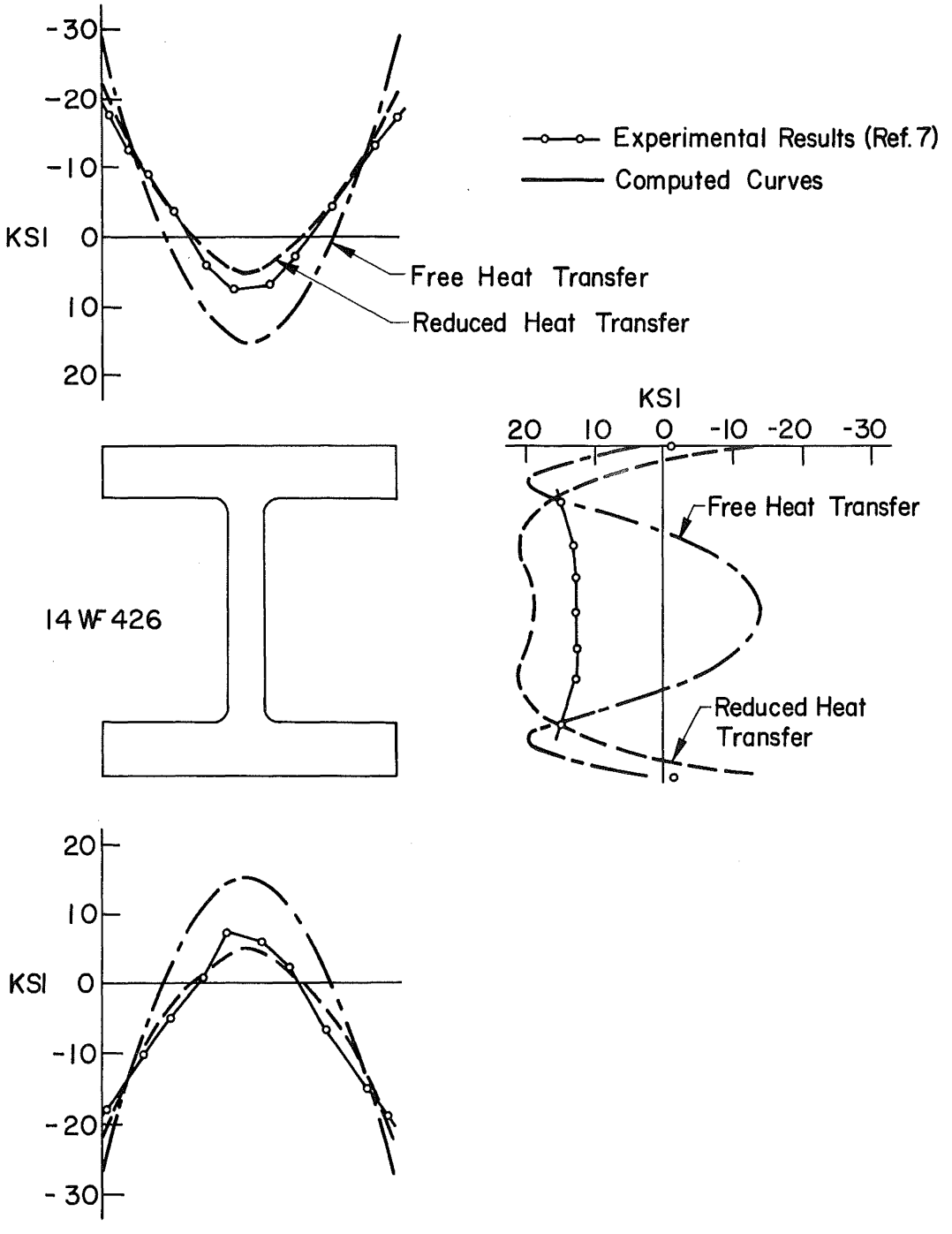

Fig. 54 Residual stresses in a 14WF426 shape

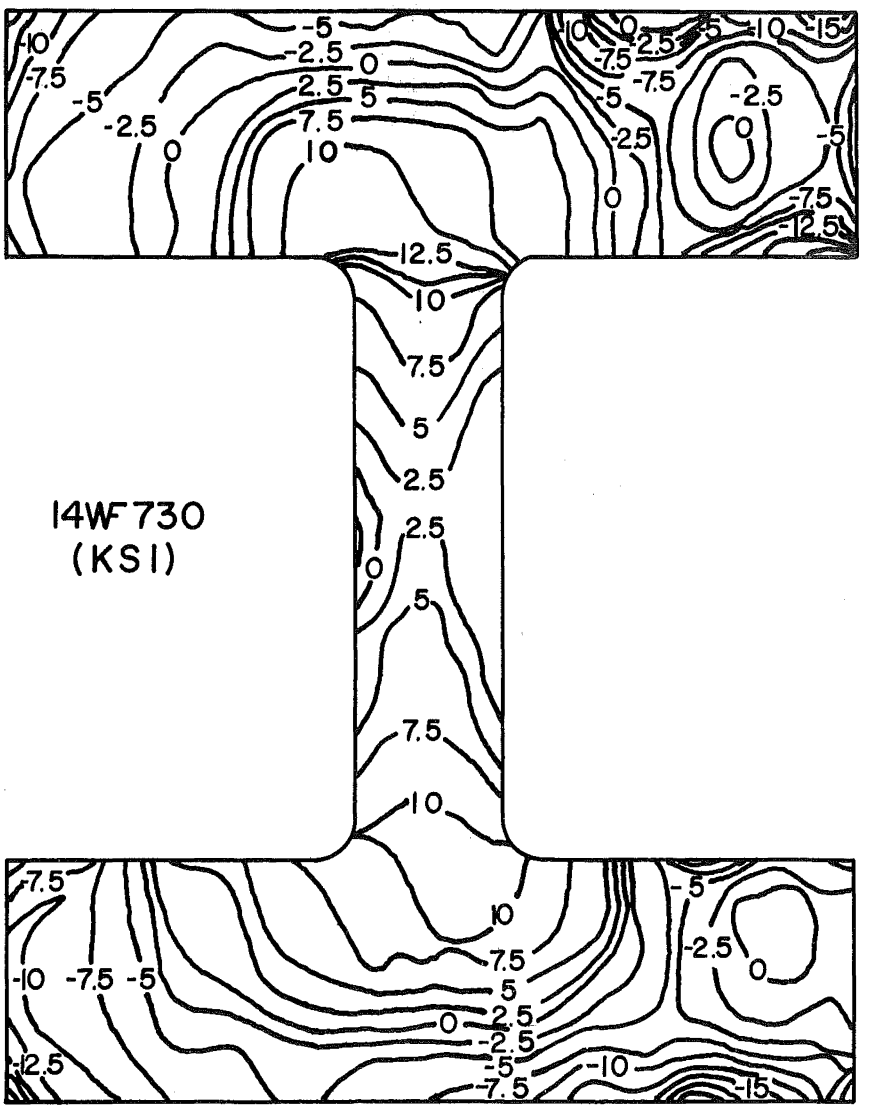

Fig. 55 Residual stresses in a 14WF730 shape

REFERENCES

1. G. A. Alpsten and L. Tall
RESIDUAL STRESSES IN HEAVY WELDED SHAPES, Fritz Laboratory Report No. 337.12, In Preparation.

2. G. Alpsten
EGENSPÄNNINGAR I VARMVALSADE STÅLPROFILER (RESIDUAL STRESSES IN HOT-ROLLED STEEL PROFILES), Tekn. Lic. Dissertation, Institution of Structural Engineering and Bridge Building, The Royal Institute of Technology, Stockholm, 1967.

3. M. Roš
DIE BREITFLANSCHIGEN DIFFERDINGER-GREY-TRÄGER (THE WIDE-FLANGE SHAPES, TYPE DIFFERDINGER-GREY), Bericht 52, Eidgen. Mat.-Prüf.-Anst., Techn. Hochsch., Zürich, 1930.

4. J. Mathar
ERMITTLUNG VON EIGENSPANNUNGEN DURCH MESSUNG VON BOHRLOCH-VERFORMUNGEN (DETERMINATION OF RESIDUAL STRESSES BY MEASURING THE DEFORMATION AROUND DRILLED HOLES), Archiv f.d. Eisenhüttenwesen Vol. 6, 1933, pp. 277-281.

5. O. Grave
DISCUSSION TO REF. 4

6. Dörnen
SCHRUMPFUNGEN AN GESCHWEISSTEN STAHLBAUTEN, Stahlbau, Vol. 6, 1933, pp. 22-24.

7. Y. Fujita
THE MAGNITUDE AND DISTRIBUTION OF RESIDUAL STRESSES, Fritz Laboratory Report No. 220A.20, May, 1955.

8. A. W. Huber
THE INFLUENCE OF RESIDUAL STRESS ON THE INSTABILITY OF COLUMNS, Ph.D. Dissertation, Lehigh University, 1956

9. L. S. Beedle and L. Tall
BASIC COLUMN STRENGTH, Proc. ASCE, Vol. 86, 1960, pp. 139-173.

10. B. A. Boley and J. H. Weiner
THEORY OF THERMAL STRESS, John Wiley & Sons, Inc., 1960.

11. D. W. Peaceman and H. H. Rachford
THE NUMERICAL SOLUTION OF PARABOLIC AND ELLIPTIC DIFFERENTIAL EQUATIONS, J. Soc. Indust. Appl. Math., Vol. 3, 1955, pp. 28-41.

12. G. Birkhoff and R. S. Varga
IMPLICIT ALTERNATING DIRECTION METHODS, Trans. Amer. Math. Soc., Vol. 92, 1959, pp. 13-24.

13. G. A. Alpsten
THE PREDICTION OF COOLING BEHAVIOR OF HOT-ROLLED STEEL MEMBERS, Fritz Laboratory Report No. 337.13, In Preparation

14. N. R. Eyres, D. R. Hartree, J. Ingham, R. Jackson, R. J. Sarjant, and J. B. Wagstaff
THE CALCULATION OF VARIABLE HEAT FLOW IN SOLIDS, Phil. Trans., Royal Society of London, Vol. 240, 1946, Ser. A, pp. 1-57.

15. G. M. Dusinberre
NUMERICAL METHODS FOR TRANSIENT HEAT FLOW, Trans., Am. Soc. Mechanical Engrs., Vol. 67, 1945, pp. 703-712.

16. K. Ödeen
BERÄKNING AV ICKE-STATIONÄR, TVÅ-DIMENSIONELL VÄRMELEDNING I BRAND-UTSATTA BETONGKONSTRUKTIONER (CALCULATION OF NON-STATIONARY, TWO-DIMENSIONAL HEAT FLOW IN CONCRETE STRUCTURES SUBJECTED TO FIRE) Väg-och vattenbyggaren, Stockholm, No. 11, 1964, pp. 463-466.

17. L. Tall
RESIDUAL STRESSES IN WELDED PLATES -- A THEORETICAL STUDY, The Welding Journal, Vol. 43, Jan. 1964, pp. 10-s - 23-s.

18. D. V. Lindh and J. L. Tocher
HEAT GENERATION AND RESIDUAL STRESS DEVELOPMENT IN RESISTANCE SPOT WELDING, The Welding Journal, Vol. 46, Aug. 1967, pp. 351-s - 360-s.

19. F. R. Estuar
WELDING RESIDUAL STRESSES AND THE STRENGTH OF HEAVY COLUMN SHAPES, Ph.D. Dissertation, Lehigh University, Aug., 1965. (University Microfilm Inc., Ann Arbor, Michigan).

20. J. Glen
AN EXPERIMENTAL STUDY OF THE STRENGTH AND DUCTILITY OF STEEL AT ELEVATED TEMPERATURES, Symp. on Strength and Ductility of Metals, 1952, pp. 184-221.

21. B. G. Johnston (Ed.)
GUIDE TO DESIGN CRITERIA FOR METAL COMPRESSION MEMBERS, 2nd Edition, 1966, Column Research Council.

22. N. R. NagarajaRao and L. Tall
RESIDUAL STRESSES IN WELDED PLATES, Welding Journal, Vol. 40, Oct., 1961, pp. 468-s - 480-s.

23. M. Lohrmann, N. R. NagarajaRao and L. Tall
RESIDUAL STRESSES IN AUTOMATICALLY WELDED PLATES, Fritz Laboratory Report, In Preparation.

24. E. Mas and C. Massonnet
BELGIUM'S PART IN THE EXPERIMENTAL RESEARCH ON THE BUCKLING OF AXIALLY LOADED MILD-STEEL MEMBERS CONDUCTED BY THE "CONVENTION EUROPEENNE DE LA CONSTRUCTION METALLIQUE", Acier-Stahl-Steel, No. 9, Sept., 1966, pp. 385-392.

25. A. Franklin
PRIVATE COMMUNICATIONS, 1967.

26. J. Brozzetti, G. A. Alpsten, and L. Tall
RESIDUAL STRESSES IN A HEAVY ROLLED SHAPE 14WF730, Fritz Laboratory Report No. 337.10, In Preparation.

27. G. A. Alpsten and L. Tall
COLUMN STRENGTH OF HEAVY SHAPES - A PROGRESS REPORT, Fritz Laboratory Report No. 337.16, In Preparation.